Assays for Specific DNA, microRNA, and Proteins Using DNA Nanostructures

by

Rebecca E. Paliwoda

A thesis submitted in partial fulfillment of the requirements for the degree of

Doctor of Philosophy

Department of Chemistry
University of Alberta

ABSTRACT

Detection of biomolecules that are over- or under-expressed in diseases is an important field for early diagnosis, monitoring treatment, and improving patient prognosis. The main goal of my thesis is to utilize DNA nanotechnology combined with nanomaterials to provide sensitive and specific detection of the desired target molecules that exist in low abundance. I have developed three analytical assays for the detection of DNA, microRNA, proteins, and for the characterization of functionalized nanomaterials.

I have developed a binding induced three-way junction (3WJ) with fluorescence resonance energy transfer (FRET) detection using a quantum dot (QD) as both a FRET donor and scaffolding for the DNA nanostructure. I designed probes to bind different portions of the nucleic acid sequence and optimized this assay for the detection of a DNA target. When both probes bind, a short complementary sequence allows the QD FRET donor and a dye acceptor to be in close proximity; detection occurs through the generation of a fluorescent signal. This developed assay was also applied to the detection of single base mismatches in the target DNA sequence with excellent discrimination between the mismatch and the wild-type sequence. With further optimization, this developed technique was also applied to the detection of a microRNA sequence with a specific and sensitive concentration-dependent response.

Building on the QD-FRET detection technique, I have designed a binding-induced DNA assembly (BINDA) assay for the detection of a protein target. This technique utilized two aptamers, which bind to specific epitopes on target molecules. When combined with the formation of a BINDA nanostructure, the QD donor again

acted as both the FRET donor and scaffolding for other components of BINDA. This technique was able to detect trace levels of the desired protein target with minimal background signal.

I also have developed a toehold-mediated strand displacement assay for the characterization of surface coverage on DNA functionalized gold nanoparticles (AuNPs). Through these strand displacement reactions, multifunctionalized AuNPs can be characterized without needing different fluorescent labeling on each strand. This work was compared to conventional characterization methods with similar results. I also found that the use of a TAMRA fluorescent label reduced surface coverage of DNA onto AuNPs.

All of the developed assays are sensitive and specific for the desired targets, do not require any separation steps, have simple procedures, are rapid, and require only a fluorescence reader. These aspects are very important for developing point-of-care diagnostic assays to improve patient care, diagnosis, and prognosis.

PREFACE

Chapter 5 of this thesis has been published as Paliwoda, R.E.; Li, F.; Reid, M.S.; Lin, Y.; Le, X.C. Sequential Strand Displacement Beacon for Detection of DNA Coverage on Functionalized Gold Nanoparticles. *Anal. Chem.* **2014**, 86(12), 6138-6143.

I was responsible for the data collection and analysis, as well as manuscript composition. F. Li contributed to manuscript composition and concept formation. M. S. Reid and Y. Lin aided with manuscript editing. X. C. Le was the supervisory author and was involved with concept formation and manuscript composition.

ACKNOWLEDGMENTS

First, I would like to thank my supervisor, Dr. X. Chris Le, for his continued support in all of my scientific endeavors. Your encouragement and patience has helped me become increasingly independent and form innovative ideas on my own, while still being available when your expertise is needed. I would also like to thank Dr. Hongquan Zhang for your countless suggestions and guidance whenever I was lost in my research.

Thank you to my committee members, Dr. Nils Petersen and Dr. Robert Campbell for their critical suggestions and comments.

I also appreciate the support and organization of Ms. Katerina Carastathis and Ms. Anita Weiler. Thank you to Dr. Anna Jordan for being exceptionally kind by taking time out of your retirement to support young scientists.

I acknowledge how fortunate I am to have received many funding opportunities during my graduate studies, including NSERC, AITF, QEII, Jean Cooley, and multiple travel awards.

Thank you to all of the amazing friends I have made since moving to Edmonton: you have all made this city feel like home. Friends from the Chemistry department (Cassandra, Tom, Meagan, Melanie, Chris), thank you for sharing your wide range of expertise and making my years of grad school an amazing learning experience. Friends in AET, thank you for lending advice and for making everyday a little brighter in the lab. Thank you especially to Ashley and Lindsay for listening whenever I needed to complain. Thank you to friends outside of my time at the university (Jennifer, Sarah,

Rhiannon, Louise) for keeping me sane and connected to the real world. I also need to extend the biggest thank you to Mike and Aleks for being with me every step of the way over the past 6 years.

I need to thank my tiny, cuddly roommate. Though you've never helped pay rent, having you to come home to everyday has been such a joy, even on the bad days

Thank you Evan for your patience and understanding.

And last, but certainly not least, I would like to thank my parents for their blind and unwavering support, love, and encouragement. You have always cheered for me, pushed me to my full potential, and taught me to work hard to reach my goals.

TABLE OF CONTENTS

LIST OF TABLES

LIST OF FIGURES

LIST OF ABBREVIATIONS

3WJ	Three way junction
A	Adenine
AuNP	Gold nanoparticle
BINDA	Binding induced DNA assembly
BSA	Bovine serum albumin
C	Cytosine
DF	Discrimination factor
DNA	Deoxyribonucleic acid
dsDNA	Double Stranded DNA
EDTA	Ethylene diamine tetraacetic acid
ELISA	Enzyme-linked immunosorbent assay
FAM	Fluorescein amidite
FRET	Fluorescence resonance energy transfer
G	Guanine
GO	Graphene oxide
HCR	Hybridization chain reaction
LSPR	Localized surface plasmon resonance
LOD	Limit of detection
miRNA	microRNA
MB	Molecular beacon
MAB	Molecular aptamer beacon

ME	2-mercaptoethanol
nt	Nucleotide
PBS	Phosphate buffered saline
PDGF	Platelet-derived growth factor
PLA	Proximity ligation assay
POC	Point of care
PCR	Polymerase chain reaction
QD	Quantum dot
RCA	Rolling circle amplification
RNA	Ribonucleic acid
SELEX	Systematic evolution of ligands by exponential enrichment
SNP	Single nucleotide polymorphism
ssDNA	Single stranded DNA
T	Thymine
TAMRA	Tetramethylrhodamine
U	Uracil

Chapter 1: Introduction

1.1 Biomolecule Detection

Biomolecule is a broad term that is used to describe molecules that are present in biological systems. These molecules are important in the functioning of these systems, including coding for genetic information, gene expression and regulation, catalyzing metabolic reactions, structure of cells, and regulation of cell cycle. These molecules can be misregulated and are an indicator of many diseases, such as cancer. Therefore, detection and monitoring of these molecules are important for disease diagnosis, management, and prognosis.

Biological samples, such as blood, serum, and urine, are extremely complex, with many different types of biomolecules and other small molecules. Because of this, developed assays must be specific and sensitive to the desired target. This is a wide field of research with goals of developing clinically relevant results that are robust and reproducible.

1.1.1 DNA

Deoxyribo**n**ucleic **a**cid (DNA) carries the genetic information for growth, development, and functioning in all biological systems. DNA is a polymer of repeating units called nucleotides. Each unit consists of a deoxyribose sugar and a phosphate group backbone, as well as one of four nucleobases. There are 4 different nucleobases in DNA: **a**denine (A), **g**uanine (G), **t**hymine (T), and **c**ytosine (C).[1] In single stranded DNA (ssDNA), the backbone of the nucleotides is covalently bonded via a phosphodiester bond between the

sugar of one nucleotide and the phosphate group of the adjacent one. **D**ouble **s**tranded **DNA** (dsDNA) forms with strands in opposite directions as a result of hydrogen bonding between complementary nitrogenous bases: A with T and C with G. Sequences are described from 5′ phosphate to 3′ hydroxyl.

DNA sequences can be extremely long, with dynamic structure along its length. dsDNA hybridized through hydrogen bonds form a helical shape, with a radius of 10 Å and 3.4 nm per turn, with each nucleotide measuring approximately 3.4 Å.[1,2] Thus, each turn of the helix contains approximately 10 nucleotide base pairs. The dsDNA helix also has grooves between the strands that are not symmetrical, resulting in a major and minor groove. These grooves provide binding sites for proteins, enzymes, and dyes.

The dsDNA structure is maintained by the above-mentioned hydrogen bond interactions between complementary base pairs. These interactions can be disrupted and pulled apart like a zipper via enzymes or by melting the sequences by increasing the temperature, low salt content, and extreme pH.[3] The different base pairs have different amounts of hydrogen bonds that can be formed: AT pairs have 2 and GC pairs have 3.[1] Thus, DNA with a higher GC content is more stable than that with a lower content.[4,5] Length also effects stability of dsDNA: longer sequences are more stable than shorter sequences.[6] These parameters of DNA will be discussed further in section 1.2.

1.1.2 microRNA

Ribo**n**ucleic **a**cid (RNA) is a nucleic acid that plays important roles in genetic coding, regulation, and expression of genes. RNA is similar in structure to DNA, with a chain of nucleotides bound by phosphodiester interactions. Unlike DNA, RNA exists as single

stranded, the ribose sugar contains a hydroxyl (-OH) group at the 2′ location, and it contains 4 nucleobases: **a**denine (A), **c**ytosine (C), **g**uanine (G), or **u**racil (U).[7–9] RNA is synthesized via a process called transcription by RNA polymerase using a DNA template. Through this transcription process, single stranded RNA molecules can be translated further into proteins, become involved in the translation process itself, or be involved in silencing of gene expression.[10]

micro**RNA** (miRNA) are short, noncoding RNA sequences involved in post transcriptional regulation of gene expression and RNA silencing.[11,12] miRNA are encoded by DNA and can hybridize with complementary mRNA molecules, playing an important role in gene regulation and expression.[13,14] Due to this, the mRNA are silenced via destabilization of mRNA, cleavage of mRNA, and/or reduced translation efficiency.[15,16] Because miRNA are involved in the normal functioning of eukaryotic cells, their dysregulation can lead to many different diseases. miRNA-mRNA form duplexes in the process of mRNA silencing, but usually multiple miRNA sites are bound for effective repression.[17,18] There is a database, miR2Diseases,[19] which summarizes research findings of the relationships found between miRNA and the disease outcomes.

The first miRNA, miRNA lin-4 from *Caenorhabditis elegans*, was discovered in 1993,[20] but miRNA were not considered their own biomolecular class until 2001.[11,21] Since then, miRNA have become an increasingly attractive target for disease detection and treatment. Detecting over or under expression of a miRNA sequence could indicate the presence of a disease.[22–25] Also, using targeted treatment for the blocking of the miRNA could aid in disease prognosis.

1.1.3 Proteins

Proteins carry out many biological functions within organisms, including catalyzing reactions, DNA and RNA replication, regulation of biochemical activities, storage and transportation of small molecules, and providing mechanical and structural support. Proteins consist of a linear chain of amino acids formed from the translation of mRNA to a polypeptide sequence. These polypeptides undergo post-translation modifications to alter their physical and chemical properties, ensuring they are able to fold into their final active and functional protein.[26–28] Because proteins have a wide range of functions within an organism, altering their expression and distribution can lead to many diseases; this results in many proteins being biomarkers.

1.1.4 Detection of Nucleic Acids and Proteins

Detection of biomarkers is important for disease detection, diagnosis, and prognosis. These molecules are important for the normal functioning of cells and organisms, but even slight changes in their expression and distribution can lead to problems. Thus, early and accurate detection of fluctuations in their levels can lead to a better prognosis for patients.

Even though there are many clinical assays for overexpression of DNA, RNA, and proteins, there is always a need for more sensitive and accurate assays for these biomolecules. There have been many advances in the development of analytical techniques for detection of these molecules, such as amplification and non-amplification techniques, those that require enzymes and those that don't, as well as assays that require antibody molecules for target recognition. Many of these techniques have been reviewed extensively,[29–31] and selected techniques are summarized below.

1.1.4.1 Non-Amplification Techniques

Detection of biomolecules requires high specificity and sensitivity. Complex matrices make this a difficult task, but many techniques have been developed and implemented in clinical labs. The most common assay used clinically is **e**nzyme-**l**inked **i**mmuno**s**orbent **a**ssay (ELISA), which uses antibodies to detect the presence of an antigen in a liquid sample.[32,33] There are three types of ELISA assays: direct, sandwich, and competitive. In direct ELISA, a test solution is added to a plate and an enzyme-labeled primary antibody is added, which binds specifically to the target. After a washing step, detection occurs with the addition of the enzyme substrate, and a colour change or fluorescence occurs.[32,34] In sandwich ELISA, a surface is coated with an antibody, and the sample solution is applied to the surface. The antibody captures antigens present, and a washing step removes unbound antigens. Next, a specific primary antibody is introduced and binds to the antigen, forming a "sandwich", and any unbound antigens and unbound antibodies are washed away. Then, an enzyme-labeled secondary antibody directed against the primary antibody is added, unbound antibodies are washed away, and the enzyme substrate is added. Detection then occurs with a solution colour change or with fluorescence detection.[35] Lastly, in competitive ELISA, unlabeled primary antibodies and sample are incubated and then added to an antigen-coated well. Next, a washing step removes unbound antibodies that have already bound antigens from the sample. Then, a labeled secondary antibody against the primary antibody is added, and after a washing step, the enzyme substrate is added and fluorescence or colour change occurs.[35] Thus, if an antigen is present in the sample the detection signal is lower. ELISA is a powerful technique due to the specificity of the antibody-antigen interactions. However,

the process is laborious and involves many washing steps. Another technique that can be used is mass spectrometry, which is able to detect biomolecules accurately based on their mass-to-charge ratio.[36,37] This technique, however, requires specific sample preparation, typically requiring a separation step and expensive instrumentation.

Molecular **b**eacons (MBs) are simple oligonucleotide probes that are able to detect the presence of specific nucleic acid sequences in a homogeneous solution. MBs have a stem-loop structure functionalized with a fluorophore on one end and a quencher on the other.[38–40] In the closed stem-loop structure, florescence is quenched due to the efficient energy transfer from the fluorophore to the quencher that are in close proximity. In the presence of a target, which is complementary to the loop, hybridization occurs, disrupting the stem-loop structure. The quencher and fluorophore are no longer in close proximity; this allows fluorescence to be restored, and detection can occur. **M**olecular **a**ptamer **b**eacons (MABs) utilize the specific binding capabilities of aptamers (further discussed in section 1.3) with the signal detection of molecular beacons for specific biomolecules.[41] When an MAB binds to a target, it undergoes a conformational change, increasing the distance between the fluorophore and the quencher, allowing for fluorescence detection.[42–44] Figure 1.1 shows specific design examples for these MABs. Figure 1.1 (A) shows the binding of a target to two oligonucleotides from a split aptamer, allowing the hairpin to open and fluorescence to occur.[45] Figure 1.1 (B) shows the aptamer bound into a hairpin, which is allowed to open in the presence of a target.[46,47] Finally, Figure 1.1 (C) shows fluorescence quenching in the presence of a target molecule.[48]

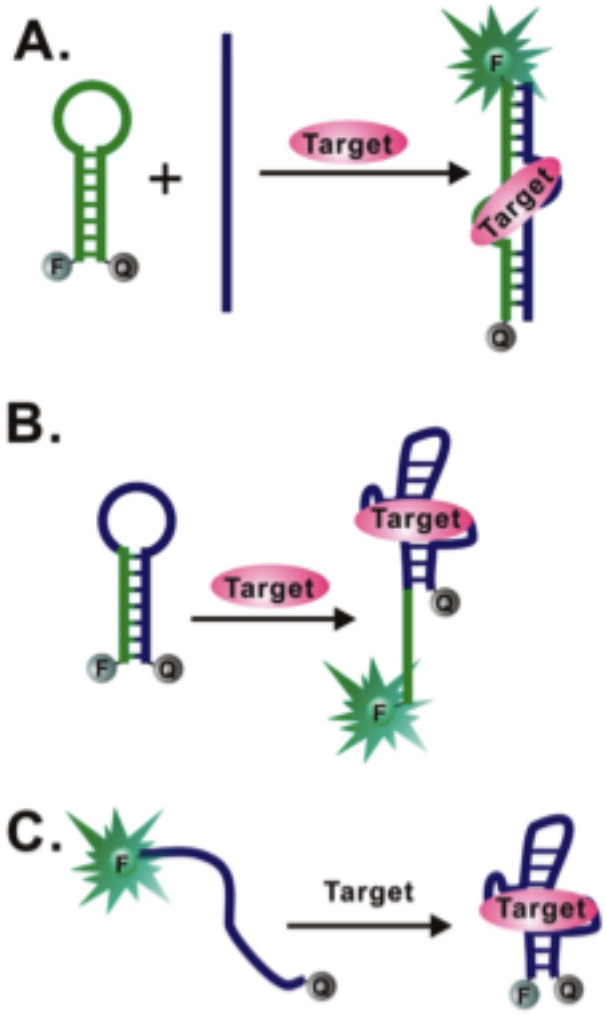

Figure 1.1 Examples of molecular aptamer beacons (MABs). (A) Binding of a target to two oligonucleotides from a split aptamer, allowing the hairpin to open and fluorescence to occur.[45] (B) Aptamer bound into a hairpin, which is allowed to open in the presence of a target.[46,47] (C) Fluorescence quenching in the presence of a target molecule.[48] Reprinted and modified with permission.[29] Copyright 2013 American Chemical Society.

1.1.4.2 Homogeneous Amplification Techniques

To detect many biomolecules, the signal must be amplified as the targets are generally in very low concentration. There are many techniques to achieve this, but the most clinically relevant and highly used technique is **p**olymerase **c**hain **r**eaction (PCR). PCR is a temperature cycled DNA amplification technique that uses a DNA template, DNA polymerase, free nucleotides, and two DNA primers. Typically, PCR goes through 20−40 cycles through initialization, denaturation, annealing, and elongation steps, resulting in 2^n copies of DNA formed, where n is the number of cycles.[49]

Like PCR, **r**olling **c**ircle **a**mplification (RCA) uses polymerase to add nucleotides continually to an annealed primer, but RCA is an isothermal DNA amplification technique for circular DNA. The result of this amplification is a long, ssDNA strand of multiple tandem repeats.[50] This can be detected using molecular beacons[51,52] and intercalating dyes.[50,53]

Hybridization **c**hain **r**eaction (HCR) is an isothermal, room temperature DNA amplification technique, in which monomers assemble in the presence of a target DNA strand. In a simple example, two DNA hairpins in solution interact in the presence of an initiator target, triggering a cascade of hybridization events, which results in alternating copolymers of nicked double helices that can be detected by gel electrophoresis or fluorescence.[54]

Proximity **l**igation **a**ssay (PLA) is a protein detection technique that uses antibody antigen interactions to allow for high specificity and sensitivity. Two primary antibodies interact with the protein of interest. Then, secondary antibodies with DNA sequences

functionalized to them are directed against the primary antibodies. When the DNA sequences are brought into close proximity due to interaction with the target complex, the DNA strands participate in RCA or other amplification detection techniques.[55] This technique converts macromolecule detection to an easily amplifiable DNA motif.[56]

1.2 Principles of Binding Induced DNA Assembly

DNA self-assembly is a common strategy for generating nanostructures where components for structures assemble due to non-covalent interactions. Advantage can be taken of the specificity of DNA base pairing to construct complex nanostructures. **B**inding **In**duced **D**NA **A**ssembly (BINDA) utilizes the binding of two affinity ligands to a single target molecule.[30,57–60] The guiding principle of BINDA is that nonspecific interaction of DNA sequences can be eliminated. This can be achieved by knowing that the DNA self-assembly is dependent on the stability of the complementary sequences, which are influenced by the complementary DNA concentration, length of complementary region, GC content, and use of blocking DNA. Figure 1.2 shows BINDA probes with blocking strands binding to the same target molecule, allowing complementary sequences to be in close proximity and hybridization can occur.

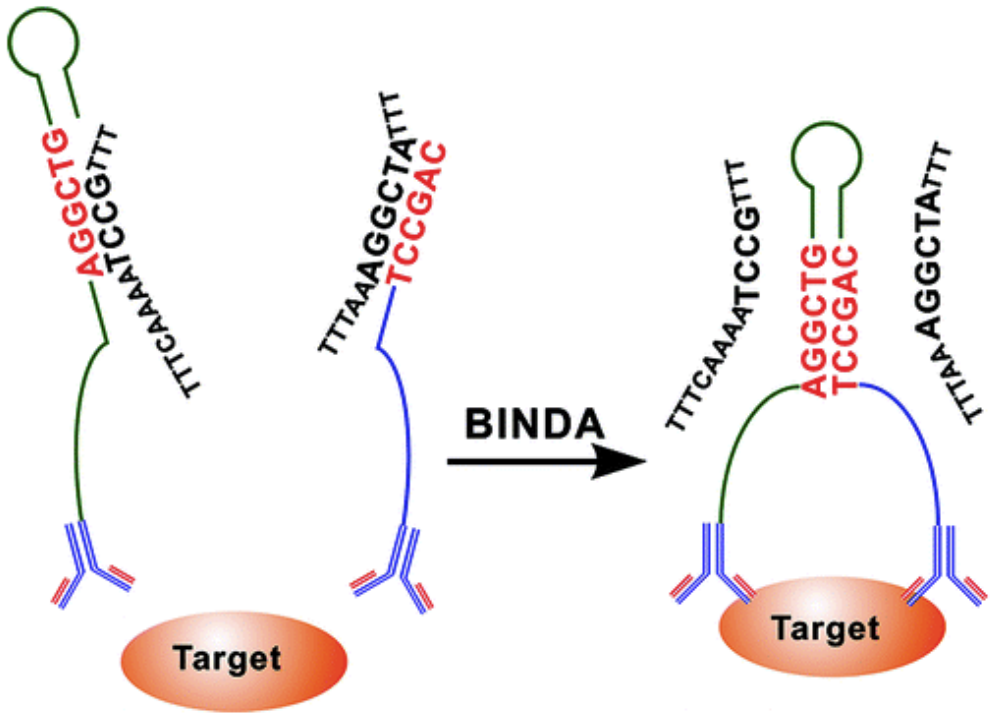

Figure 1.2 Binding Induced DNA Assembly (BINDA) with blocking DNA strands. Reprinted with permission.[57] Copyright 2012 American Chemical Society.

In BINDA, affinity ligands are functionalized with short, complementary DNA sequences so that the binding of the two ligands to the target molecule brings the sequences into close proximity, and hybridization is favorable. The affinity ligands used for BINDA can be antibodies or aptamers, but they must be able to bind to the same target molecule. In terms of experimental design, the length of complementarity and GC content is easy to achieve as the sequences are custom designed and synthesized. For BINDA, the concentration of complementary DNA is drastically increased in a local environment when the two affinity ligands are able to bind to a single target molecule.

This binding increases the melting temperature of the complementary DNA sequences, which mimics the formation of a DNA hairpin. Essentially, the interaction converts from an intermolecular interaction to mimicking an intramolecular interaction. The melting temperature of the two sequences unbound and bound to the target molecule can be estimated using the Integrated DNA Technology's OligoAnalyzer program. For example, a 6 nucleotide long sequence (50% GC content, 10 mM Na^+ and 1 mM Mg^{2+}) does not form a stable duplex in solution (T_m= 0°C), but by mimicking a hairpin the melting temperature is increased to around 44°C, shown in Figure 1.3.

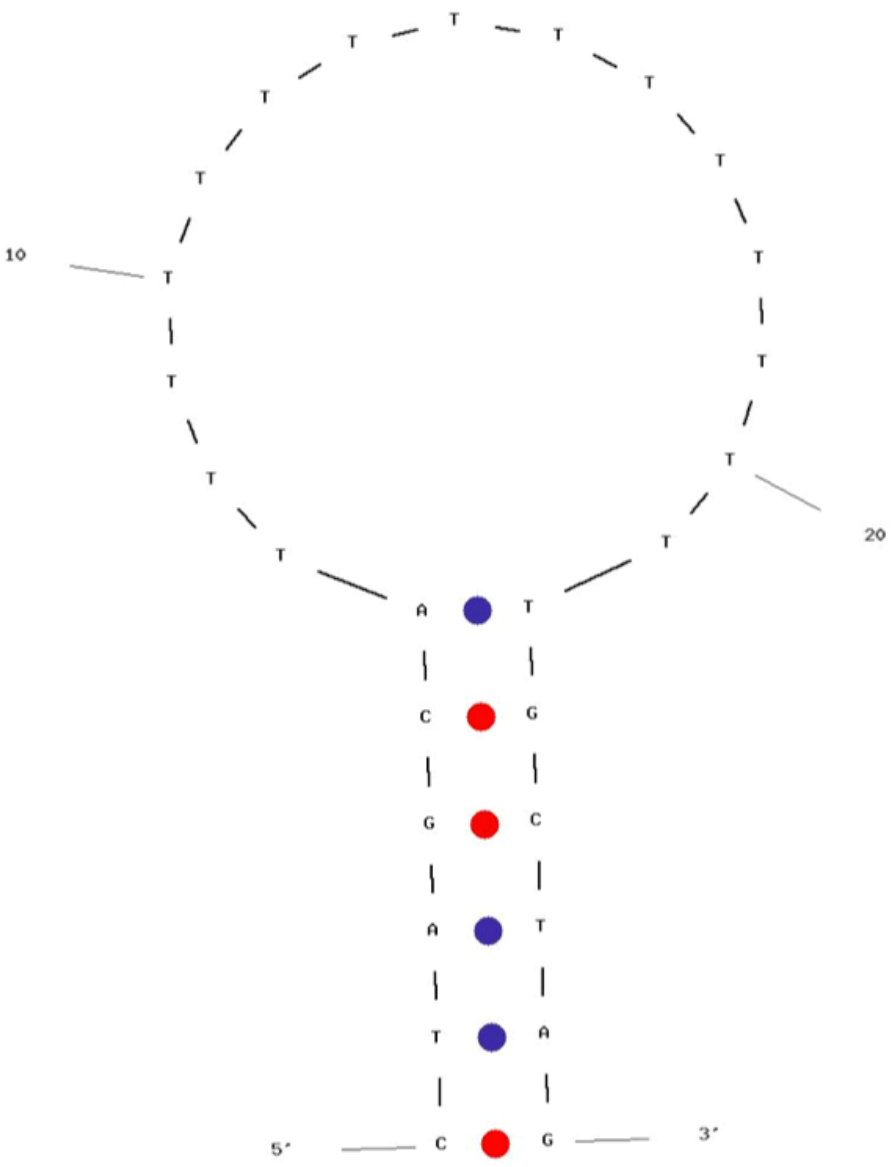

Figure 1.3 Use of IDT OligoAnalyzer software to mimic the hairpin formed when BINDA probes are in close proximity.

BINDA has many advantages for biological assays. First, BINDA is highly specific as it requires the binding of two different affinity ligands to a single target molecule; the probability of this occurring to allow hybridization of complementary sequences is very low. Secondly, this assay is able to occur in a single tube due to its high specificity. The homogeneous assay is able to detect its target without the need for a separation step, like many biological assays, meaning that the assay is technically simple to perform. Thirdly, detection of proteins is easily converted into an amplifiable and detectable DNA assembly. Lastly, a BINDA assay can be amendable to many targets by simply changing the affinity ligand to be specific for the desired target.

1.2.2 BINDA Detection Methods

BINDA inherently has high specificity and sensitivity, but molecules of interest are still in low abundance, so signal amplification is necessary. Commonly, real-time PCR is used for BINDA detection.[57,59] This process is similar to PCR, described in section 1.1.4.2, where there are denaturation, annealing, and elongation steps. But, in real-time PCR, reporter probes are added that are specific for the sequence to be amplified.[61–64] These probes are labeled with a fluorophore on one end and a quencher on the other. During the annealing stage both primers and reporter probes hybridize with the DNA sequence, and the 5′ to 3′ exonuclease activity of the polymerase digests the reporter probe, releasing the fluorophore from the quencher, and fluorescence can be detected. As PCR involves thermocycles, this process is repeated at each cycle, and fluorescence increases as the DNA sequence is amplified. The reporter probes used in real-time PCR allow the detection to be specific for the desired amplified DNA sequence. However, DNA intercalating dyes also can be used as a less expensive option for the quantification

of PCR products during thermocycling. Specifically, SYBR Green intercalating dye binds preferentially to double stranded DNA and has been used for early BINDA detection work.[57,59,65]

Using real-time PCR for BINDA detection improves detection limits, but it requires the use of a thermocycler. For detection without an amplification step, simple fluorescence detection can be used for detection of targets.[58] For fluorescence detection, a fluorescence microplate reader is the most common instrumentation. Microplate readers are an important instrument for time saving, lower cost, and simple procedures compared to other analytical techniques. In a plate reader for fluorescence detection, a light source passes light through the excitation filter, which allows light of a specific wavelength to pass through. This excitation incident light is directed towards the assay well of the microplate, which then emits light. Next, the emitted light is directed towards an emission filter, allowing light of only a specific wavelength to pass towards a photomultiplier, which increases the signal before going to the computer software. Many microplate readers are "multi-mode", meaning that they have the ability to detect not only fluorescence but also absorbance.

1.3 Aptamers

Aptamers are short DNA or RNA molecules that are selected to bind to a target molecule with high specificity and affinity.[66–68] Aptamers are selected for in vitro and are useful in many biotechnological applications and increasingly in therapeutic and

clinical settings.[69,70] Similar to antibodies, aptamers bind to specific epitopes on the target molecule with dissociation constants in the pico- to nano-molar range.[71]

Aptamers have many advantages compared to antibodies for biological research. Firstly, aptamers can be generated for any protein or small molecule target through the selection process described in Section 1.3.1.[72] This process is performed in vitro and does not require cell lines for producing more aptamers. Secondly, this selection process can be optimized under many different conditions, including higher temperatures, varying salt concentrations, and different buffers.[73] These conditions can be manipulated, resulting in aptamers with properties optimal for the designed analysis. Antibody selection only occurs under biological conditions, meaning that antibody−ligand binding is optimal under these same conditions. Thirdly, aptamers can be synthesized easily once the sequence is known, including reporter or attachment molecules at precise locations.[73] This synthesis process is rapid and costs much less than monoclonal antibodies, if they are even available for the target of interest. Lastly, aptamers are much more stable than antibodies. Performing an assay with aptamers can be optimized under many conditions, but with antibodies, conditions are much more limited. Also, oligonucleotide aptamers have a much longer shelf life than antibodies.[73] Antibodies do have the potential to be more specific for a target than aptamers as antibodies are made of amino acids, of which there are 20 naturally occurring, while aptamers are made of 5 nucleotides.

1.3.1 Selection of Aptamers

Aptamers are selected through a process called **S**ystematic **E**volution of **L**igands by **Ex**ponential Enrichment (SELEX).[72] The SELEX method has four steps: library

generation, partition, elution, and amplification. This process starts with a large library of random single stranded sequences of fixed length with consistent 5′ and 3′ primer binding ends. The library is exposed to the target molecule and the unbound sequences are removed. Next, the bound sequences are eluted and amplified via PCR for subsequent selection rounds. This process continues with increasingly stringent binding conditions, and then the tightest binding sequences can be obtained. Because these libraries have common primer regions, these portions of the sequence can be removed for further analysis of specificity.

1.4 Fluorescence Resonance Energy Transfer

Fluorescence **r**esonance **e**nergy **t**ransfer (FRET) is a mechanism that describes energy transfer between an excited donor molecule and an acceptor molecule without photon emission through non-radiative dipole-dipole coupling. When incident light excites the donor molecule, energy is emitted by the donor and is absorbed instantly by the acceptor molecule.[74,75]

1.4.1 FRET Theoretical Parameters

The FRET process can occur only if the donor and acceptor are in close proximity. This energy transfer process is explained by the Jablonski diagram (Figure 1.4), which shows the electronic states of a molecule and the transitions between the donor and acceptor molecule.[75,76] When incident light excites the donor molecule, its electrons jump from the ground state (S_0) to an excited state (S_1, S_2, S_3, etc.). Under typical fluorescence conditions, relaxation of these excited electrons to the lowest excited state (S_1) and the

further relaxation to the ground state (S_0) results in the emission of a photon as fluorescence. In the proximity of an acceptor molecule, the donor energy is transferred to the acceptor, which excites its electrons from S_0 to an excited state (S_1, S_2, S_3, etc.).

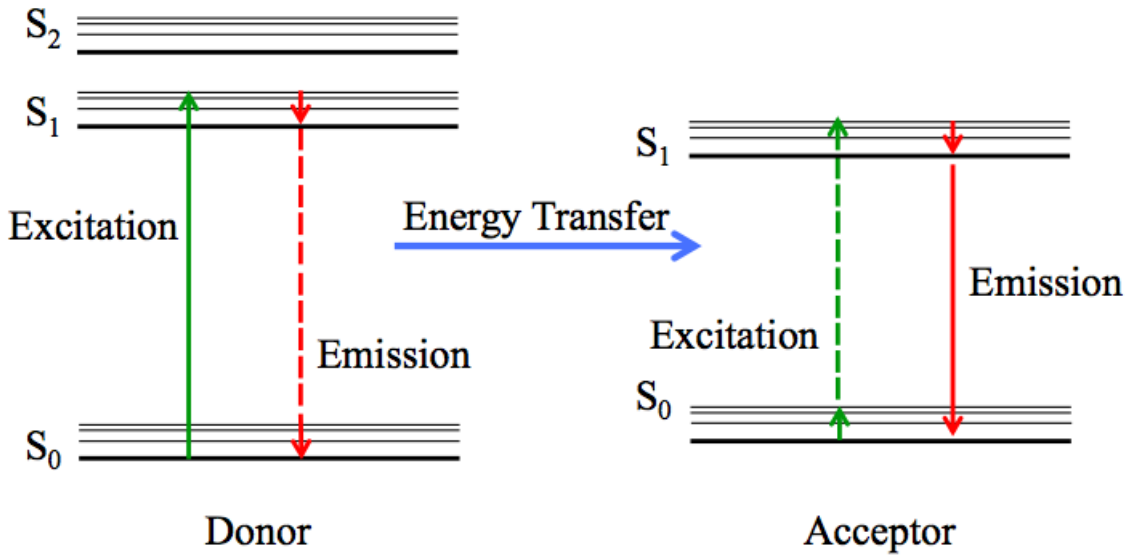

These excited electrons eventually relax to the ground state (S_0), resulting in the emission of a photon of light. This process is summarized in Figure 1.4. The wavelength of light emitted is longer and has less energy than the original exciting wavelength.

Figure 1.4 Jablonski diagram showing the excitation of the FRET donor with donor emission energy transfer to excite acceptor, with detectable emission.

The FRET efficiency (E) is defined as the quantum yield of the energy transfer, or the amount of energy transferred to the acceptor for every donor excitation event. This efficiency depends on physical parameters, specifically the distance between the

donor and acceptor (usually 1−10 nm) and the spectral overlap of the donor emission with the acceptor absorption.

The rate of energy transfer, $k_T(r)$, is given by:

$$k_T(r) = \frac{1}{\tau_D} \left(\frac{R_0}{r}\right)^6 \quad \text{(Eq. 1-1)}$$

where r is the distance between the donor (D) and the acceptor (A), R_0 is the Förster distance, and τ_D is the emission lifetime of the donor without an energy transfer process. When the Förster distance (R_0) is equal to the D to A distance (r), the rate of transfer is equal to the rate of decay of the donor ($1/\tau_D$).[75]

The Förster distance (R_0) is the distance at which energy transfer is 50% efficient and is given by:[74]

$$R_0^6 = \frac{9000 \ln 10}{128 \pi^5 N_A} \frac{\kappa^2 Q_D}{n^4} J \quad \text{(Eq. 1-2)}$$

where Q_D is the quantum yield of the donor in the absence of acceptor, n is the refractive index (1.4 for biomolecules in aqueous solution), N_A is Avagadro's number, J is the degree of overlap between the donor emission spectrum and the acceptor absorption spectrum, and κ^2 is a term that describes the relative orientation between the donor and acceptor and is assumed to be equal to 2/3 due to fast isotropic motion of donor and acceptor entities.

The overall efficiency of the energy transfer in a single donor-acceptor pair as a function of the distance, *r*, is:

$$E = \frac{R_0^6}{(R_0^6 + r^6)} \quad \text{(Eq. 1-3)}$$

Therefore, the amount of energy transferred is dependent on the distance (*r*) between the donor and acceptor.[75]

1.4.2 Choice of Donor-Acceptor Pairs

The choice of donor-acceptor pairs in FRET is extremely important. The most important aspect of this pair is that the emission spectrum of the donor molecule overlaps with the excitation spectrum of the acceptor molecule, the overlap integral *J* in Equation 1-2.[75] This will ensure that energy is transferred efficiently from the donor fluorophore to the acceptor fluorophore with minimal photon emission of the donor. This will minimize background fluorescence, making the **l**imit **o**f **d**etection (LOD) lower. Another important aspect of choosing a donor-acceptor pair is ensuring that the apex of the absorption and emission spectra of both the donor and acceptor are wide enough for appropriate filters to be used in the fluorescence instrument.[75] This difference is called the Stokes Shift. Similarly, it is optimal for the emission of the donor molecule to have a much lower wavelength than the emission of the acceptor molecule. This will ensure that the fluorescence emission detected at the longer wavelength is due exclusively to the emission of the acceptor molecule and not from the donor. The larger the difference in wavelength, the more likely the emission is due to the acceptor molecule. It is also important that the donor-acceptor pair chosen is suitable for the environment that the analysis will be done in. For example, if the analysis will be done with a biological

sample or for the end goal of a biological sample, it is important to choose a pair that is compatible with a physiological environment. Figure 1.5 shows the absorbance and emission spectra of a quantum dot donor and a dye acceptor. In this example, the donor emission spectrum (purple trace) overlaps the excitation spectrum of the acceptor (green trace), allowing for a large wavelength difference between the quantum dot donor excitation (blue trace) the emission of the acceptor (red trace). The use of quantum dots as FRET donors in bioprobes has been extensively reviewed for the detection of many biological molecules.[77,78]

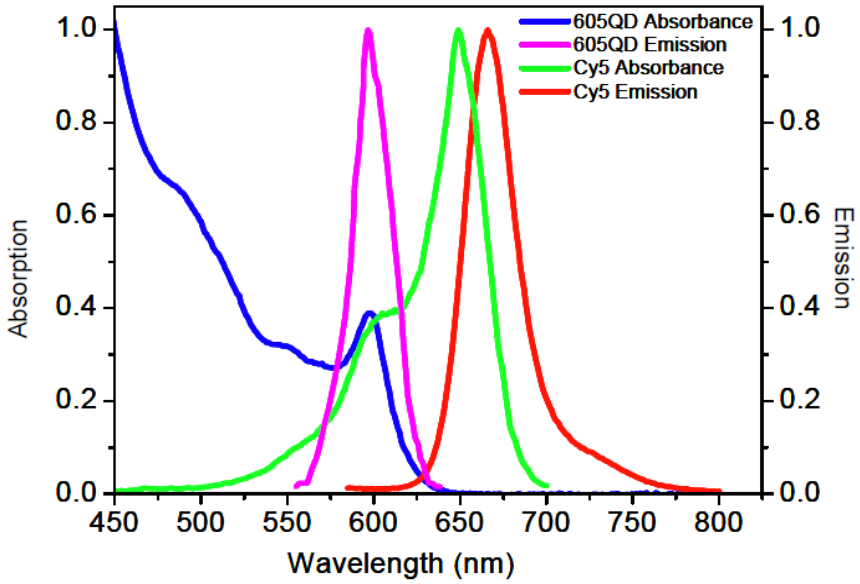

Figure 1.5 Absorption and emission spectra of a quantum dot donor with Cy5 dye acceptor for FRET. Reprinted with permission.[79] Copyright 2005 Nature.

1.4.3 Coupling with BINDA

Coupling of FRET detection with BINDA is a logical progression: FRET cannot occur unless the donor and acceptor are in close proximity. The intrinsic property of proximity hybridization in BINDA establishes the close distance required for FRET to occur. Without both probes binding to the same target, the distance between the FRET donor and acceptor is too great, and FRET cannot occur. This pairing also helps in maintaining a low background signal. The complementary region between the FRET donor and acceptor is too short to be stable in bulk solution, therefore, the hybridization won't allow the close interaction to occur. Also, because two binding events need to occur on the same target molecule, the likelihood of target non-specific interaction is very low, thus, the background is also low.

1.5 Nanomaterials

Nanomaterials are materials in which a single unit is between 1 and 1000 nm in at least one dimension. However, typically, nanomaterials are usually described as materials on the nanoscale, between 1 and 100 nm.[80,81] Nanoparticles, in particular, have great scientific interest as they are a bridge between atomic or molecular structures and bulk materials. Nanoparticles have many unique properties due to the high surface area to volume ratio as the particles get smaller.[82] Importantly, nanoparticles can be functionalized with organic molecules or polymers to change their physical and chemical properties, such as stability, solubility, and their ability to target.[83] This is especially important in biological applications when using nanomaterials for disease diagnosis, cell imaging, and targeted drug delivery.

1.5.1 Quantum Dots

Quantum **d**ots (QDs) are inorganic, semiconductor nanocrystals with sizes ranging from 1 to 20 nm.[84] QDs have many unique photophysical properties: broad absorption/excitation spectrum ranging from visible to UV spectrum, narrow emission spectrum (typically ranging 25-35 nm, full width at half maximum) that is size controlled, high fluorescent quantum yield, and strong stability against photo-bleaching.[85] Both the absorption and emission spectra are scalable with the size of the QD; this means that changing the diameter of the particle will shift the spectra.[85,86] This makes QDs ideal candidates for FRET donors due to their tunable sizing and the selection of a donor-acceptor pair. For example, changing the diameter of a CdSe QD from 20 to 2 nm shifts the emission spectrum from red (700−800 nm) to green (550 nm); therefore, smaller QDs emit shorter wavelengths of light (higher E). Also, there are approaches for stable synthesis, resulting in production of uniform QDs with narrow size distribution,[87] as well as methods for modifying these QDs to include surface functional ligands, allowing them to be used in a variety of biosensors for imaging, labeling, and sensing.[88]

The increased use of QDs in fluorescence-based analysis has increased the popularity of CdSe QDs as the QD of choice. These QDs are the typical core-shell QDs, with the core consisting of CdSe and the shell of ZnS. In this configuration, the ZnS shell protects the CdSe core from oxidation and from leaching into the buffer solution. This results in higher stability and an improved quantum yield of the CdSe core.[89] The ZnS shell thickness also can be varied for different purposes: thinner shells (4−6 monolayers) provide increased protection of the CdSe core from extreme buffer

conditions. These CdSe QDs have many advantages, including a single-step synthesis, high water solubility, high fluorescence quantum yield, narrow size distribution, and commercially available with surface modifications.

1.5.2 Gold Nanoparticles

Colloidal gold is a solution of **gold** **n**ano**p**articles (AuNPs) in solution and can exist in many different morphologies, including rods and spheres. These different shapes and sizes exhibit different optical, electronic, and molecular recognition properties.[90–92] Colloidal gold solutions have been used for centuries to stain glass and other artistic works because of the nanoparticle's interactions with light. AuNP solutions range from reds to blues, depending on size, shape, and aggregation state due to **l**ocalized **s**urface **p**lasmon **r**esonance (LSPR),[93,94] where surface electrons oscillate with incident light. In general, smaller particles appear red in solution, and increasing size shifts the colour to blue.[93] There is a similar observation with aggregation: as AuNPs aggregate, a colourmetric change of solution occurs from red to blue.[95] This colourmetric change has been employed for biological assays by functionalizing the AuNP surface with DNA.[96] In the presence of a target, the AuNPs aggregate, and a colourmetric change occurs.

AuNPs functionalized with DNA are increasingly promising candidates for precise, multifunctional materials that integrate nano-assemblies,[97] drug delivery,[98,99] and imaging moieties for sensing.[58,100–104] This is an important aspect of DNA nanomaterials and the development of bioassays. Recent efforts have emphasized the development of preparation methods that are able to control functional groups precisely, allowing for well-defined materials in many applications, including diagnostic, imaging, and drug delivery.[105,106] In aims to be clinically relevant, assays and therapeutic agents

utilizing DNA functionalized AuNPs must be fully characterized and have the ability to be quantitative, not just qualitative. Thus, in characterizing the surface coverage of DNA functionalized onto an AuNP surface, it is important to understand the DNA and nanoparticle interactions and to optimize the sensitivity, stability, and efficiency of nanoparticle-based sensors and therapeutic carriers.

1.6 DNA Technology

Watson−Crick base pairing is understood and extremely predictable,[1] making its specificity a powerful and versatile tool for constructing diverse structures and devices on the nanoscale. Specifically, DNA nanotechnology utilizes complementary DNA strands to hybridize and manipulate their shapes in static structural or dynamic ways.[107] Structural DNA nanotechnology can construct two- and three-dimensional objects of varying complexities in a bottom-up DNA self-assembly to form well-defined structures. Dynamic DNA nanotechnology utilizes DNA thermodynamics to reconfigure nanostructures mechanistically. Both static and dynamic DNA nanotechnology play an important role for development of relevant analytical assays, especially for the detection of disease biomarkers.

1.6.1 Static DNA Nanotechnology

Static DNA nanotechnology involves the formation of DNA complexes, such as two- and three-dimensional DNA helices. These formed materials generally are used in structural DNA nanotechnology and, based on well-established Watson−Crick base pairing, can form predictable and well-defined geometries. These robustly formed

double helices can be characterized easily many ways, most simply using DNA intercalating dyes specific for double stranded DNA, such as ethidium bromide.[108]

An example of a static DNA structure is the formation of a DNA **three** **w**ay **j**unction (3WJ). A DNA 3WJ is a Y-shaped structure formed by three strands that hybridize with each other.[109] This technique can be target responsive by detecting a target ssDNA where two probes are designed to be partially complementary to the target and partially complementary to each other. The most important aspect of this design is that the length of complementarity between the two probes is short so that stable hybridization does not occur without the presence of the target ssDNA. This idea of target-responsive DNA 3WJ can be applied to not only ssDNA targets but also proteins.[110] Furthermore, these static DNA 3WJ can be used in dynamic DNA nanotechnology, as well as being coupled with BINDA for protein detection (Figure 1.6).[110]

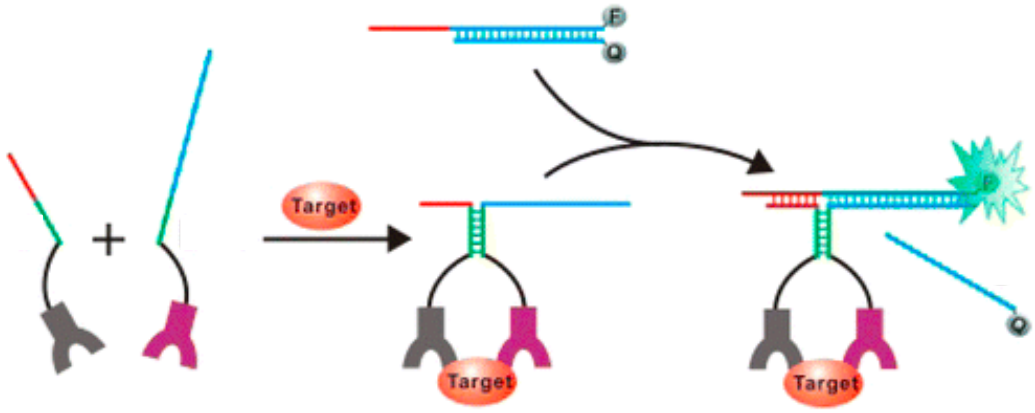

Figure 1.6 Example of BINDA coupled with a DNA 3WJ. The formation of the 3WJ isn't favorable until the BINDA probes bind the target, which then allows for fluorescence detection. Reprinted and modified with permission.[110] Copyright 2013 American Chemical Society.

1.6.2 Dynamic Strand Displacement Reactions

Initially, DNA structures focused on self-assembly as static structures, but recently, focus on dynamic structures has been emphasized. DNA nanotechnology utilizes non-covalent interactions in an aim to design higher ordered assemblies that have new functions. This is the premise of strand displacement, in which none of the covalent bonds of the nucleic acid backbone are modified but the non-covalent interactions between strands are. These DNA strand displacement reactions play a central role in dynamic DNA nanotechnology.[111]

Dynamic DNA nanotechnology often uses toehold-mediated strand displacement reactions for detection or formation of further DNA structures. DNA strand displacement is a process where two strands with partial or full complementarity hybridize in aims to displace another pre-hybridized strand in order to reconfigure these nanostructures. DNA strand displacement reactions are initiated through a short sticky end of DNA, called a toehold. This sticky toehold is typically 5−8 **n**ucleo**t**ides (nt) in length and is complementary to a toehold of a second DNA structure. This second structure has a strand that is completely complementary to the toehold strand, meaning that upon its hybridization, it is more stable than the initial sequence bound to it. In practice, the toehold of the initial strand hybridizes to the toehold of the second DNA structure, and branch migration occurs, "kicking off" a ssDNA sequence that was initially bound to the first toehold. This free ssDNA then can be quantified or further used for subsequent DNA interactions. This process is summarized in Figure 1.7 (A). In this reaction, an increase in the reaction rates can be achieved by increasing the length of the toehold region. This causes the product to be more favored thermodynamically.

Similar to strand displacement reactions, toehold exchange involves the interaction of an initial toehold from a dsDNA with the toehold of another sequence, creating a dsDNA sequence more stable than the initial dsDNA sequence and a ssDNA sequence, which can further proceed to interact in other displacement reactions.[112] This process initially yields two reactive products from two reactive reactants rather than one product in toehold-mediated strand displacement. In these toehold exchange reactions, the invading and the resulting toeholds result in stronger interactions, increasing the rate of the reaction.[112] This is summarized in Figure 1.7 (B).

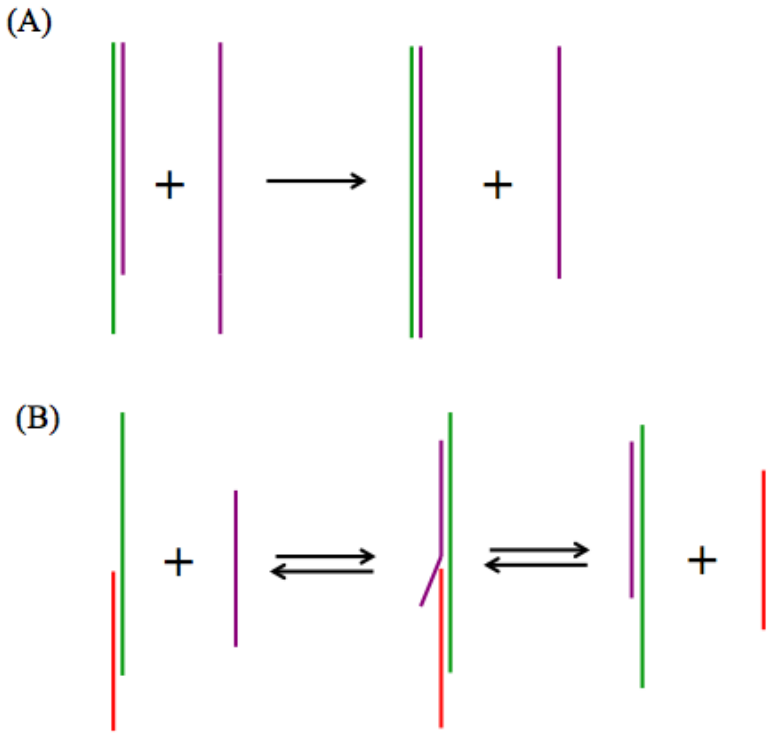

Figure 1.7 Examples of dynamic strand displacement reactions. (A) Strand displacement reaction using a toehold. (B) Toehold exchange reaction where the invading strand has a longer complementary region than the original DNA structure, resulting in a more stable interaction and the release of a DNA strand.

1.7 Thesis Objectives

The combined use of nanomaterials and DNA nanotechnology provides a powerful tool capable of detecting biomoleucles in a variety of environments with high specificity and sensitivity. The initial aim of this thesis was to utilize the properties of nucleic acid functionalized nanoparticles to develop homogeneous assays for the detection of

biomolecules. My initial work was to characterize the surface coverage of AuNPs that are used in therapeutic settings for imaging and drug delivery. After completion of this work, I realized that the quenching abilities of AuNPs were more suited for a "turn-off" assay. I, therefore, focused on the use of QDs as scaffolding and signal transduction during FRET detection of nucleic acids and proteins. By developing a nucleic acid triggered 3WJ assay with QDs as a FRET donor for detection, a sensitive and specific assay can be developed with homogenous detection without the need of an amplification step. This technique is unique in the use of QDs as a scaffold and signal transducer for both the detection of DNA and microRNA. This technique was extended to the detection of a protein target by combining the same FRET detection and DNA assembly with BINDA by using two different aptamers.

This thesis consists of six chapters. **Chapter 1** gives a general overview of the importance of biomolecules and their detection. The chapter focuses on detection techniques and relevant theoretical discussions behind their principles. Also discussed is the importance of nanomaterials and DNA technology in the detection of these biomolecules. **Chapter 2** describes a binding-induced 3WJ technique for a specific DNA sequence using a FRET detection scheme. This Chapter will outline important optimization steps that lead to the development of a linear calibration curve over three orders of magnitude with pM detection limits. Also investigated is detection of the DNA target but with single base mismatches. This research utilizes a QD FRET donor in the presence of a FRET dye acceptor, which has not yet reportedly been used in a binding induced detection scheme. **Chapter 3** builds on the work done in Chapter 2 and demonstrates the detection of a microRNA target using the same 3WJ probes with

FRET detection. microRNA has unique challenges, such as low stability and lower binding affinity with DNA probes. Despite this, a linear calibration curve was constructed over three orders of magnitude with pM detection limits. **Chapter 4** describes the development of a binding-induced assay using two aptamers for the detection of human α-thrombin with FRET detection. This chapter outlines the optimization steps needed to develop a linear calibration curve over three orders of magnitude with pM detection levels. **Chapter 5** describes the characterization of surface coverage of gold nanoparticles using DNA strand displacement reactions. This technique was able to quantify singly functional nanoparticles with comparable results to conventional methods and was able to characterize multiplexed nanoparticles, which cannot be done using conventional methods. **Chapter 6** summarizes the conclusions from all research chapters and discusses the implications from these findings, as well as future directions for the research.

Chapter 2: Development of a Binding-Induced Three-Way Junction Fluorescence Energy Transfer Method for the Detection of a DNA Target

2.1 Introduction

DNA carries the genetic code for growth, development, and functioning in all biological systems. The specific sequences in the DNA structure are unique to every living organism and can be targets for the identification and diagnosis of many diseases. With advancements in sequencing capabilities, the DNA sequences of the whole human genome,[113,114] as well as many organisms, is now available and can allow for early and accurate detection of DNA as a biomarker.[115] **S**ingle **n**ucleotide **p**olymorphisms (SNPs) are a single point mutation that occurs at a specific position in the genome with a small, but regular frequency within the population(>1%). If this variation falls within the coding region of a gene, it can lead to nonfunctional proteins and potentially many types of diseases.[116] Knowing the location of common mutations is important from an assay development standpoint as probes can be designed to test for these mismatches at a genetic level rapidly and specifically.

DNA-3D structures are used as tools for the detection of many specific DNA sequences. Particularly, DNA 3WJs utilize well-established Watson−Crick base pairing to construct DNA assemblies.[117–123] Specifically, target responsive 3WJs have been used for molecular detection, sensing, and imaging.[124–128] These techniques use dye detection, atomic force microscopy imaging, and crystal growing for imaging, which are all non-specific techniques. By utilizing known base-pairing and QDs as a scaffold and donor

for FRET detection, detection can be simple, sensitive, and specific for a target sequence.

The objective of this chapter is to optimize and demonstrate the ability of a DNA 3WJ structure, in combination with QD, to detect a specific DNA target sequence. This FRET assay is used also to investigate mismatch detection in the target DNA sequence. This technique utilizes FRET detection that can only occur when all components of the 3WJ are together to form the 3WJ.

2.1.1 Principle of the Binding-Induced 3WJ FRET Assay

Figure 2.1 shows the detection scheme for the DNA target. In this assay, QD probes are prepared by functionalizing them with a sequence (**QD5**) containing two domains, **c** (blue) and **a*** (purple). These are mixed with a dye sequence (**DS**), which is functionalized with a dye and also has two domains, **c*** (blue) and **b*** (green). When in the presence of a DNA target, the **a*** domain of the QD hybridizes with the **a** domain of the target, and the **b*** domain of DS hybridizes with the **b** domain of the target. This brings **c** and **c*** into close proximity, making hybridization favorable, bringing the dye into close proximity of the QD, and FRET detection can occur. The emission from both QD donor and Cy5 acceptor are detected. If the target DNA is not present, the complementary region of **c** and **c*** is not sufficiently long enough for stable hybridization to occur in bulk solution, and FRET detection cannot occur.

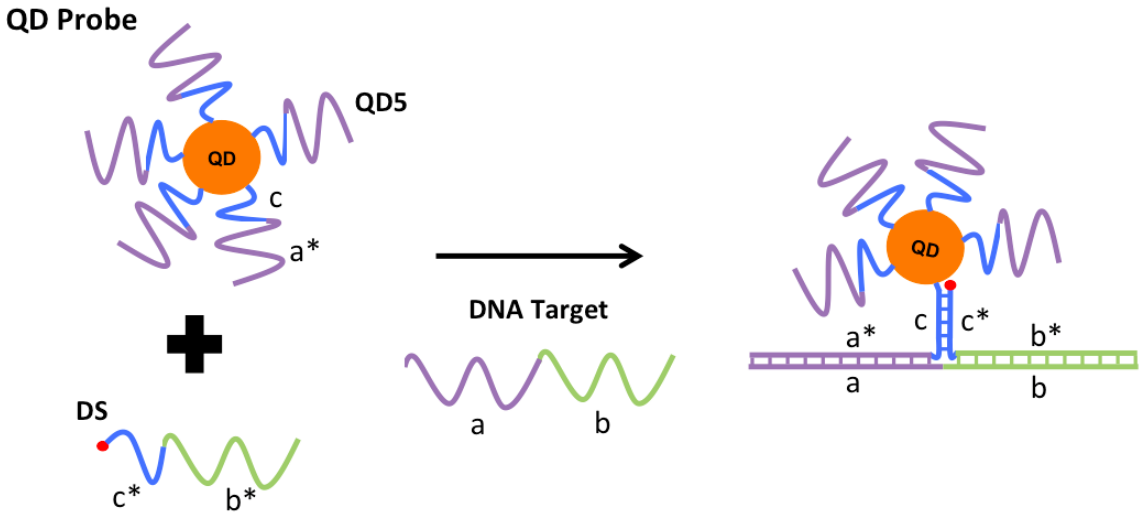

Figure 2.1 Scheme for the detection of a DNA target with a 3WJ. Functionalized quantum dot (QD) probes are mixed with the dye sequence (DS). When in the presence of a DNA target, probes hybridize with the complementary target (**a** with **a*** and **b** with **b***), allowing complementary sequences **c** and **c*** to hybridize, bringing the dye to close proximity of QD, and FRET detection can occur.

2.2 Experimental Methods

2.2.1 Materials and Reagents

The DNA oligonucleotides sequences (Tables 2.1 and 2.2) were custom synthesized, labeled, and HPLC purified by Integrated DNA Technologies (IDT, Coralville, IA). A solution of Qdot^{TM} 605 ITK streptavidin conjugate QDs (2.0 μM) was obtained from ThermoFisher (Eugene, OR). Bovine serum albumin (BSA) was obtained from Sigma-

Aldrich (Oakville, ON). Phosphate buffered saline (1X PBS) (pH 7.4) was obtained from Sigma-Aldrich (Oakville, ON). All other reagents were of analytical grade.

Table 2.1 DNA sequences for three-way junction FRET detection of DNA. The colour codes of the nucleotides (green, blue, purple) match those in Figure 2.1. The same colours indicate complementary sequences.

DNA Name	Sequence
DNA Target	5′- TAG CTT ATC AGA CTG ATG TTG A -3′
QD 5Comp (**QD5**)	5′- Biotin - CGT AG TT CT GAT AAG CTA -3′
QD 6Comp (**QD6**)	5′- Biotin - CGT AGT TT CT GAT AAG CTA -3′
QD 7 Comp (**QD7**)	5′- Biotin - CGT AGT G TT CT GAT AAG CTA -3′
Dye Sequence (**DS**)	5′- TCA ACA TCA GT TT CAC TAC G / T – Cy5 -3′
QD 5Comp 2T (**QD5-2T**)	5′- Biotin - TT CGT AG TT CT GAT AAG CTA -3′
QD 5 Comp 5T (**QD5-5T**)	5′- Biotin – TTT TT CGT AG TT CT GAT AAG CTA -3′
QD 5Comp 10T (**QD5-10T**)	5′- Biotin – TTT TTT TTT T CGT AG TT CT GAT AAG CTA -3′
20Biotin Control (**C**)	5'- Biotin - TT - ATG GCT GTC ACA TAC TTC GC -3'
20Dye Control (**DC**)	5'- GCG AAG TAT GTG ACA GCC AT - Cy5 -3'

Table 2.2 Mismatches in the DNA Target. The site of mismatch is underlined.

Mismatch DNA	Sequence
1.01	5′- AAG CTT ATC AG A CTG ATG TTG A -3′
1.02	5′- TTG CTT ATC AG A CTG ATG TTG A -3′
1.03	5′- TAA CTT ATC AG A CTG ATG TTG A -3′
1.04	5′- TAG ATT ATC AG A CTG ATG TTG A -3′
1.05	5′- TAG CAT ATC AG A CTG ATG TTG A -3′
1.06	5′- TAG CTA ATC AG A CTG ATG TTG A -3′
1.07	5′- TAG CTT TTC AG A CTG ATG TTG A -3′
1.08	5′- TAG CTT AAC AG A CTG ATG TTG A -3′
1.09	5′- TAG CTT ATA AG A CTG ATG TTG A -3′
1.10	5′- TAG CTT ATC TG A CTG ATG TTG A -3′
1.11	5′- TAG CTT ATC AA A CTG ATG TTG A -3′
2.01	5′- TAG CTT ATC AG T CTG ATG TTG A -3′
2.02	5′- TAG CTT ATC AG A ATG ATG TTG A -3′
2.03	5′- TAG CTT ATC AG A CAG ATG TTG A -3′
2.04	5′- TAG CTT ATC AG A CTA ATG TTG A -3′
2.05	5′- TAG CTT ATC AG A CTG TTG TTG A -3′
2.06	5′- TAG CTT ATC AG A CTG AAG TTG A -3′
2.07	5′- TAG CTT ATC AG A CTG ATA TTG A -3′
2.08	5′- TAG CTT ATC AG A CTG ATG ATG A -3′
2.09	5′- TAG CTT ATC AG A CTG ATG TAG A -3′
2.10	5′- TAG CTT ATC AG A CTG ATG TTA A -3′
2.11	5′- TAG CTT ATC AG A CTG ATG TTG T -3′
1.20	5′- TAA GTT ATC AG A CTG ATG TTG A -3′
1.21	5′- TAA CTT ATT AG A CTG ATG TTG A -3′
2.20	5′- TAG CTT ATC AG A CTG ATC ATG A -3′
2.21	5′- TAG CTT ATC AG A TTG ATC TTG A -3′
Double	5′- TAA CTT ATC AG A CTG ATC TTG A -3′

2.2.2 Preparation of QD Probe

QD probes were prepared fresh each day. Probe preparation buffer contains 1X PBS with 0.1% BSA. Biotinylated QD sequence (**QD5**, **QD6, QD7, QD5-2T**, **QD-5T**, or **QD-10T**) was mixed with streptavidin coated QDs in a 15:1 (DNA:QD) ratio, unless otherwise stated. This was allowed to incubate at room temperature for 30 min. The final prepared QD probe concentration was 50 nM and the volume needed for experiments that day.

2.2.3 Development of a Positive Control

Streptavidin coated QDs were functionalized with biotinylated 20 nt long sequences (**C**) by mixing DNA with QDs in a 20:1 (DNA:QD) ratio. In 1X PBS with 0.1% BSA and 1 mM Mg^{2+}, 1 nM functionalized QDs were mixed with varying concentrations of complementary control dye labeled sequence (**DC**) in triplicate. These were left to incubate for 30 min at room temperature, and then transferred to a 96 well plate for fluorescence detection.

During all subsequent experiments, a positive control was run with **C** functionalized QDs (20:1 ratio) (final concentration 1 nM) to detect 5 nM **DC** to ensure experiments are running as expected.

2.2.4 Fluorescence Detection of a DNA target

A mix of QD probe and dye sequence were prepared in 1X PBS with 0.1% BSA and 1 mM Mg^{2+} for final detection concentrations of 1 nM QD probe and 45 nM **DS**, unless otherwise specified. This master mix was added to all triplicate samples and blank (without DNA target) solutions to a final volume of 100 μL. Samples were left to

incubate for 30 min at room temperature, and then transferred to a 96 well plate for fluorescence detection.

Fluorescence signal was detected with a multi-mode microplate reader (DTX 880 Multimode Detector) with excitation at 475 nm and emission at 605 nm for QDs and emission at 680 nm for Cy5 fluorescence.

The FRET response (fold change) is defined as:

$$\text{FRET Fold Change} = \frac{\left(\frac{S_{680}}{S_{605}} - \frac{B_{680}}{B_{605}}\right)}{\frac{B_{680}}{B_{605}}} \quad \text{(Eq. 2-1)}$$

where S_{680} and B_{680} are the fluorescence emission intensities at 680 nm in the presence and absence of target, respectively; and S_{605} and B_{605} are the fluorescence emission intensities at 605 nm in the presence and absence of target, respectively. Fluorescence emission for the Cy5 dye at 680 nm is due to energy transfer occurring because of FRET, meaning that the dye and the QD are in close proximity. Due to the short length of the complementary region, this only occurs when both the QD probe and dye probe bind to the protein target. Fluorescence emission at 605 nm is due to the QD emission.

2.2.5 Optimization of Assay Parameters for DNA Target Detection

Assay parameters were optimized to achieve high signal to noise ratios to improve detection limits. QD probes were prepared fresh each day for optimization of the following: length of complementary region **c** and **c***, QD probe preparation, ratio and concentration of the QD probe and the **DS**, and length of spacer on **QD5**. For each optimization step, the target DNA was detected at 2 nM (green hatched) and 5 nM (solid blue) in triplicate, unless otherwise shown. Also detected at each optimization were

blanks (no DNA target, only QD probe, only **DS**) and positive controls (described in section 2.2.3).

2.2.6 Calibration Curve for a DNA Target by 3WJ-FRET Detection

With optimized conditions, a series dilution of the DNA target was detected. All samples were tested in triplicate, 9 sample blanks were tested, and positive control was tested in triplicate. From this data, a calibration curve was created, and standard deviations of the blanks were used to calculate detection limits.

2.2.7 Detection of Mismatches using the 3WJ-FRET Assay

Detection of mismatched sequences (Table 2.2) was conducted under the optimized conditions as was for the generation of the calibration curve. Forced detection of mismatches was attempted by increasing the mismatch sequence concentration 100x to 1 μM (orange hatched) compared to the DNA target at 10 nM (solid blue). Detection of mismatches at 10 nM was used for calculation of discrimination factor compared to the DNA target. The discrimination factor is the ratio of the difference in FRET fold change of the target compared to the mismatch fold change.[129]

2.3 Results and Discussion

2.3.1 Development of a Positive Control

An important aspect in the development of any analytical technique is the ability to trust that the results obtained are the true values. One way to ensure this is to include controls that should have no signal response (negative control) and that always have a strong signal response (positive control). For positive controls for FRET signal response, it is

important to ensure that the dye is always brought to a close proximity with the QD donor. To do this, a biotinylated 20-nucleotide long sequence (**C**) was designed, functionalized to QDs, and mixed with varying amounts of completely complementary dye labeled sequence (**DC**). This design is similar to that of Zhang et al.[79] but without the use of a target DNA. Figure 2.2 shows the increasing FRET fold change response for increasing amounts of **DC**. The final detection concentration of QDs is 1 nM, and each QD is functionalized with 20 **C** sequences; and it can be seen that the calibration curve is no longer linear at the 20 nM **DC** concentration. This is logical as the overall concentration of **C** sequences and **DC** sequences is approximately equal, making the signal become saturated.

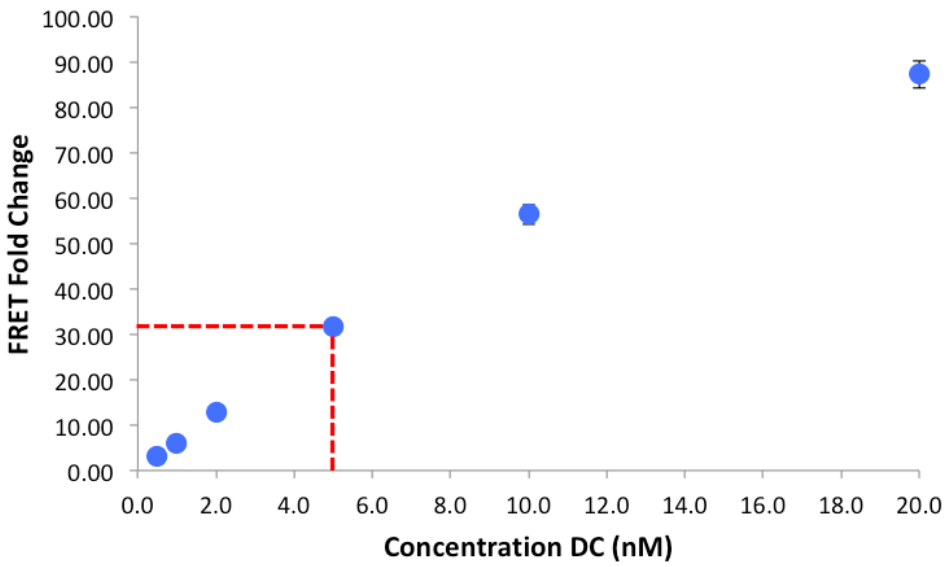

Figure 2.2 Calibration curve for the detection of the dye control (**DC**) as a positive control.

This design accounts for a perfect hybridization situation and shows what the signal should be in ideal circumstances. The signal at 5 nM is well within the linear range of the calibration curve and has a very strong FRET fold change signal around 30. For all subsequent experiments in Chapters 2−4, a positive control detecting 5 nM **DC** with 1 nM QD functionalized with 20 **C** sequences was used.

2.3.2 Optimizing Assay Parameters for Detection of a DNA Target

The first optimized parameter for the FRET BINDA assay is the length of the complementary region **c** and **c***, shown in Figure 2.1. If this length is too long, the **DS** and the QD probe could hybridize nonspecifically, resulting in an increased background signal. As described in Table 2.1, the length of the complementary region is increased by varying the **c** region of the QD sequence (**QD5, QD6, QD7**). Figure 2.3 shows the FRET fold change results as the length of this region is increased. From the figure, **QD5** gave the best fold change response for both concentrations of target sequence tested. This is due to the overall low background signal at 680 nm, suggesting that there is little nonspecific hybridization between the **DS** and the QD probe without target present. As the length of **c** increased (in **QD6** and **QD7**), the background signal at 680 nm increased, resulting in lowered fold change signal for these sequences. This suggests that increasing the complementary length between **c** and **c*** increases the target nonspecific hybridization of probes. Because of this, **QD5** was chosen for further optimization of the assay.

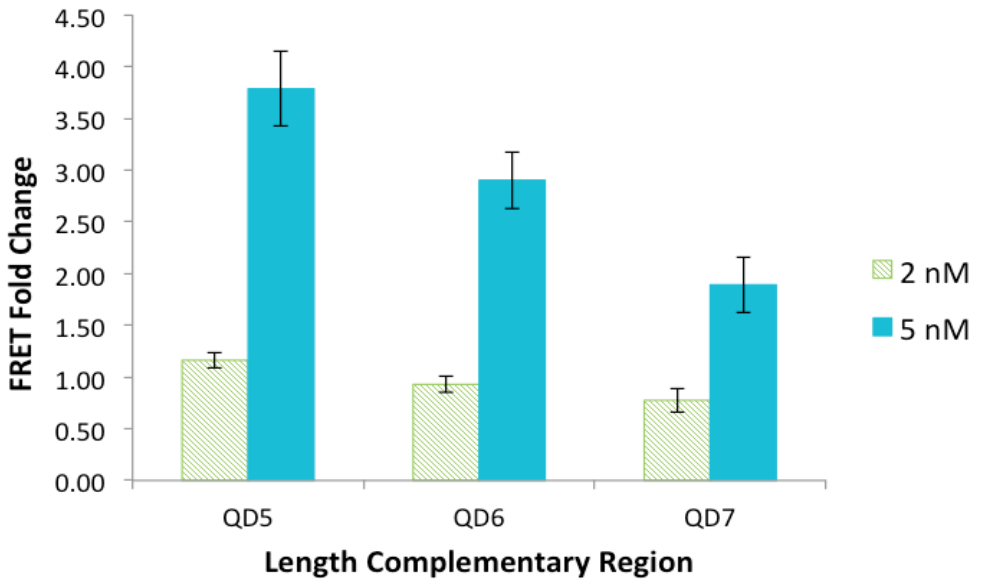

Figure 2.3 Optimization of the length of the complementary region between the QD probe and the DS. The green hatched bars were the results from the detection of 2 nM DNA target; the solid blue bars show results from the detection of 5 nM DNA target.

The preparation of QD probes is important for optimizing the FRET fold change signal. The commercially available QDs are functionalized with multiple molecules, therefore, can be functionalized with multiple **QD5** DNA sequences. Figure 2.4 shows the detection of a target sequence with varying amounts of **QD5** functionalized to QD, with a final detection concentration of 1 nM. It appears that all amounts have the same FRET fold change signal within the error limits. According to the manual for the QDs, each QD is functionalized with 5−10 streptavidin molecules, and as each streptavidin molecule has four biotin binding sites, a maximum of 20−40 **QD5** sequences can be functionalized per QD. This, however, is in an ideal situation where the manufacturer

functionalization of QDs is optimal, and DNA functionalization occurs at 100%. Because of this, QDs functionalized with 15 **QD5** sequences was chosen for subsequent experiments as it allows for a high signal but doesn't allow for excess **QD5** in solution that could bind targets but not be hybridized to the QD probe.

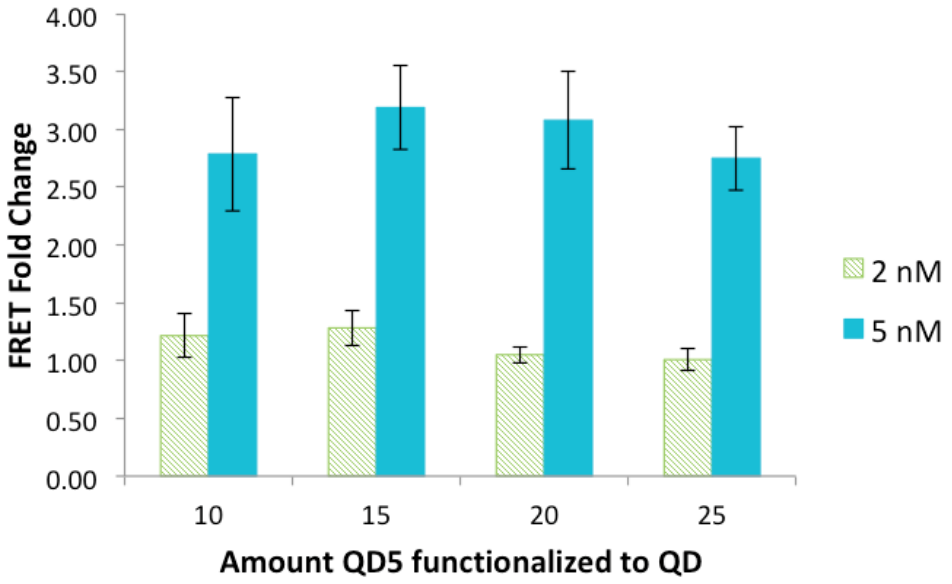

Figure 2.4 Preparation of the QD probe by varying the amount of **QD5** functionalized to the QD.

The ratio and concentration of the **DS** to the QD probes is important in order to ensure that the highest fold change can occur. As each QD is functionalized with 15 **QD5** sequences, each probe has the opportunity to detect up to 15 target sequences. By optimizing the ratio of the **DS** to the QD probe, the highest FRET fold change with the lowest background signal can be determined. Figure 2.5 (A) shows this optimization by varying the amount of **DS** and maintaining the QD probe at 1 nM. It appears that the

signals for 30, 45, 60, and 75 nM of **DS** are all similar. This makes sense as the actual concentration of **QD5** is only 15 nM, and the signal is saturated. To ensure that the **DS** is not the limiting factor in subsequent experiments, a ratio of 1:45 (QD probe:**DS**) was chosen as it maintains the **DS** in a 3x excess of the QD probe but does not have a negative effect by increasing the background signal. Figure 2.5 (B) uses the 1:45 ratio but looks at the effect of varying the probe concentration. It can be seen that decreasing the probe concentration decreases the FRET fold change signal as there are fewer probes in solution. Increasing the probes to above 1 nM QD and 45 nM **DS** increases the background signal at 680 nm, decreasing the overall fold change. Thus, for subsequent experiments, 1 nM QD and 45 nM **DS** was used.

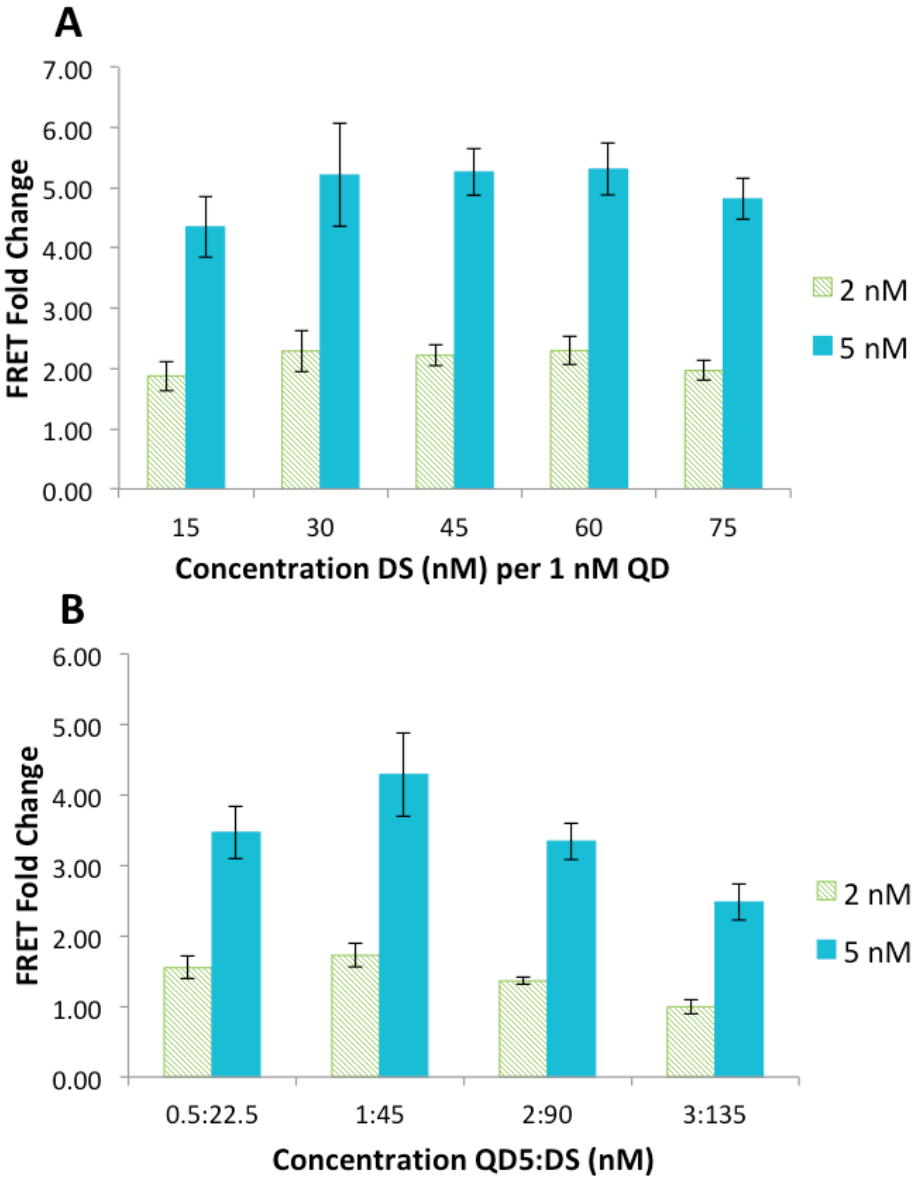

Figure 2.5 Optimization of probe ratio (**A**) and probe concentration (**B**).

The final optimization is done by varying the dye distance from the QD donor for FRET detection. For FRET to occur, the donor (QD) and dye (acceptor) must be within an optimal distance. For this particular system, the Förster distance is 6.94 nm.[79]

For all the **QD5** sequences, the biotin used has an intrinsic 15-atom long tetraethylene glycol spacer, but by adding polyT sequences to the sequence, the distance of the QD donor to the Cy5 acceptor can be tuned and varied. Figure 2.6 shows the effect of increasing this distance. All previous optimization experiments simply used **QD5** functionalized to QDs, however, it appears that the addition of a 2T (**QD5-2T**) spacer gives a stronger FRET fold change. This small increase in distance (~0.64 nm) may give the DS more flexibility to hybridize with **QD5**, allowing for a stronger interaction when both probes are bound to the target sequence. As the polyT spacer is further increased to 5T and 10T, the FRET fold change signal decreases. This suggests that the dye has moved further away from the QD donor and that FRET efficiency decreased as (*r*) from equation 1-3 increased.

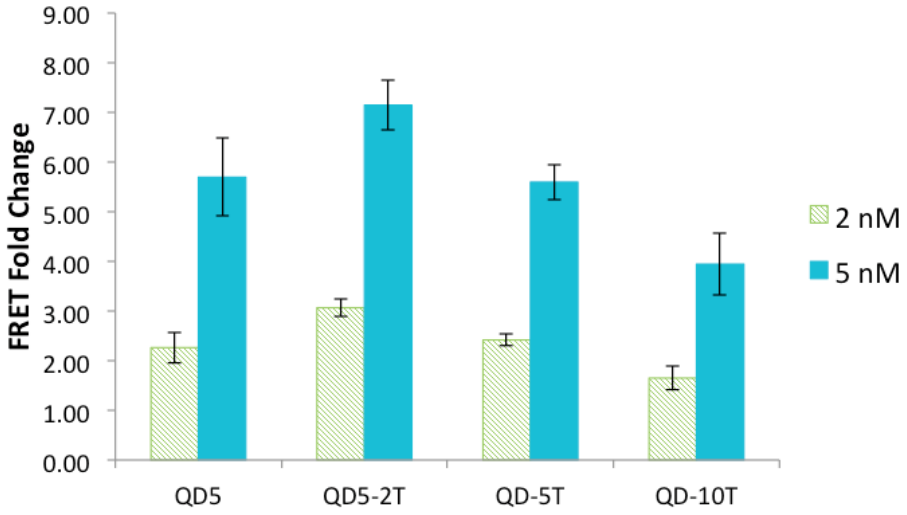

Figure 2.6 Optimization of the dye distance from the QD by varying the length of the T spacer on **QD5** sequence functionalized to the QD.

2.3.3 Calibration Curve for the Detection of the DNA Target Using the Developed 3WJ-FRET Assay

With all optimized conditions, calibration curves were constructed for both **QD5** with no additional spacer (blue diamonds) and **QD5-2T** (orange squares), as seen in Figure 2.7. The **QD5** curve is linear from 0.1−15.0 nM target DNA concentration, but the **QD5-2T** curve is linear only up to 10 nM target DNA concentration. These linear ranges result in the **QD5-2T** curve being slightly more sensitive and to have a much lower y-intercept, suggesting that it could have a lower LOD, but the standard deviation of the blank signal is greater than for **QD5**. In both curves, the 100 pM signal is discernable from the blank, but limits of detection are 164 pM (**QD5**) and 279 pM (**QD5-2T**).

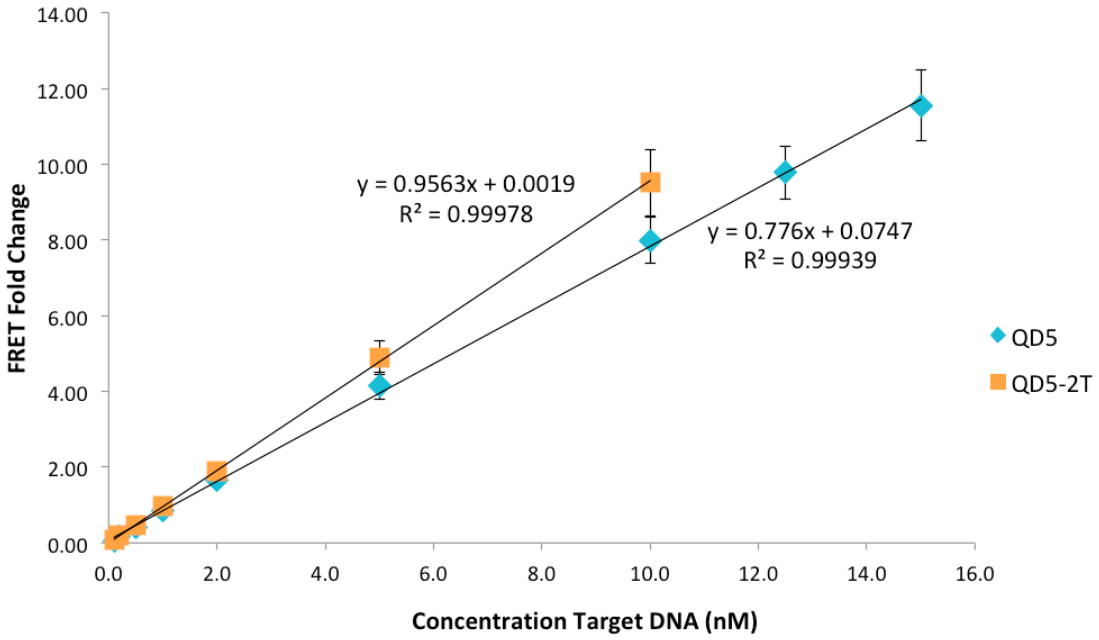

Figure 2.7 Calibration curves for the detection of the target DNA using a 3WJ FRET detection system for no spacer **QD5** (blue diamonds) and spacer **QD5-2T** (orange squares).

Studies have shown that there are approximately 6−7 pg of DNA per cell;[130,131] this is a very small amount. However, when analyzing biological samples, thousands of cells are taken, lysed, and the contents analyzed. This increases DNA concentrations drastically to bring concentrations into the calibration range. From these samples, the DNA can be isolated and concentrated for analysis by the developed method. Other assays have been developed using aptamers and 3WJ strategies for the detection of nucleotide, protein, and small molecules, and the detection limits are in the pM to nM

range.[41] This suggests that this developed assay has potential to be used in real samples for the detection of cellular DNA.

2.3.4 Detection of Mismatches Using the 3WJ-FRET Assay

Detection of single base mismatches is important as these mutations can lead to non-functional proteins and result in many diseases. Specific detection is important as these mismatches can be in low concentration. By using the developed 3WJ FRET method with **QD5**, this research further explored whether mismatches could be detected. Table 2.2 summarizes the mismatch sequences tested compared to the DNA target in Table 2.1. These sequences were designed by changing the base to an A, unless the base was already an A, then it was changed to a T. These sequences were designed to determine where in the probe binding region (**a** and **b**) a mismatch could be detected. If there is a mismatch in **a** or **b**, the QD probe or the **DS** cannot hybridize with the target sequence, and FRET detection cannot occur.

Figure 2.8 shows the detection of mismatch sequences (1 μM) at 100x the concentration of the target sequence (10 nM). This was done as an attempt to force interaction between the probes and the target, even though the stability of that interaction is much lower than the prefect target match. From the Figure, binding of the QD probe in region **a** (mismatches 1.01−1.11) is higher than binding of the **DS** to region **b** (mismatches 2.01−2.11). For both probes, it appears that mismatches near the ends of the regions are more tolerated and still allow the QD probe or the **DS** to bind compared to mismatches in the middle of the binding regions.

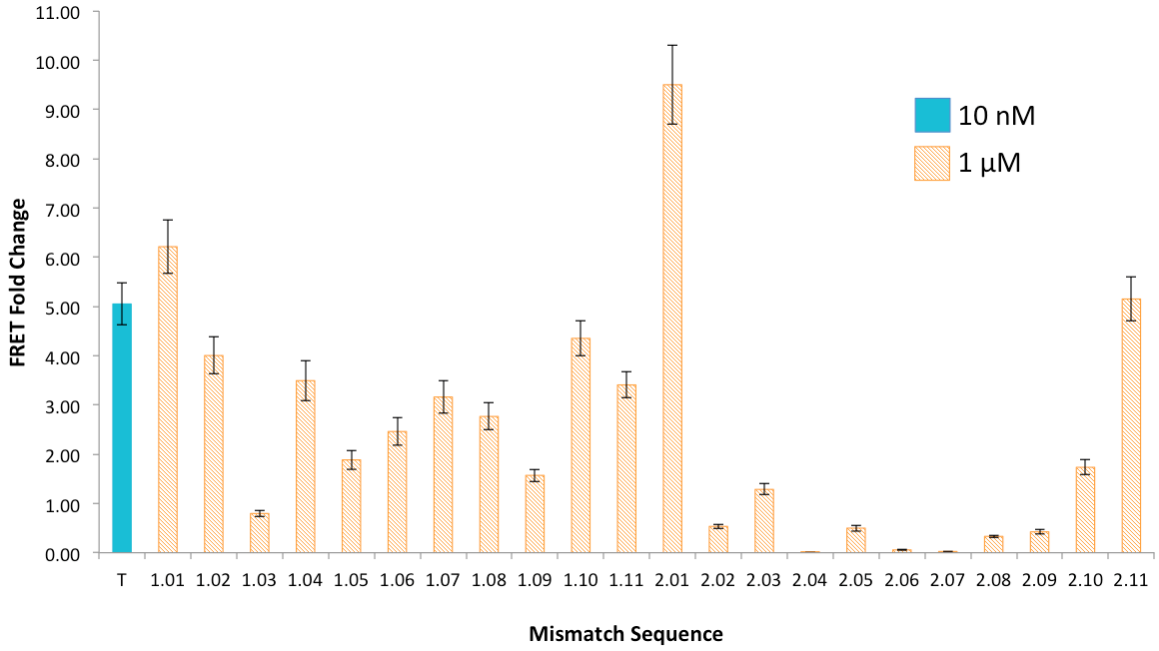

Figure 2.8 Detection of single mismatch sequences (orange) at an elevated concentration (1 µM) compared to the 10 nM target sequence (blue). The mismatch locations in the sequences are shown in Table 2.2.

Figure 2.9 shows the detection of double mismatch sequences (1 µM) at 100x the concentration of the target sequence (10 nM). Sequences 1.20 and 1.21 have double mismatches in the **a** binding region for the QD probe, and sequences 2.20 and 2.21 have double mismatches in the **b** binding region for the **DS**. The double mismatch has a mismatch in both the **a** binding region and in the **b** binding region. Unsurprisingly, there is no FRET fold change for any of these double mismatches. This is due to the probes not hybridizing with the target sequence and FRET detection being unable to occur.

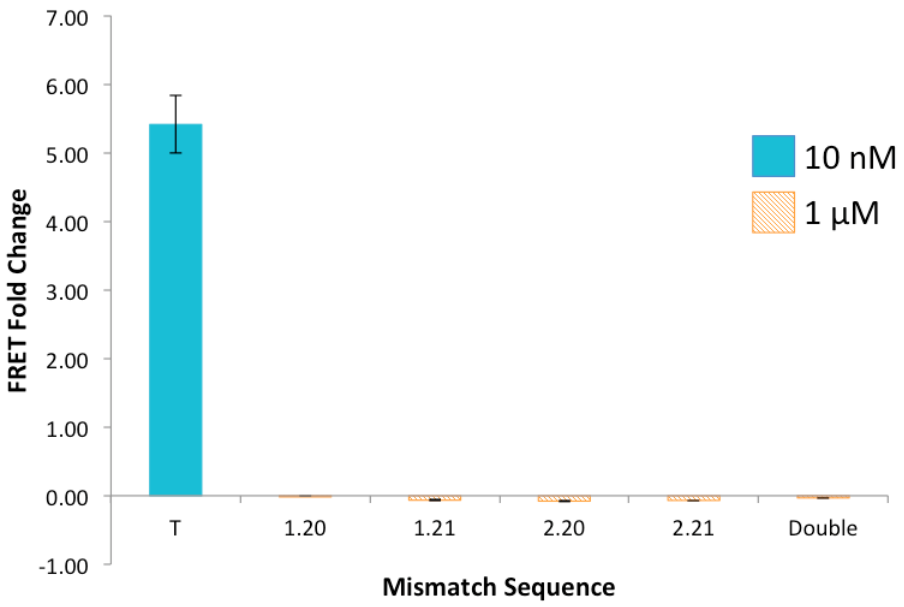

Figure 2.9 Detection of double mismatch sequences at an elevated concentration (1 µM) compared to the 10 nM target sequence to force detection.

Figure 2.10 shows the detection of mismatch sequences at the same concentration as the target sequence (10 nM). This data gives a true picture of how the developed assay performs for detecting SNPs. From this data, it appears that the detection of SNPs cannot be discriminated from target detection if the mismatch is near the end of the binding regions **a** and **b**. Mismatch sequences 1.01, 1.02, 2.01, and 2.11 have similar FRET fold change as the target DNA sequence, and sequences 1.10, 1.11, and 2.10 have slightly lowered fold change. This likely is due to the ability of the QD probe and the **DS** still being able to bind to the target despite a single base mismatche being present. Alternatively, if the mismatch occurs in the middle of binding regions **a** and **b** (sequences 1.03−1.09 and 2.02−2.09), the FRET fold change is very low

compared to the perfect target sequence, and discrimination is simple to observe. This likely is due to the mismatch disrupting the ability of the QD probe to hybridize with region **a** and the **DS** to hybridize with region **b**. If either of the probes do not hybridize with the target, FRET detection cannot occur.

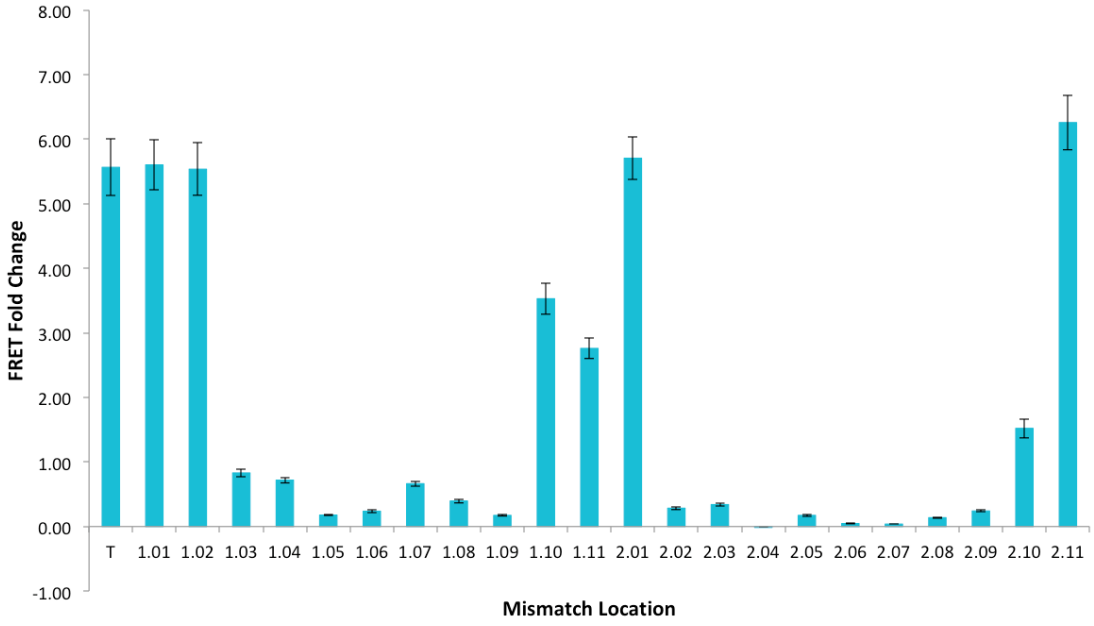

Figure 2.10 Detection of single mismatch sequences at 10 nM for the determination of the discrimination factor compared to the target sequence (T). The mismatch locations are show in Table 2.2.

Table 2.3 summarizes the ability of the developed assay to discriminate between the target sequence and any SNPs. The discrimination factor (DF) is the ratio of the difference in detection of the target compared to the mismatch.[129] A DF value of approximately 1 means that there is little to no discrimination between the target and the

mismatch sequence. A DF value less that 1 indicates that the mismatch has a higher detection signal than the target, while a DF value greater than 1 indicates that the target has a higher detection than the mismatch sequence. A comparison of Figure 2.10 and Table 2.3 shows agreement between the recorded signal and the calculated DF. Sequences 1.01, 1.11, and 2.01 have DF values of approximately 1, suggesting there is no discrimination between these and the perfect target. Sequence 2.11 has a DF less than 1, which is not surprising as it is a mismatch at the 3′ end of the target sequence and is less significant for hybridization than those bases in the middle of the sequence. For the mismatches that occur in the middle of binding regions **a** and **b** (sequences 1.02−1.10 and 2.02−2.10), the DF values are all much greater than 1, again suggesting that the QD probe or the **DS** do not hybridize, and there is little to no FRET signal.

Table 2.3 Discrimination factors (DF) of mismatches compared to the target DNA sequence.

DNA Sequence	Discrimination Factor (DF)
T	1.01 ± 0.05
1.01	0.97 ± 0.06
1.02	5.4 ± 0.1
1.03	6.03 ± 0.07
1.04	21.7 ± 0.1
1.05	16.5 ± 0.1
1.06	6.49 ± 0.08
1.07	10.4 ± 0.2
1.08	18.6 ± 0.2
1.09	1.41 ± 0.06
1.10	1.73 ± 0.04
1.11	1.01 ± 0.05
2.01	0.94 ± 0.04
2.02	14.3 ± 0.2
2.03	10.8 ± 0.1
2.04	54.0 ± 0.4
2.05	15.7 ± 0.3
2.06	30.1 ± 0.4
2.07	32.5 ± 0.3
2.08	20.3 ± 0.2
2.09	11.12 ± 0.09
2.10	2.6 ± 0.1
2.11	0.80 ± 0.05

The results of Figure 2.10 and Table 2.3 indicate that this optimized assay could be used easily for the detection of SNPs in samples. By designing the **QD5** probe

sequence or the **DS** sequence to include the mismatch in the middle of binding region **a** or **b**, there would be very little FRET signal compared to the perfect target sequence. These discrimination factors are specific to this sequence and would need to be optimized for other targets.

Other SNP detection methods using nanomaterials have achieved attomolar levels of detection, but these methods require amplification steps.[132] Other nanomaterial based methods do not have amplification steps but require much more time and complex instrumentation.[133–135] This developed 3WJ with FRET detection method has a pM detection limit, has very simple operation and instrumentation, and detection is able to occur in less than 30 min.

2.4 Conclusions

A sensitive and specific assay for the detection of a target DNA sequence was developed using a DNA 3WJ FRET technique. This assay is technically simple to perform, occurs in a homogeneous solution, is rapid, and all the mixing and detection occurs at room temperature without the need for complex instrumentation. The technique has the novelty of using a DNA functionalized QD as a FRET donor, with the functionalized DNA used for the construct of a DNA 3WJ. This developed assay is sensitive to a specific target sequence and is able to achieve picomolar detection limits without the need to amplify the target sequence. This assay also can be used to detect SNPs by designing the QD probe or the **DS** to have the mismatch in the middle of the hybridization region. Further research could be conducted to test the application of this

technique to real-world examples, such as serum or cell lysate. For detection of low concentrations of SNPs, additional amplification of signals would be useful.

Chapter 3: Binding-Induced Three-Way Junction Fluorescence Energy Transfer Method for the Detection of a microRNA Target

3.1 Introduction

miRNA have many functions in cells, mostly affecting gene expression through interaction with mRNA targets.[13–16] microRNA 21 is one of the most frequently over-expressed microRNA sequences in solid tumors and has shown the ability to inhibit phosphatase expression, limiting the activity of many signaling pathways.[136,137] microRNA 21 targets many different tumor suppressors; its over expression results in a tumor growth in many types of cancers, such as gastric,[138] ovarian,[139,140] cervical,[141] and leukemic cancers,[142] as well as head and neck cell lines,[143] papillary thyroid carcinoma,[144] and hepatocellular carcinomas.[145] Because of the wide range of cancers associated with microRNA 21, development of an assay for early detection is important for rapid diagnosis allowing for earlier treatment of patients.

The aim of this chapter is to extend the DNA-3WJ assay developed in Chapter 2 to the detection of microRNA by changing the DNA target to microRNA 21. This technique utilizes FRET detection that can only occur when all components of the 3WJ are together to form the 3WJ.

3.1.1 Principle of the Binding-Induced 3WJ FRET Assay

Figure 3.1 shows the detection scheme for the microRNA target. In this assay, QD probes are prepared by functionalizing them with a sequence (**QD5, QD6, QD7**)

containing two domains, **c** (blue) and **a*** (purple). These are mixed with a dye sequence (**DS**), which is functionalized with a dye and also has two domains, **c*** (blue) and **b*** (green). When in the presence of a microRNA target, the **a*** domain of the QD hybridizes with the ***a*** domain of the target, and the **b*** domain of the **DS** hybridizes with the ***b*** domain of the target. This brings **c** and **c*** into close proximity, making hybridization favorable, bringing the dye into close proximity of the QD, and FRET detection can occur. The emission from both the QD donor and the Cy5 acceptor are detected. If the microRNA target is not present, the complementary region of **c** and **c*** is not sufficiently long enough for stable hybridization to occur in bulk solution, and FRET detection cannot occur.

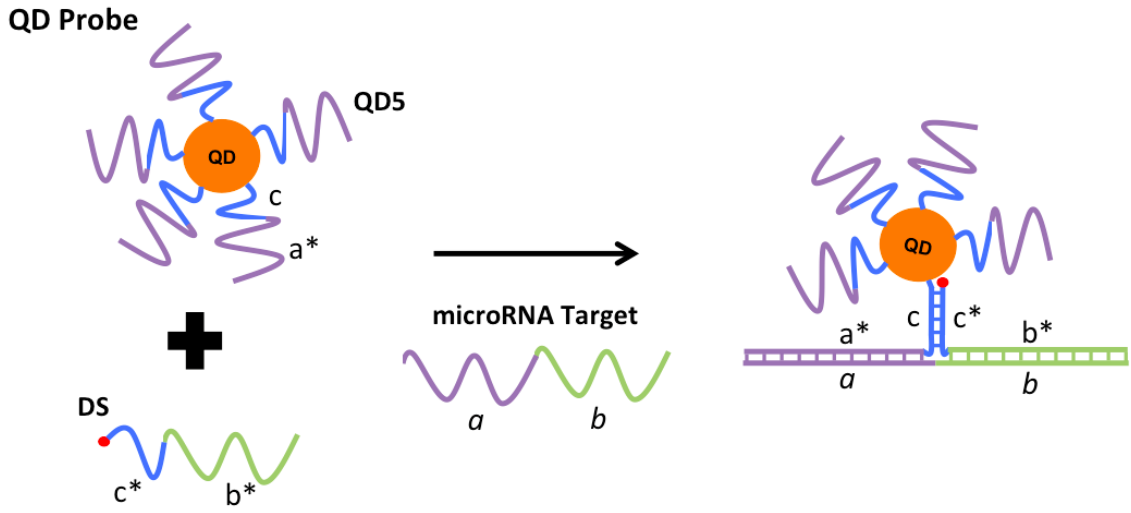

Figure 3.1 Scheme for the detection of a microRNA target with a 3WJ. Functionalized QD probes are mixed with a dye sequence (**DS)**. When in the presence of a microRNA target, probes hybridize with the complementary target (***a*** with **a*** and ***b*** with **b***), allowing complementary sequences **c** and **c*** to hybridize, bringing the dye to close proximity of QD, and FRET detection can occur.

3.2 Experimental Methods

3.2.1 Materials and Reagents

The DNA and RNA oligonucleotides sequences (Table 3.1) were custom synthesized, labeled, and HPLC purified by Integrated DNA Technologies (IDT, Coralville, IA). A solution of Qdot^{TM} 605 ITK streptavidin conjugate QDs (2.0 μM) was obtained from ThermoFisher (Eugene, OR). Bovine serum albumin (BSA) was obtained from Sigma-Aldrich (Oakville, ON). Phosphate buffered saline (1X PBS) (pH 7.4) was obtained

from Sigma-Aldrich (Oakville, ON). RNAse Away™ was obtained from ThermoFisher (Eugene, OR). Tween 20 was obtained from Sigma-Aldrich (Oakville, ON). All other reagents were of analytical grade.

Table 3.1 DNA and RNA sequences for three-way junction FRET detection of microRNA 21. The colour codes of the nucleotides (green, blue, purple) match those in Figure 3.1. The same colours indicate complementary sequences.

Nucleic Acid Name	Sequence
microRNA 21	5′- UAG CUU AUC AGA CUG AUG UUG A -3′
microRNA 10b	5′- UAC CCU GUA GAA CCG AAU UUG UG-3′
QD 5Comp (**QD5**)	5′- Biotin - CGT AG TT CT GAT AAG CTA -3′
QD 6Comp (**QD6**)	5′- Biotin - CGT AGT TT CT GAT AAG CTA -3′
QD 7 Comp (**QD7**)	5′- Biotin - CGT AGT G TT CT GAT AAG CTA -3′
Dye Sequence (**DS**)	5′- TCA ACA TCA GT TT CAC TAC G / T – Cy5 -3′

3.2.2 Preparation of QD Probe

QD probes were prepared fresh each day. To avoid contamination, all lab supplies were autoclaved and kept in a sterile cabinet. At the start of each day, the equipment was treated with RNAse Away™ in order to avoid degradation of the microRNA 21 target. The probe preparation buffer contains commercially available 1X PBS with Mg^{2+}/Ca^{2+} and additional Mg^{2+} added. Biotinylated QD sequence (**QD5, QD6, QD7**) was mixed with streptavidin coated QDs in a 15:1 (DNA:QD) ratio. This was allowed to incubate at

room temperature for 30 min. The final prepared QD probe concentration is 50 nM and the volume needed for experiments that day.

3.2.3 Fluorescence Detection of a microRNA target

A mix of QD probe and dye sequence were prepared in 1X PBS buffer with Mg^{2+}/Ca^{2+} with optimized nonspecific blocking agent (BSA or Tween 20) and added Mg^{2+} for final detection concentrations of 1 nM QD probe and 45 nM **DS**, unless otherwise specified. This master mix was added to all triplicate samples and blank (without microRNA target) solutions to a final volume of 100 μL. Samples were left to incubate for 30 min at room temperature and then transferred to a 96-well plate for fluorescence detection.

The fluorescence signal was detected with a multi-mode microplate reader (DTX 880 Multimode Detector) with excitation at 475 nm and emission at 605 nm for QDs and emission at 680 nm for Cy5. FRET fold change is calculated from formula (Eq. 2-1), as described in section 2.2.4. The fluorescence signal of blanks also was examined at 680 nm as it is only due to Cy5 emission originating from energy transfer from the QD donor and shows background signal clearly.

3.2.4 Optimization of Assay Parameters for microRNA Target Detection

Parameters optimized in Chapter 2 were used initially for the detection of microRNA 21. As the DNA/RNA hybridization is not as stable as DNA/DNA hybridization, several parameters were further optimized to improve this hybridization and detection. Optimization included the buffer composition, by adjusting the salt concentration, and the length of the complementary region **c**. All optimizations used commercially available 1X PBS buffer with Mg^{2+}/Ca^{2+} that was not autoclaved due to precipitation of

salts during the process. For each optimization step, the target microRNA was detected at 2 nM (green hatched) and 5 nM (solid blue) in triplicate, unless otherwise shown. Also detected at each optimization were blanks (no DNA target, only QD probe, only **DS**) and positive controls (described in section 2.2.3).

3.2.5 Calibration Curve for a microRNA Target by 3WJ-FRET Detection

With optimized conditions, a series dilution of microRNA was detected. All samples were tested in triplicate, 9 sample blanks were tested, and positive control was tested in triplicate. From this data, a calibration curve was created, and standard deviations of the blanks were used to calculate detection limits. Detection of a different microRNA target (microRNA 10b) also was tested to show assay specificity.

3.3 Results and Discussion

3.3.1 Optimization of Buffer Conditions

Buffer conditions for miRNA detection are critical for stabilizing DNA/RNA hybridization. There also is the potential risk of RNAse contamination, which would degrade miRNA in samples; therefore, buffers and equipment must be sterile. Optimized parameters from Chapter 2 (15 **QD5** sequences functionalized to QDs, 45 nM **DS** with 1 nM QD) were used to assess buffers for detection of the microRNA 21 target. Figure 3.2 shows FRET fold change with different buffer conditions. Buffer 1 used in DNA detection showed no FRET signal. This buffer was not sterile and had very little Mg^{2+} ions. Mg^{2+} aids in the hybridization of nucleic acids into duplexes by stabilizing the negative charges in the sugar-phosphate backbones. Buffer 2 showed a low fold change

signal when using a sterile, commercially available 1X PBS buffer with Mg^{2+}/Ca^{2+}. The concentration of the cations is not sufficient to stabilize the negatively charged backbones. Buffer 3 also had a low fold change signal with the 1X PBS buffer with Mg^{2+}/Ca^{2+} and added 0.1% BSA. The addition of BSA in previous experiments was used to prevent adsorption of assay components to the reaction vessel walls. Buffer 4 had a slightly elevated FRET fold change signal when using commercial 1X PBS with Mg^{2+}/Ca^{2+} and added 0.05% Tween 20. In this case, the addition of Tween 20 is used to replace the addition of BSA and prevent adsorption. Buffer 5 had a much higher fold change signal when using commercial 1X PBS with Mg^{2+}/Ca^{2+} and added 20 mM Mg^{2+}. The addition of a high concentration of cation helps stabilize the DNA/RNA duplex. When increasing the added cation concentration to 50 mM Mg^{2+}, as in Buffer 6, the signal decreased. Comparing Buffer 5 with Buffer 7, the addition of 0.05% Tween 20 did not improve the fold change signal. Comparing Buffer 6 with Buffer 8, similar to Buffer 7, the addition of 0.05% Tween 20 did not improve the fold change signal.

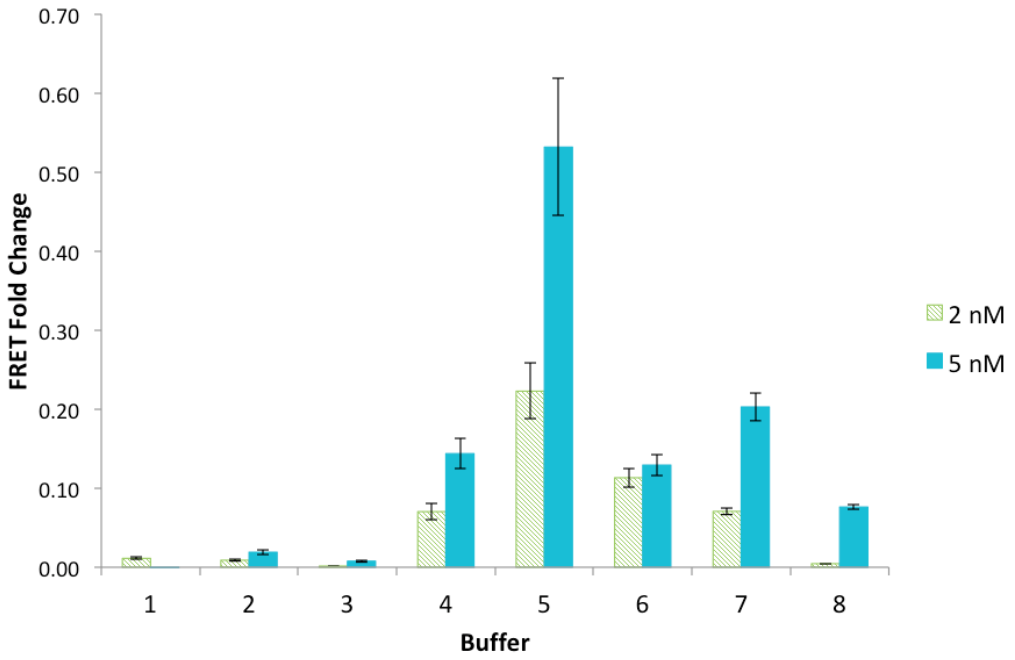

Figure 3.2 Optimization of buffer conditions with **QD5** functionalized QD probes. (**1**) Buffer conditions in Chapter 2: 1X PBS with added 1 mM Mg^{2+} and 0.1% BSA. (**2**) Commercial 1X PBS with Mg^{2+}/Ca^{2+}. (**3**) Commercial 1X PBS with Mg^{2+}/Ca^{2+} and 0.1% BSA. (**4**) Commercial 1X PBS with Mg^{2+}/Ca^{2+} and 0.05% Tween 20. (**5**) Commercial 1X PBS with Mg^{2+}/Ca^{2+} and additional 20 mM Mg^{2+}. (**6**) Commercial 1X PBS with Mg^{2+}/Ca^{2+} and additional 50 mM Mg^{2+}. (**7**) Commercial 1X PBS with Mg^{2+}/Ca^{2+} and additional 20 mM Mg^{2+} and 0.05% Tween 20. (**8**) Commercial 1X PBS with Mg^{2+}/Ca^{2+} and additional 50 mM $Mg^{2+}$and 0.05% Tween 20. The green hatched bars were the results from the detection of 2 nM DNA target; the solid blue bars show results from the detection of 5 nM DNA target.

3.3.2 Optimization of Complementary Region

From the buffer optimization in Figure 3.2, Buffer 5 appears to have the best conditions for FRET fold change response. However, these conditions are optimal for QD probes with a **QD5** sequence. Increasing the length of the complementary region **c** could help stabilize the 3WJ, allowing for stronger detection of the microRNA target.

Figure 3.3 shows the increase in the length of region **c** by changing the sequence functionalized to QD probes (15 sequences per QD) using Buffer 5. The Figure shows that **QD6** gives the strongest fold change signal under these conditions. The increase in one nucleotide in the complementary region compared to **QD5** appears to aid in the stabilization of the 3WJ. Under Buffer 5 conditions, **QD7** gave the lowest fold change signal due to a higher background signal. However, as this is the longest complementary region, it provides the highest stability for the binding induced 3WJ.

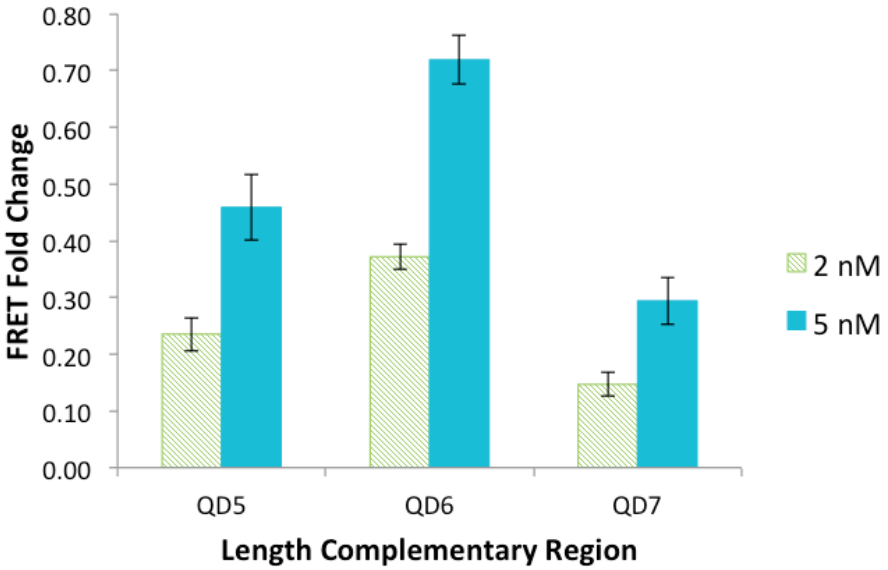

Figure 3.3 Optimization of the length of the complementary region between the QD probe and the **DS**.

In order to improve the FRET fold change signal with **QD7**, the background signal should be decreased. Since Buffer 5 has a high added cation concentration, reducing this should decrease the target nonspecific hybridization, thereby increasing the FRET signal. Figure 3.4 shows the optimization of buffer conditions by varying the amount of added Mg^{2+} to the commercial 1X PBS buffer with Mg^{2+}/Ca^{2+}. The aim of varying the added cation is to stabilize the DNA/RNA duplex. However, too high a concentration stablilizes the hybridization of the QD probe and the **DS** not in the presence of microRNA target, which results in a higher background and reduced FRET fold change signal. From the Figure, it appears that with **QD7** functionalized QDs, the

addition of 1 mM Mg^{2+} gives the strongest fold change signal due to minimal background signal.

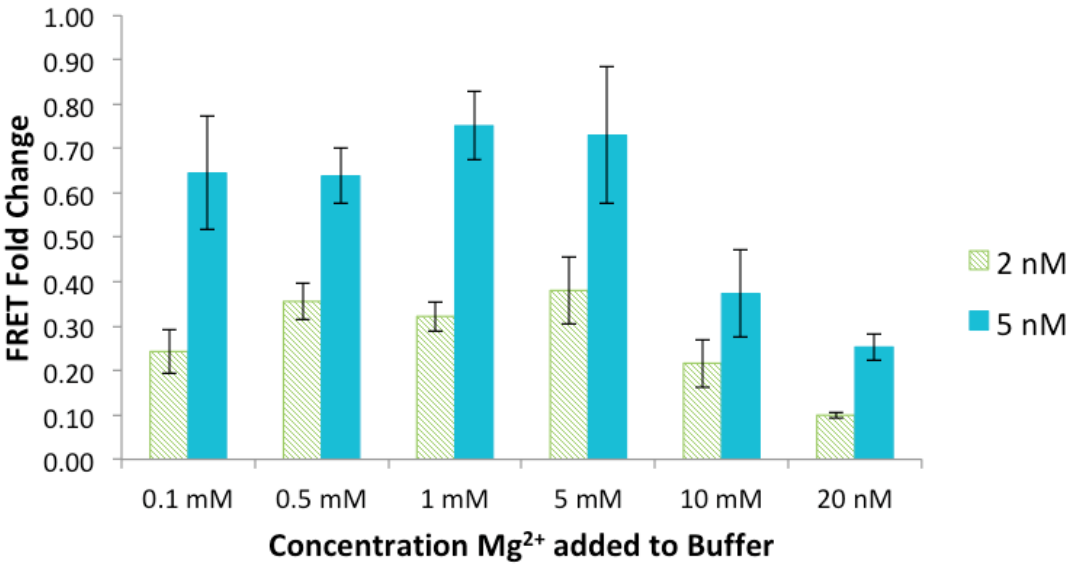

Figure 3.4 Optimization of buffer conditions with **QD7** on the QD probe.

Using the commercial 1X PBS buffer with Mg^{2+}/Ca^{2+} and added 1mM Mg^{2+}, the concentration of **DS** is optimized with **QD7** functionalized QD probes maintained at 1 nM. From Figure 3.5, maintaining the **DS** at 45 nM gave the strongest fold change signal. This concentration is the same concentration as the one optimized for DNA detection, making the **DS** a 3x excess of the **QD7** sequence with the final QD probe concentration. This excess ensures that there are many **DS** sequences for detection, without having such a high excess as to increase the background signal. However, when

assessing the overall absolute FRET fold change signal, even with the optimized buffer conditions, the signal is not as high as with **QD6**.

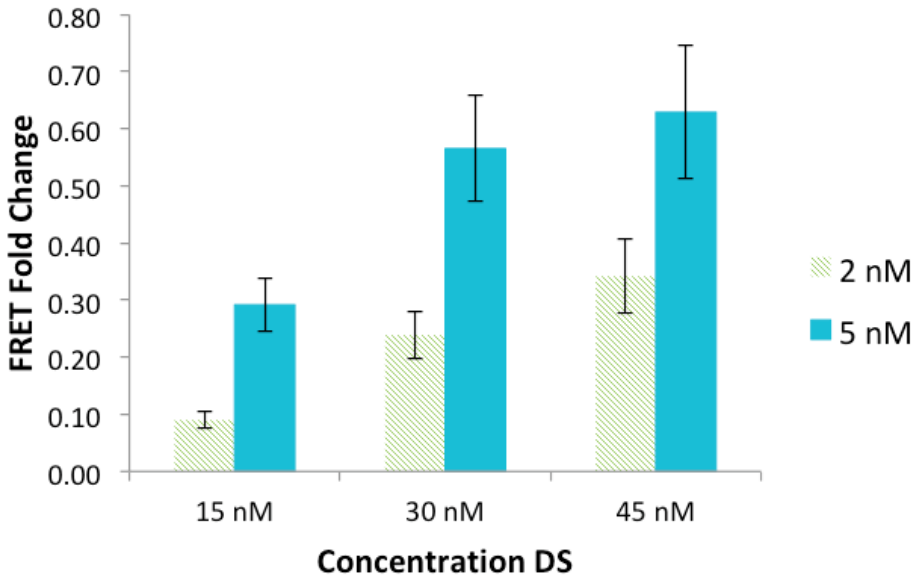

Figure 3.5 Optimization of the **DS** concentration with **QD7** on the QD probe.

From Figure 3.3, **QD6** functionalized QD probes gave the strongest fold change signal. Optimizing the concentration of added cation to the buffer conditions could increase this overall signal further. Figure 3.6 show the optimization of buffer conditions by varying the amount of added Mg^{2+} to the commercial 1X PBS buffer with Mg^{2+}/Ca^{2+} for **QD6** functionalized QD probes. It can be seen that the addition of 10 mM Mg^{2+} gives the strongest fold change signal. This amount helps strengthen the DNA/RNA hybridization without strengthening the non-specific hybridization of the **DS** with the QD probe.

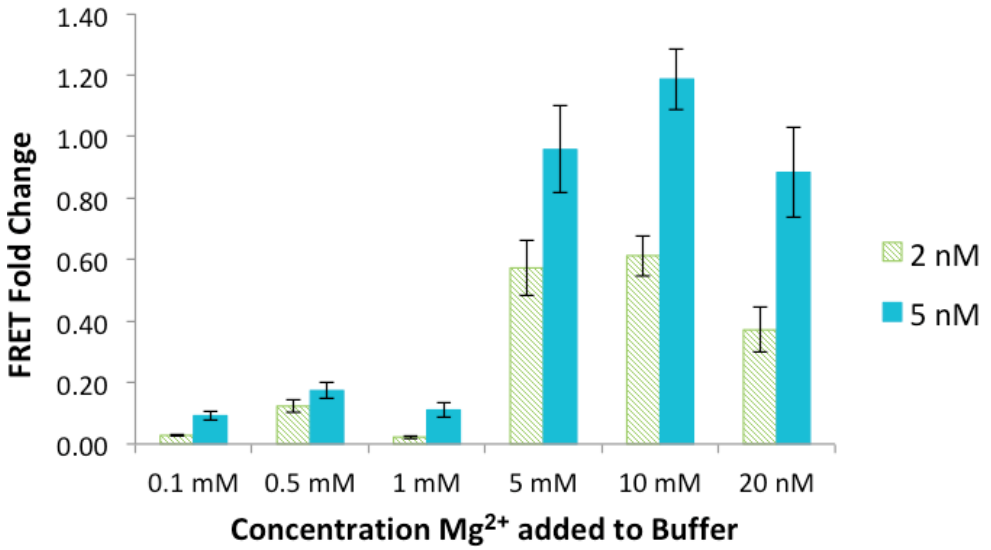

Figure 3.6 Optimization of buffer conditions with **QD6** on the QD probe.

Using optimized buffer conditions (1X PBS buffer with Mg^{2+}/Ca^{2+} and added 10 mM Mg^{2+}), the concentration of **DS** is optimized with **QD6** functionalized QD probes maintained at 1 nM. Figure 3.7 shows that 45 nM **DS** gives the highest FRET fold change response. As with DNA detection and with **QD7** functionalized QD probes, this concentration allows **DS** to be 3x excess **QD6** so detection of microRNA can occur with minimal background signal.

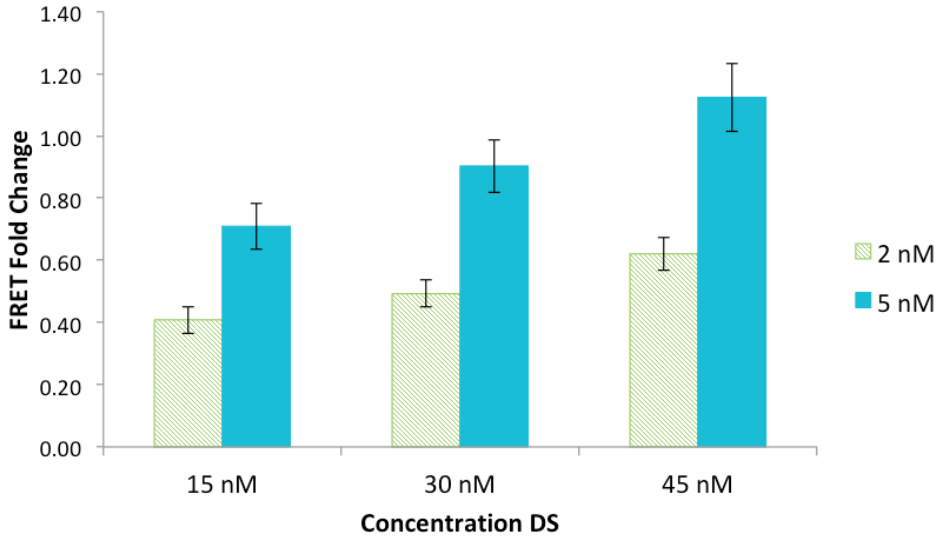

Figure 3.7 Optimization of the **DS** concentration with **QD6** on the QD probe.

3.3.3 Calibration Curve for the Detection of a microRNA Target by 3WJ-FRET Detection

With all optimized conditions, a calibration curve for the detection of microRNA 21 (blue diamonds) is shown in Figure 3.8. The data is linear from 0.2−15.0 nM microRNA 21 target with an LOD of 720 pM. Also shown in Figure 3.8 is the detection of a microRNA 10b (orange squares) using the assay and specific probes for microRNA 21; there is no fold change signal for the non-specific sequence. This shows that the developed assay is specific for the desired target as the QD probe sequence and the **DS** are designed for that target.

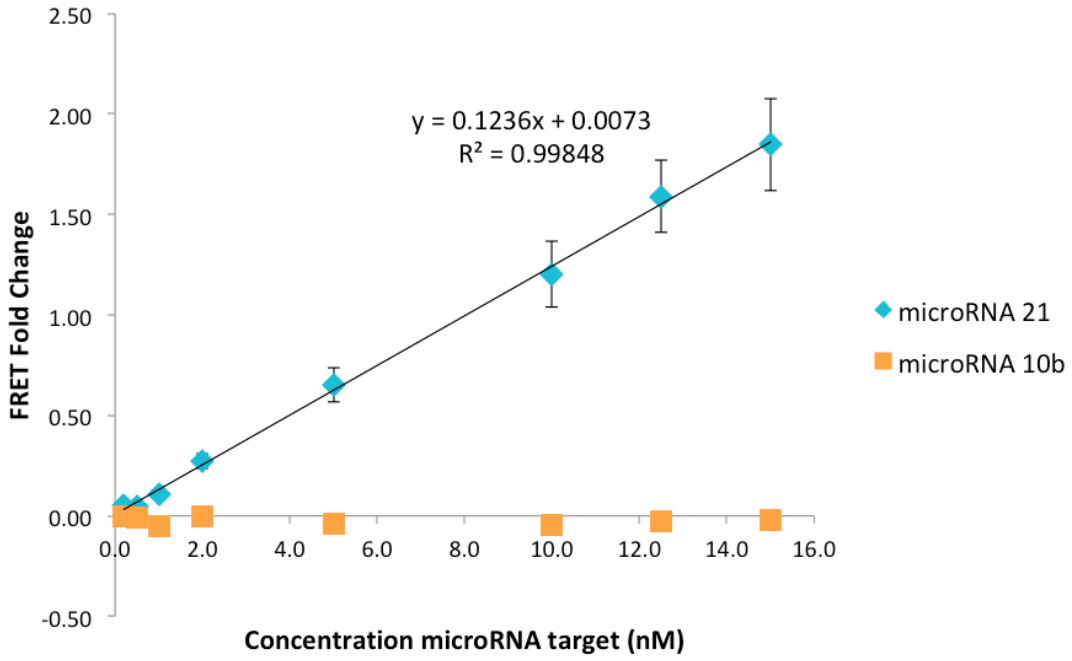

Figure 3.8 Calibration curves for the detection of microRNA 21 (blue diamonds) and non-specific microRNA 10b (orange squares) using the developed 3WJ FRET detection system.

Detection of specific miRNA targets is important for disease detection, diagnosis, and prognosis. The developed miRNA assay has a higher LOD compared to DNA from Chapter 2 (720 pM vs. 163 pM), but the LODs are within the same order of magnitude. This difference can be due to many factors, including the potential lowered hybridization stability between DNA:RNA duplexes compared to DNA:DNA and RNA:RNA duplexes.[146] This can be observed in the overall lower absolute FRET fold change values in the calibration curves. The absolute fold change values for miRNA can be increased by increasing the hybridization between the QD probes, the **DS**, and the

microRNA target. This increased hybridization would bring more **DS** to close proximity of the QD probe, increasing FRET detection.

Another important aspect of hybridization in this assay is accounting for the GC content of sequences. As GC pairs form 3 hydrogen bonds upon hybridization, their contribution to the overall stability is greater than an AT pair, which only forms 2. The 22 nucleotide long sequence of microRNA 21 only has 36% GC content, while other microRNA targets may have higher (10b has 44%). This lowered GC content means that forming duplexes with microRNA 21 will not be as stable as those with higher GC content. The developed assay was able to detect microRNA 21 despite this lowered content, but the conclusions made in this Chapter can be applied only to microRNA 21. If this assay is applied to other microRNA targets, optimization of complementary region length and salt content must be optimized.

As microRNA 21 plays an important role in many diseases,[136] sensitive detection is important. Yang et al.[147] recently developed a sensitive strategy for in vivo detection using **g**raphene **o**xide (GO) and a dually labeled molecular beacon (MB). Introduction of the microRNA target removes the MB from the GO surface and restores fluorescence to the dye labels. This assay has a 2:1 (target: dye response) resulting in a detection limit of 30 pM. It is only an order of magnitude less than the developed 3WJ assay and can be used in cells. Another FRET based assay was able to achieve detection limits of 200−900 pM in small volumes.[148] This assay has a detection limit range similar to the developed 3WJ assay but has a ligation step, increasing analysis time. Clinical detection of microRNAs includes quantitative PCR, microarrays, next generation sequencing, and Northern blotting.[149–151] Though these techniques are powerful and well-established,

they can be time consuming and may require reverse transcription for the detection of synthesized complementary DNA to the microRNA target. Overall, the developed 3WJ assay with FRET detection compares well with other simple microRNA detection methods, with the advantage of extremely simple methods, instrumentation, and rapid detection. This developed technique also holds the advantage of short probe binging length, which is ideal for short microRNA sequences.

3.4 Conclusions

A sensitive and specific assay for the detection of a miRNA sequence was developed using a DNA 3WJ FRET technique. This assay is technically simple to perform, occurs in a homogeneous solution with rapid detection, and with all steps occurring at room temperature without the need for complex instrumentation. The technique has the novelty of using a DNA functionalized QD as a FRET donor, with the functionalized DNA used for the construct of a DNA 3WJ. This developed assay is sensitive and is able to achieve pM detection limits without the need to amplify the target sequence. The assay is also specific for a desired target, with no detection occurring upon the introduction of a non-specific microRNA sequence. The specificity of this assay suggests that it could be used to detect miRNA targets in biological samples.

Chapter 4: Detection of Human α-Thrombin using a Binding-Induced Fluorescence Energy Transfer Detection Method

4.1 Introduction

Thrombin is a protease that acts in the coagulation cascade.[152–155] After an injury, thrombin is enzymatically cleaved from its inactive form (prothrombin) into its active form, where it is able to aid in the formation of clots to prevent further bleeding. Due to its critical role in the coagulation cascade, thrombin has been found to be involved with diseases such as Alzheimer's disease and cancers.[156,157] Under normal conditions, thrombin is not present in blood, but inactive prothrombin is secreted into blood at a concentration of about 1.2 μM. After injury and during coagulation, concentrations of thrombin cleaved from prothrombin can vary from pM to μM.[158,159]

Thrombin is a frequently used target molecule for proof of concept assays. An extensive review of over 100 aptamer-based assays for thrombin detection was published in 2014.[160] Most assays detect human α-thrombin, which is the most biologically significant form of thrombin. There are 2 aptamers for α-thrombin: a 15 nucleotide long sequence (K_d = 100 nM)[68] and a 29 nucleotide long sequence (K_d = 0.5 nM).[161] Both aptamer sequences form stable intramolecular G-quadruplex structures, which can be used as DNAzymes for the detection of thrombin.[162] There are many factors that contribute to the use of thrombin for proof of concept assays. Both thrombin aptamers are short sequences with 15 or 29 nucleotides, making them simple and inexpensive to synthesize even with affinity or reporter molecule modifications. Also, the two aptamers bind to two distinct epitopes on the thrombin molecule without

interfering with each other's binding or with the catalytic activity of thrombin itself. The 15−nt aptamer binds to the heparin-binding site of thrombin, and the 29−nt aptamer binds to the fibrinogen-recognition site of thrombin. The binding of the two aptamers makes a "sandwich" format assay that is well established in many other techniques.

The aim of this chapter is to develop a BINDA based assay coupled with FRET detection for human α-thrombin as a proof of principle method for other protein targets. These techniques pair well due to their intrinsic properties: BINDA cannot occur unless both probes bind to bring complementary sequences to close proximity, and FRET cannot occur unless the donor and acceptor are also in close proximity.

4.1.1 Principle of the Binding-Induced FRET Assay

Figure 4.1 shows the scheme for the detection of human α-thrombin. In this assay, QD probes are prepared by functionalizing a thrombin aptamer (purple) and a short complementary sequence (green). Dye probes are prepared with another thrombin aptamer (blue) and a dye labeled sequence complementary to the green sequence on QDs (black and green). In the presence of a target human α-thrombin protein, the two aptamer probes bind to the same α-thrombin protein, bringing the complementary sequences together for hybridization and bringing the dye into close proximity of QD. Thus, FRET detection can occur. The emission from both the QD donor and the Cy5 acceptor are detected. If the target protein is not present, there is no binding-induced assembly. The inter-molecular hybridization between the probes is not stable hybridization in bulk solution. The Cy5 acceptor is not brought to close proximity of the QD donor, and FRET detection cannot occur.

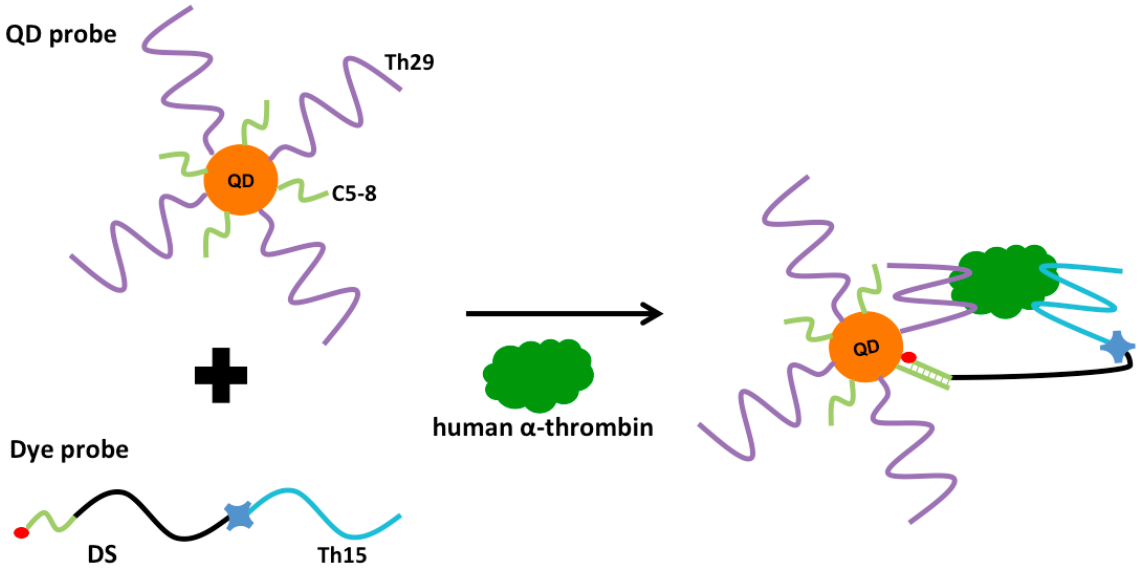

Figure 4.1 Scheme for the detection of human α-thrombin. Functionalized QD probes are mixed with dye probes. When in the presence of a protein target, the two aptamer probes bind to the same target protein, facilitating complementary sequences to hybridize, bringing the dye to close proximity of QD, and FRET detection can occur. **Th15** denotes the 15−mer thrombin aptamer and **Th29** denotes the 29−mer thrombin aptamer.

4.2 Experimental Methods

4.2.1 Materials and Reagents

The DNA oligonucleotides sequences (Table 4.1) were custom synthesized, labeled, and HPLC purified by Integrated DNA Technologies (IDT, Coralville, IA). A solution of Qdot^{TM} 605 ITK streptavidin conjugate QDs (2.0 μM) was obtained from ThermoFisher

(Eugene, OR). Human α-thrombin was purchased from Haematologic Technologies Inc. (Essex Junction, VT). Bovine serum albumin (BSA) was obtained from Sigma-Aldrich (Oakville, ON). Phosphate buffered saline (1X PBS) (pH 7.4) was obtained from Sigma-Aldrich (Oakville, ON). All other reagents were of analytical grade. Nanopure H_2O (>18MΩ), purified by an Ultrapure Milli-Q water system, was used for all experiments.

Table 4.1 DNA sequences and modifications for the detection of human α-thrombin.

DNA Name	Sequence
Comp 5 (**C5**)	5′- Biotin- TT C GAG A - 3′
Comp 6 (**C6**)	5′- Biotin- TT CGA GAT - 3′
Comp 7 (**C7**)	5′- Biotin- TT CGA GAT A - 3′
Comp 8 (**C8**)	5′- Biotin- TT CGA GAT AA - 3′
Dye Sequence (**DS**) (11 nm)	5′- Biotin- TTT TTT TTT TTT TTT TTT TTT TTT TTT TTT T ATC TCG T- Cy5- 3′
Long Dye Sequence (**DS-L**) (15 nm)	5′- Biotin- iSp18- TTT TTT TTT TTT TTT TTT TTT TTT TTT T ATC TCG T- Cy5- 3′
Thrombin 29 (**Th29**)	5′- Biotin- TTT TTT AGT CCG TGG TAG GGC AGG TTG GGG TGA CT - 3′
Thrombin 15 (**Th15**)	5′- Biotin- TTT TTT GGT TGG TGT GGT TGG - 3′

4.2.2 Preparation of Aptamer Functionalized Probes

Two aptamers that bind to human α-thrombin were used: the 29−nt aptamer (**Th29**) and the 15−nt aptamer (**Th15**). QD and Dye probes were prepared fresh each day. Probe preparation buffer contains 1X PBS with 0.1% BSA. QD probes were prepared by mixing equal concentrations of biotinylated **Th29** with biotinylated complementary

sequence (**C5, C6, C7, C8**). This DNA mixture was added to streptavidin coated QDs so that they are in a 10:10:1 ratio (**Th29**:**CX**:QD), unless otherwise specified. This was allowed to incubate at room temperature for 30 min. To this mixture, a 10x excess biotin mixture was added to block unbound sites on streptavidin QDs and was left to incubate at room temperature for 30 min. The final prepared QD probe concentration is 50 nM and the volume needed for the experiments that day.

Dye probes were prepared by mixing equal concentrations of biotinylated **Th15** with biotinylated dye labeled sequence (**DS**). This DNA mixture was incubated with an equal concentration of streptavidin for 30 min at room temperature. To this mixture, a 10x excess biotin mixture was added to block unbound sites on streptavidin QDs. This was left to incubate at room temperature for 30 min. The final prepared dye probe concentration is 500 nM and the volume needed for the experiments that day.

4.2.3 Fluorescence Detection of Human α-Thrombin

A mixture of QD probe and dye probe were prepared in 1X PBS with 0.1% BSA and 1 mM Mg^{2+} for final detection concentrations of 1 nM QD probe and 10 nM dye probe, unless otherwise specified. This master mix was added to all triplicate samples and blank (without protein target) solutions to a final volume of 100 μL. Samples were left to incubate for 30 min at room temperature and then transferred to a 96-well plate for fluorescence detection.

Fluorescence signal was detected with a multi-mode microplate reader (DTX 880 Multimode Detector) with excitation at 475 nm and emission at 605 nm for QDs and emission at 680 nm for Cy5. FRET fold change is calculated from formula (Eq. 2-

1), as described in section 2.2.4. Fluorescence signal of blanks also was examined at 680 nm as it is only due to the Cy5 emission originating from energy transfer from the QD donor and represents background.

4.2.4 Optimization of Assay Parameters

Assay parameters were optimized to achieve high signal to noise ratios to improve detection limits. Probes were prepared fresh for each experiment according to the following experimental parameters being optimized: length of complementary region (**C5, C6, C7, C8**), probe ratio and concentration, probe preparation procedures, and probe stability. For each optimization step, human α-thrombin was detected at 2 (green hatched) and 5 nM (solid blue) in triplicate, unless otherwise shown. Also detected at each optimization were blanks (no protein target, only QD probe, only dye probe) and positive controls (described in section 2.2.3).

4.2.5 Calibration Curve for Human α-Thrombin

Under the optimized conditions, human α-thrombin at a series of concentrations was detected. All samples were tested in triplicate, 9 sample blanks were tested, and positive control was tested in triplicate. From this data, a calibration curve was generated and standard deviations of the blanks were used to calculate detection limits.

4.3 Results and Discussion

4.3.1 Optimization and Proof of Concept of Initial Assay

The first optimized parameter in the FRET BINDA assay is the length of the complementary region from 5−nt to 8−nt (**C5, C6, C7, C8**). If this complementary

length is too short, binding of the dye sequence and the short complementary region would not be stable even when both probes are bound to the protein target. Alternatively, if the complementary length is too long, the two probes could hybridize without the need for target binding, thus generating background signal. The latter has a larger effect on lower target concentrations; if the background is too high, lower concentrations may not be able to be detected. In Figure 4.2, the FRET fold change signal for both **C5** and **C6** is low. This is due to an overall low signal at 680 nm, meaning that even if the QD and Dye probes are both binding to thrombin; the complementary region is too short to form stable hybridization. In the same Figure, we can see that both **C7** and **C8** give strong FRET fold change signal for both 2 nM and 5 nM thrombin targets. However, **C8** increased the stability of hybridization without the presence of the thrombin target. Due to this, **C7** was chosen for all subsequent experiments. The use of **C7** ensures that the complementary regions hybridize when both probes are bound to the target, while the potential for target-independent hybridization is lowered, minimizing the background signal.

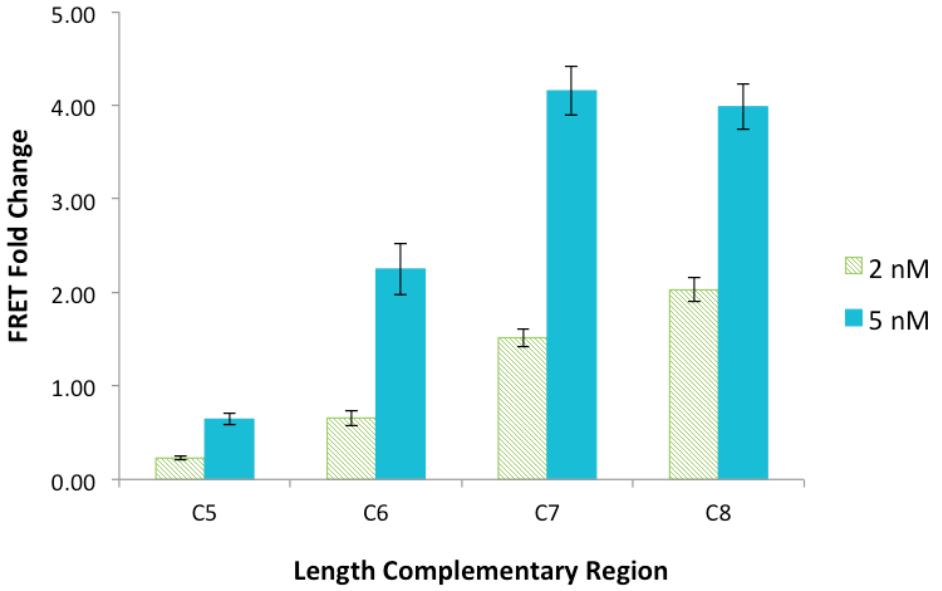

Figure 4.2 Optimization of the length of the complementary region (**C5−8**) between the QD probe and the dye probe. The green hatched bars were the results from the detection of 2 nM human α-thrombin target; the solid blue bars show results from the detection of 5 nM human α-thrombin target.

Other important parameters of this FRET-BINDA assay are the ratio and concentration of the dye probe and the QD probe. The QDs are functionalized with multiple streptavidin molecules, allowing them to be functionalized with multiple DNA sequences (**Th29** and **C7** sequences). The multiple sequences not only increase the probability that the probe will bind the target molecule but also increase the likelihood that the dye sequence will hybridize with the short complementary sequence. By having the dye probe in excess of the QD probe, the amount of dye acceptors to QD donors is increased, increasing the FRET fold change. In Figure 4.3 (A), multiple ratios of

Dye:QD probe were tested, and the results indicate that both 10:1 and 15:1 gave similar results; this equates to 10x and 15x excess dye to QD, respectively. For further optimization, 10:1 (Dye:QD probe) was used as the overall background signal was higher than for 15:1. In Figure 4.3 (B), the concentration of the dye and the QD probes was optimized while maintaining the 10:1 ratio. These results indicate that increasing the concentrations of probes gave a lower FRET fold change signal. This is due to an increase in the background signal. Thus, for subsequent experiments, a 10 nM dye probe and a 1 nM QD probe were used.

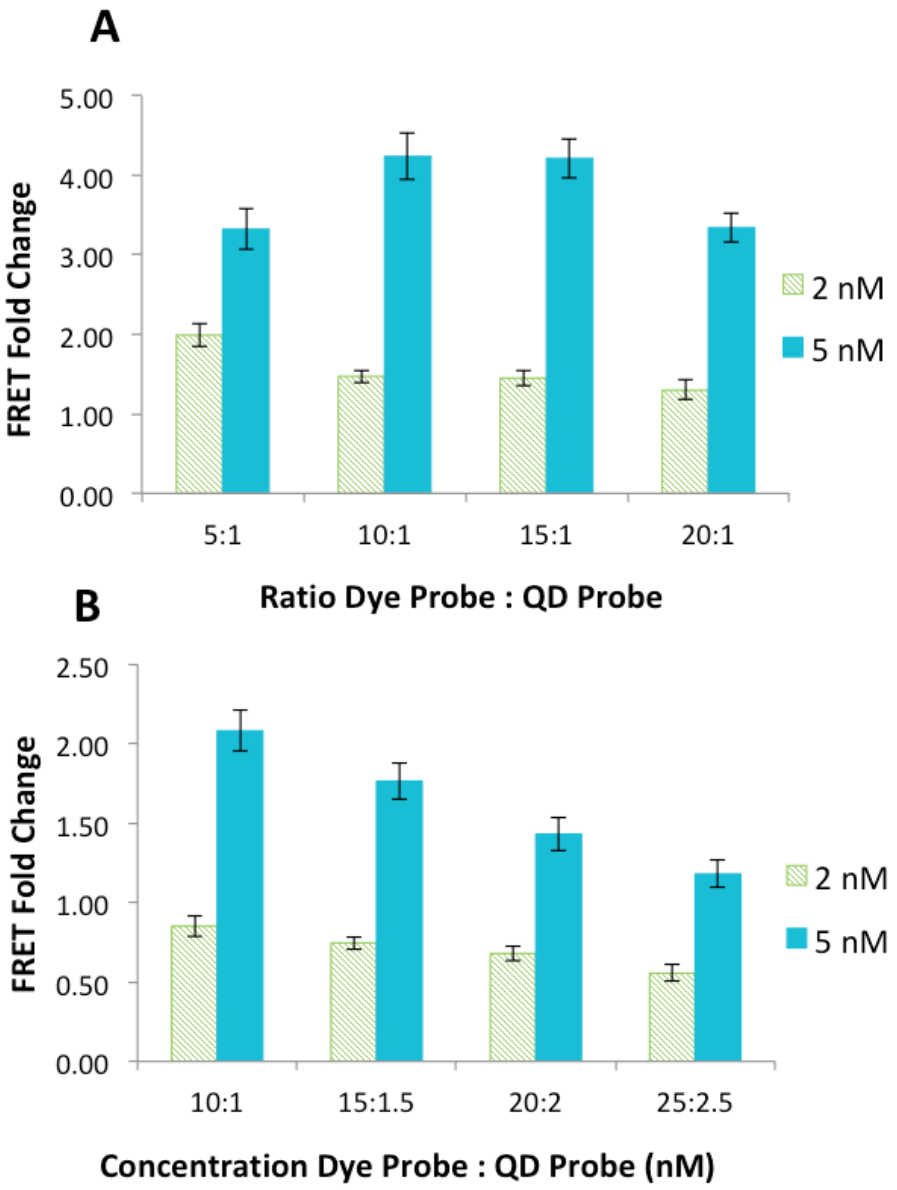

Figure 4.3 Optimization of probe ratio (**A**) and probe concentration (**B**).

4.3.2 Optimization of Probe Preparation

The preparation of both QD and dye probes also is important for optimizing the FRET fold change signal. As previously stated, the commercially available QDs are functionalized with multiple streptavidin molecules and can be functionalized with multiple DNA sequences. In Figure 4.4, QD probes are optimized with varying ratios of **Th29** aptamers and **C7** short complementary sequences. The results indicate that QD probes functionalized with 10 **Th29** aptamers and 10 **C7** short complementary sequences showed the highest FRET fold change with the lowest background signal. This allows for a high probability for the probe to interact with the thrombin target and have up to 10 short, complementary sequences for the dye probe to hybridize. This QD configuration was used for all subsequent experiments.

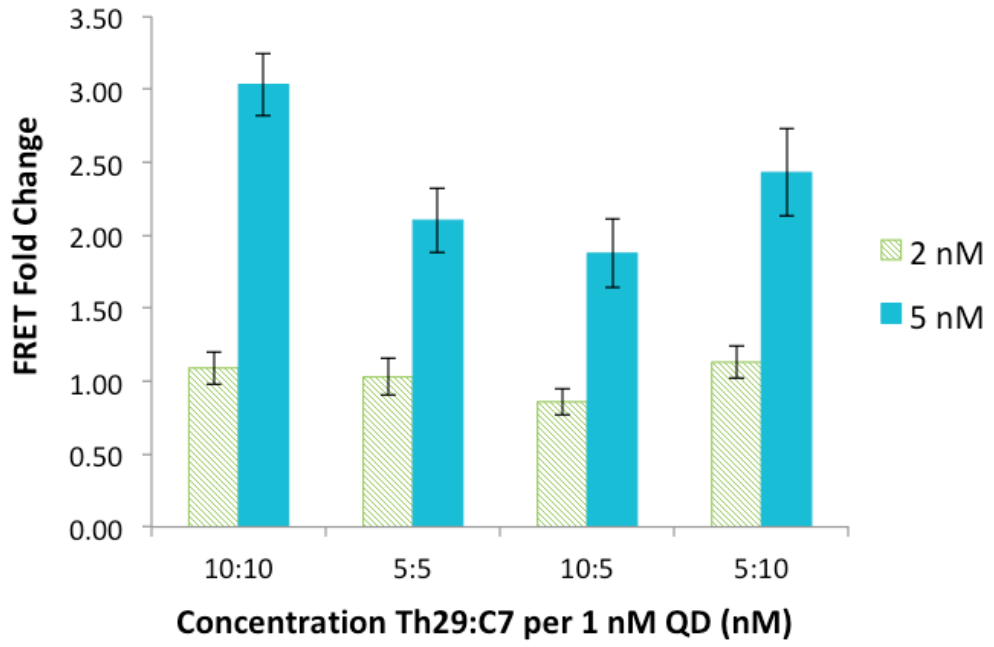

Figure 4.4 Optimization of QD probe preparation by varying the amount and ratio of **Th29** aptamer and **C7**.

Streptavidin has 4 binding sites per molecule that are able to interact with biotin. Dye probes are prepared with biotin/streptavidin interactions and can have multiple configurations. Figure 4.5 (A) shows different configurations of the dye probe. All previous experiments had utilized a 1:1 **Th15** to **DS** configuration but, the FRET fold change from this probe configuration does not appear to be the highest. The best FRET fold change result appears to be from the 1:2 (**Th15**:**DS**) configuration. This configuration allows for 2 dye acceptors (**DS**) for every probe that interacts with the thrombin target. However, this configuration had a higher background signal than the 1:1 configuration, which could effect the eventual LOD. In Figure 4.5 (B) the length of the spacer region of the dye labeled sequence is optimized. The 11-nm sequence (**DS**) had been used for all previous experiments, using only a polyT spacer to achieve this length. If this length is insufficient and both the QD and dye probes bind to the target protein, the dye sequence would not be long enough to hybridize with the complementary sequence on the QD for FRET detection. By modifying the sequence to include an internal spacer, the length can be increased to 15 nm (**DS-L**), as shown in Table 5.1. From Figure 4.5 (B) it appears that both the shorter **DS** and the longer **DS-L** give similar results, within error. This suggests that the **DS** has sufficient length to allow hybridization with the complementary sequence to occur, and FRET detection can be achieved.

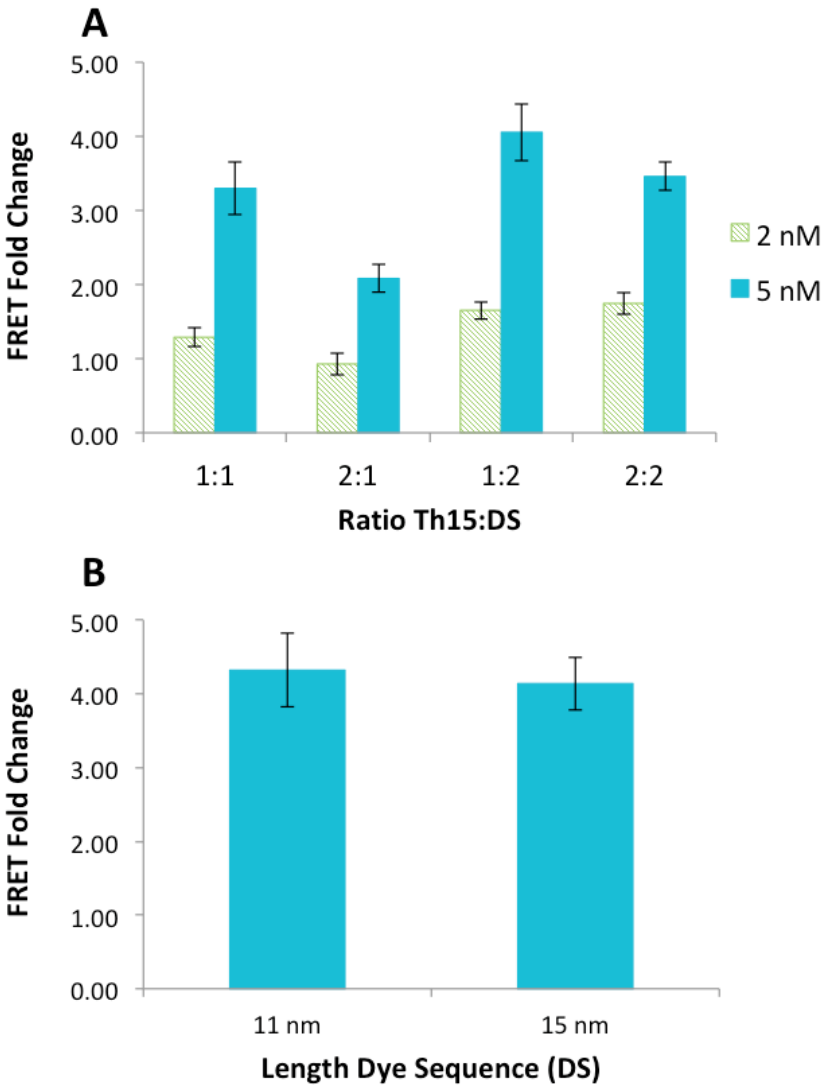

Figure 4.5 Optimization of dye probe preparation. (**A**) Ratio of **Th15** aptamer to **DS**. (**B**) Length of dye sequence.

The choice of using **Th29** for the QD probe and **Th15** for the dye probe was a starting point. Using the previously described optimized conditions, the assay was tested by exchanging the aptamers on each probe. Figure 4.6 shows that the original QD with

the **Th29** aptamer and the Dye with the **Th15** aptamer have the same results as the reverse of this situation. This suggests that the binding of probes to the thrombin target occurs in either situation.

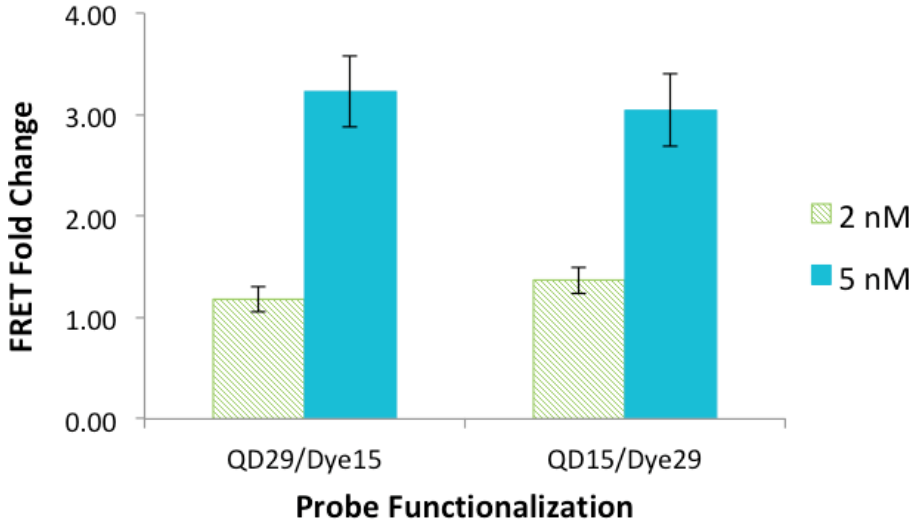

Figure 4.6 Optimization of a specific aptamer on a specific probe. In the case of QD29/Dye15, the 29−nt aptamer was conjugated onto the QD and the 15−nt aptamer was on the dye sequence (**DS**). The two aptamers were switched in the QD15/Dye29 design.

Figure 4.7 shows the probe stability during storage at 4°C. QD and Dye probes were prepared on Day 1, and fresh protein samples were prepared each day for FRET detection. On Day 1 of preparation, the FRET fold change signal is strong, however, even after storage for 2 days, the signal decreased. As storage time increases, the FRET fold change signal decreased further. These results suggest that with storage of prepared probes at 4°C, the probes begin to degrade even after 2 days. To avoid probe

degradation, probes were prepared fresh each day for thrombin detection, according to the procedure described in 4.2.2.

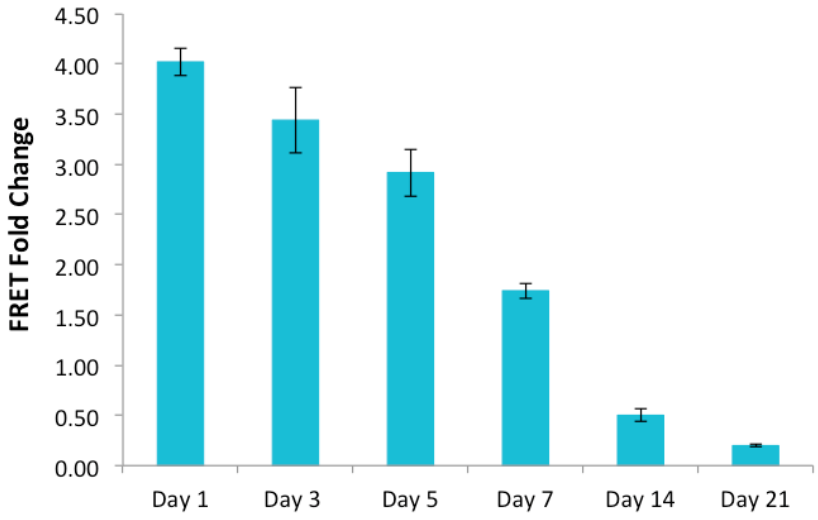

Figure 4.7 Test of probe stability with storage at 4°C. The probes stored for 1-21 days were used for the detection of freshly prepared 5 nM thrombin.

4.3.3 Optimization of Assay with 2 Dye Sequences per Th15 Aptamer on Probe

For all the above optimization experiments, a ratio of 1 **DS** to 1 **Th15** sequence was used. From Figure 4.5 (A) it appears that this dye probe configuration may not give the best FRET fold change for thrombin detection. Figure 4.8 shows the re-optimization of the assay, but with a ratio of 2 **DS** per 1 **Th15** sequence. Figure 4.8 (A) shows the optimization of the QD probe preparation by varying the amounts of **Th29** aptamer and **C7** sequence functionalized to the particle. From these results, it is clear that 10 **Th29** sequences and 10 **C7** sequences gave the best FRET fold change and proportional signal

between the two concentrations tested. Figure 4.8 (B) shows the optimization of the probe ratio by varying the ratio of dye probe to QD probe. By maintaining the QD probe at 1 nM, the dye probe ratio at 5x and 10x excess showed the highest FRET fold change. By utilizing the 10:1 dye probe to QD probe ratio, the overall concentration of thrombin aptamers between probes was consistent, allowing for equal binding of probes to the same protein target. In Figure 4.8 (C), the concentration of probes was optimized while maintaining a 10:1 dye probe to QD probe ratio. These results indicate that increasing the concentrations of probes gave lower FRET fold change signal due to an increase in the background signal. Thus, for subsequent experiments, a 10 nM Dye probe and a 1 nM QD probe were used.

Overall, the re-optimization of assay parameters with the 2 **DS** per **Th15** aptamer dye probe configuration yielded the same optimized conditions as with the 1 **DS** per **Th15** aptamer. The overall FRET fold change signal was slightly higher than that for 1 **DS**, which is due to the extra **DS** brought into close proximity to QD donors. This, however, also resulted in a higher background signal at 680 nm, which is an important parameter in the calculation of FRET fold change. For higher sample concentrations, this has minimal effect, but for low concentrations, the background signal could limit the assay.

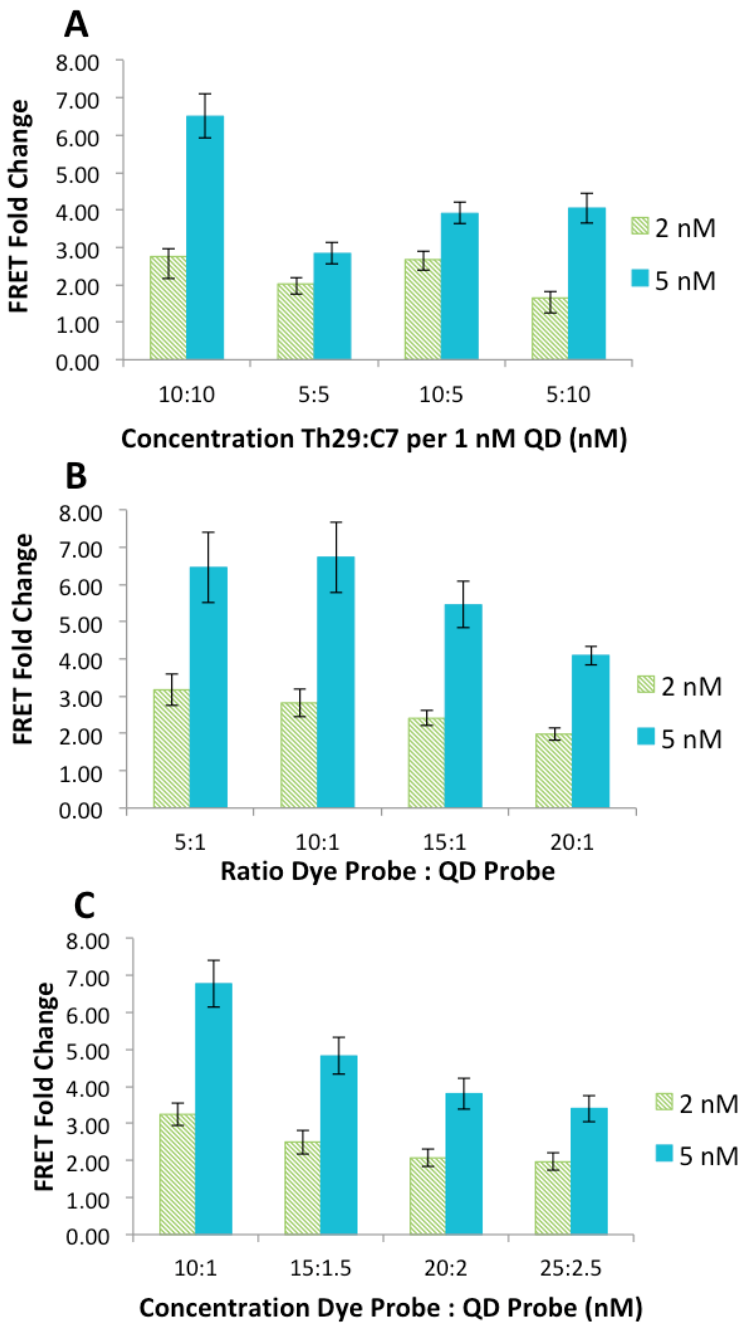

Figure 4.8 Optimization of the assay with 2 **DS** per **Th15** aptamer sequence. (**A**) Optimization of the QD probe preparation by varying the amount and ratio of **Th29** aptamer and 7 nucleotide long complementary sequence. (**B**) Optimization of the probe, while maintaining the QD probe at 1 nM. (**C**) Optimization of the probe concentration.

4.3.4 Calibration Curves for the Detection of Human α-Thrombin

With all optimized conditions, calibration curves were constructed for both the 1:1 (blue diamond) and 2:1 (orange square) (**DS**:**Th15**) dye probe configuration (Figure 4.9). For both cases, the data was linear from 0.1−5.0 nM human α-thrombin. The 1:2 configuration has a slightly larger slope, but as the intercept is higher, LOD is higher. This is due to a higher background. The 1:1 configuration has a slightly smaller slope, but the intercept is lower with less error, resulting in a lower detection limit. From this data, the LOD is 67 pM for the 1:1 configuration and 233 pM for the 2:1 configuration.

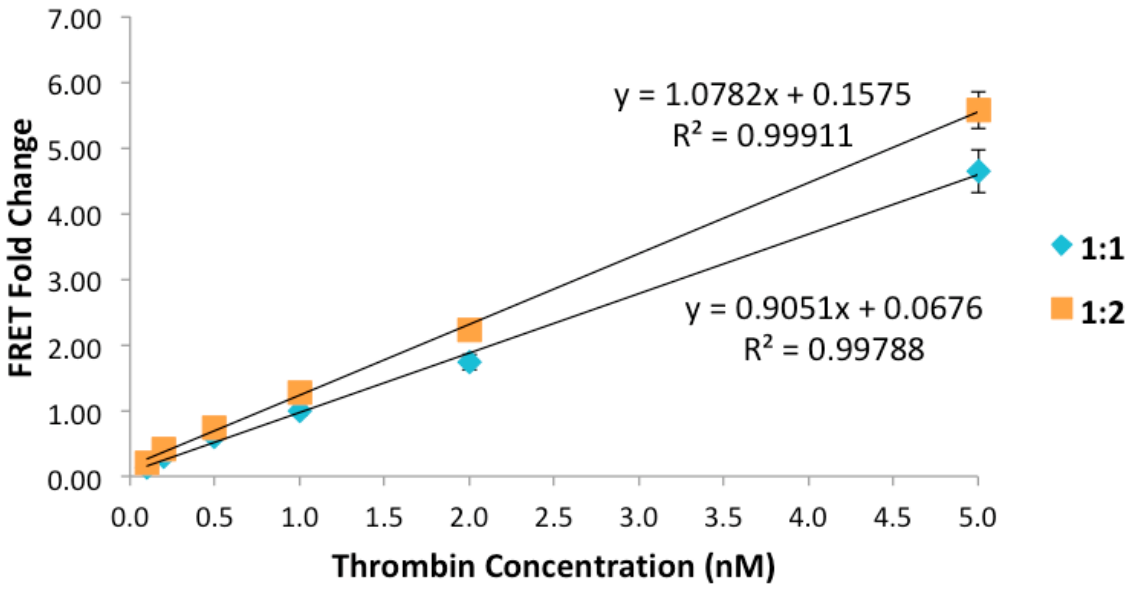

Figure 4.9 Calibration curves for the detection of human α-thrombin for both 1 dye sequence (blue diamonds) and 2 dye sequences (orange squares) per dye probe.

As previously stated, the biologically relevant concentration of α-thrombin can range from pM to μM.[158,159] This developed assay does not have such a large linear range. However, the probe concentrations are low (1 nM QD probe and 10 nM dye probe). By tuning these probe concentrations, the linear range of the assay could be adjusted for relevant protein levels.

There have been other examples of thrombin detection using a single molecular aptamer beacon (MAB). Hamaguchi et al.[46] developed a molecular aptamer beacon technique involving conformational changes in the aptamer upon protein recognition. This conformation change increased the distance between a fluorophore and quencher, increasing the fluorescence signal. Li et al.[48] used a similar process of conformational change of an aptamer beacon to increase the proximity of a fluorophore and quencher, creating a "turn off" assay with a detection limit of 112 pM. Another group used this MAB conformational change upon protein binding with rt-PCR detection by including PCR primers and the appropriate enzymes.[163] This work was able to detect thrombin in cell lysate, but with a detection limit around 0.8 nM.

Heyduk et al.[164] utilized a FRET detection scheme with 2 thrombin aptamers, both functionalized with compatable dyes. Upon both binding to the protein target, the dyes are brought into close proximity and detected with a limit of 50 pM in buffer and low nanomolar concentrations in the cell extract. This reported assay is similar to the developed FRET-BINDA assay, which utilizes QDs as a nanomaterial scaffold and reporter. As the QDs are functionalized with multiple **Th29** aptamers and complementary sequences, an opportunity exists for the detection of multiple targets with one probe, resulting in higher signals.

4.4 Conclusions

A sensitive and specific assay based on binding induced DNA assembly with FRET detection for thrombin has been developed. This BINDA-FRET assay is simple to perform, homogenous, rapid, with mixing and detection carried out at room temperature. The novel use of an aptamer functionalized QD donor and an aptamer functionalized dye acceptor allows for sensitive FRET detection with BINDA specificity to achieve low pM detection limits without the need for an amplification step. This assay can be amended easily for other targets (proteins, DNA, or RNA) by simply changing the affinity ligands and optimizing conditions, as described in this Chapter.

Chapter 5: Sequential Strand Displacement Beacon for Detection of DNA Coverage on Functionalized Gold Nanoparticles[1]

5.1 Introduction

Characterization of surface coverage of DNA functionalized AuNPs is critical for using AuNPs in therapeutic settings for diagnostics, imaging, and drug delivery.[105,106] The current conventional method uses a fluorescence turn-on assay to measure the density of fluorescently labeled DNA functionalized to AuNPs, but this method cannot measure unlabeled DNA.[165,166] If the AuNP is multi-functionalized, each different DNA sequence must be labeled with a different dye, which increases the cost. When multiple dyes are used, it is also important to note that overlap of emission spectra is an increased concern; this limits the choice of dyes. Other methods include DNA intercalating dye (e.g., OliGreen for ssDNA)[167] and real-time PCR.[168] However, these methods lack the specificity to distinguish different DNA sequences co-functionalized to the same AuNP.

The objective of this chapter is to develop a simple, low-cost, label-free method for the characterization of AuNPs functionalized with multiple DNA oligonucleotides. Figure 5.1 shows the schematic of how characterization occurs. Sequences are released from the AuNP (**D_1** and **D_2**) and mixed with DNA probes (**D_1'I_1** or **D_2'I_2** and **I_1'O** or **I_2'O**) and the universal translator (FQ) to produce a fluorescence signal through strand

[1] This chapter has been published as Paliwoda, R.E.; Li, F.; Reid, M.S.; Lin, Y.; Le, X.C. Sequential Strand Displacement Beacon for Detection of DNA Coverage on Functionalized Gold Nanoparticles. *Anal. Chem.* **2014**, 86(12), 6138-6143.[183] Reprinted and adapted with permission. Copyright 2014 American Chemical Society.

displacement reactions. Without the initial DNA released from the AuNP (**D_1** or **D_2**), these reactions cannot occur.

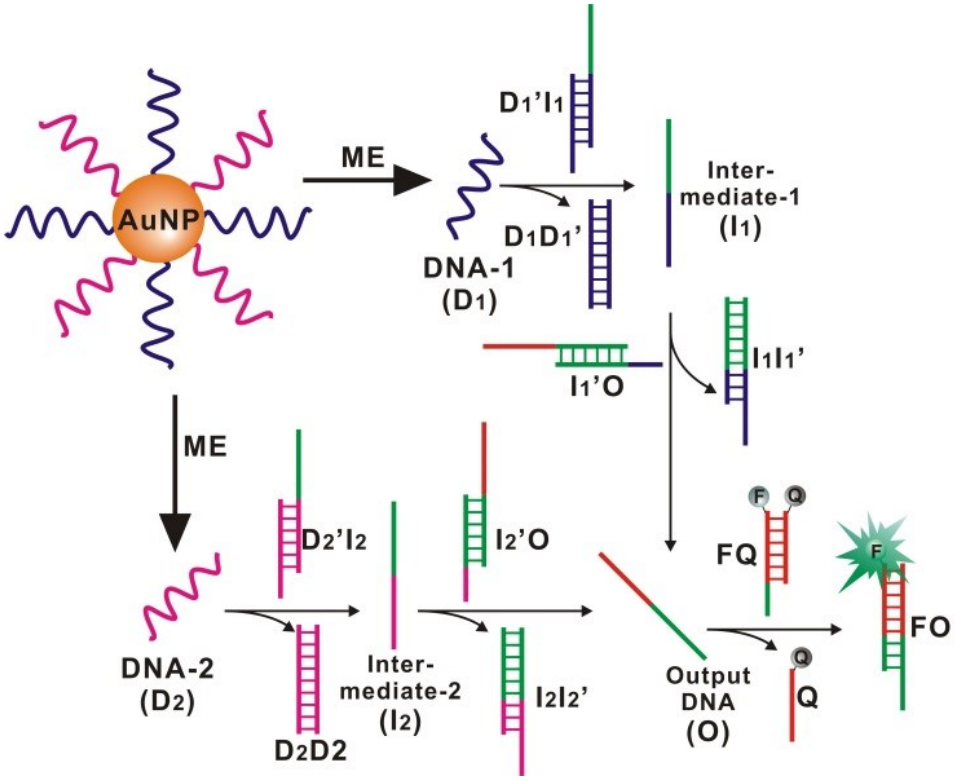

Figure 5.1. Schematic illustrating the use of sequential DNA strand displacement reactions and displacement beacon to quantify multiple DNA oligonucleotides on the same AuNP.

5.2 Experimental Methods

5.2.1 Materials and Reagents

The solution of gold nanoparticles (AuNPs) (20 nm in diameter, 7.0×10^{11}) was purchased from Ted Pella (Redding, CA). Tris−HCl buffer (1 M, pH 7.4), NaCl, 100x Tris EDTA buffer (1.0 M Tris−HCl, 0.1 M EDTA, pH 8), and 2-mercaptoethanol (ME)

were purchased from Sigma-Aldrich (Oakville, ON, Canada). Tween20 and $MgCl_2$ were purchased from Fisher Scientific (Nepean, ON, Canada). OliGreen ssDNA binding dye was purchased from Life Technologies (Burlington, ON, Canada). All DNA (Table 5.1) were synthesized and purified by Integrated DNA Technologies Inc. (Coralville, IA). Nanopure H_2O (>18.0 MΩ), purified using an Ultrapure Milli-Q water system, was used for all experiments.

Table 5.1 DNA sequences and modifications for sequential strand displacement.

DNA Name	Sequence
DNA-1 (**D_1**)	5′ - SH -TTT TTT TTT GAG TCT TCC AGT GTG ATG ATG GTG A - 3′
D_1'	5′ - T CAC CAT CAT CAC ACT GGA AGA CTC - 3′
I_1	5′ - C AGT GTG ATG ATG GTG ACG TAA TCA GGC TAC ACT CAG ACC TTG - 3′
I_1'	5′ - CAA GGT CTG AGT GTA GCC TGA TTA CGT CAC CAT C - 3′
O	5′ - CG TAA TCA GGC TAC ACT CAG ACC TTG CGA TAG CAG TAC ATT CCG AT - 3′
F	5′ - FAM - AT CGG AAT GTA CTG CTA TCG CAA GGT CT - 3′
Q	5′ - CGA TAG CAG TAC ATT CCG AT – IowaBlack - 3′
D_1-FAM	5′ - TTT TTT TTT GAG TCT TCC AGT GTG ATG ATG GTG A – FAM - 3′
D_1-TAMRA	5′ - TTT TTT TTT GAG TCT TCC AGT GTG ATG ATG GTG A – TAMRA - 3′
DNA-2 (**D_2**)	5′ - SH-TTT TTT TTT ATC GAC ATC ACC TAC GAT CTA TCA A - 3′
D_2'	5′ - T TGA TAG ATC GTA GGT GAT GTC GAT - 3′
I_2	5′ - C ACC TAC GAT CTA TCA ACG TAA TCA GGC TAC ACT CAG ACC TTG - 3′
I_2'	5′ - CAA GGT CTG AGT GTA GCC TGA TTA CGT TGA TAG C - 3′

5.2.2 Preparation of DNA Functionalized Gold Nanoparticle

Thiolated DNA oligonucleotides (Table 5.1) were used in the preparation of DNA−AuNPs. These DNA oligonucleotides were diluted to 5 μM in 200 μL with Tris−HCl buffer. This solution was mixed with 1 mL of AuNPs (1 nM) and left to incubate in the dark overnight. To this mixture, 50 μL of 3 M NaCl was added slowly, followed by 15 sec of sonication. This process was repeated 3 times with 30 min intervals to a final salt concentration of 300mM. After incubation overnight in the dark, the solution of DNA-AuNPs was centrifuged at 13,000 rpm for 30 min to separate DNA−AuNPs from the unreacted reagents. Then, the DNA−AuNPs were washed twice with 10 mM Tris−HCl (pH 7.4) and finally redispersed in 200 μL 20 mM Tris−HCl. Functionalized AuNPs were stored at 4°C in the dark until used.

5.2.3 Preparation of DNA Probes for Strand Displacement Beacon FQ and Sequential Strand Displacement Reactions

The DNA probe (**D_1'I_1** as an example) was prepared for sequential strand displacement reaction by mixing 100 μL 5 μM **D_1'** and 100 μL 5 μM intermediate strands **I_1** in TE−Mg buffer. The mixture was heated to 90°C for 5 min, and then the solution was allowed to cool down slowly to 25°C for 2 h. Similarly, the displacement beacon **FQ** was prepared by mixing 100 μL of 5 μM DNA probe **F** and 100 μL of 10 μM probe **Q**. The mixture was heated to 90°C for 5 min, and then the solution was allowed to cool down slowly to 25°C for 2 h.

5.2.4 Measuring DNA Density on AuNPs Using Sequential DNA Strand Displacement Reactions

DNA oligonucleotides were released first from the AuNPs by adding 80 μL of freshly prepared 50 mM ME into 20 μL of the DNA-AuNP solution, and this mixture was incubated in the dark at room temperature for 3 h. A solution containing DNA strand displacement probes and a displacement beacon was added to the mixture to a final concentration of 50 nM each. An aliquot of this mixture (90 μL) was added to a 96-well microplate, and fluorescence was measured using a multimode microplate reader with an excitation/emission wavelength of 485 nm/535 nm for FAM labelled DNA and excitation/emission wavelength of 535 nm/595 nm for TAMRA labelled DNA. All DNA−AuNPs were prepared in duplicate under identical conditions, and each DNA−AuNP solution was analyzed in triplicate. Therefore, each DNA density value was obtained from an average of 6 measurements. For calibration, external DNA standards (identical DNA oligonucleotides but not conjugated to AuNP) with varying concentrations were treated and measured under the same conditions as for DNA−AuNP samples.

5.2.5 Measuring DNA Density on AuNPs Using Fluorescence Turn-On Assay

Similar to the sequential strand displacement assay, FAM-labelled or TAMRA-labelled DNA oligonucleotides were released first from DNA−AuNPs by adding 80 μL of freshly prepared 50 mM ME into 20 μL of the DNA−AuNP solutions. After incubating in the dark for 3 h, fluorescence measurements were performed using a multimode microplate reader, as described above. For calibration, FAM-labelled or TAMRA-

labelled DNA oligonucleotides with varying concentrations were used as external standards and were measured in the same way as the DNA−AuNPs.

5.2.6 Measuring DNA Density on AuNPs Using OliGreen Assay

Similar to the sequential strand displacement assay, unlabelled DNA oligonucleotides were released first from 20 μL DNA−AuNPs with 80 μL of freshly prepared 50 mM ME. Standard DNA oligonucleotides with varying concentrations were treated the same way as the DNA−AuNPs. OliGreen dye was prepared as specified by the manufacturer and added to DNA solutions. After 5 min, 100 μL of each mixture was transferred into a 96-well microplate. Fluorescence was measured using the multimode microplate reader with an excitation/emission wavelength of 485 nm/535 nm for Oligreen dyes. Intercalation of the Oligreen dye into the targeted DNA oligonucleotides gave rise to fluorescence.

5.3 Results and Discussion

5.3.1 Feasibility of Sequential Strand Displacement

A specific target DNA **D_1**, output DNA **O,** and strand displacement beacon **FQ** that can only be specifically turned on by **O** was designed first to examine the feasibility of the sequential strand displacement strategy. Based on the DNA sequences of **D_1** and **O** (Table 5.1), a pair of DNA probes (**D_1'I_1** and **I_1'O)** was designed next. **I_1** consists of two pre-designed sequences: a 17-n.t. region (blue color in Table 5.1) that is identical to a

portion of the target DNA **D_1** and a 26-n.t. sequence (green) that is identical to a portion of the output DNA **O** (Figure 5.2 and Table 5.1).

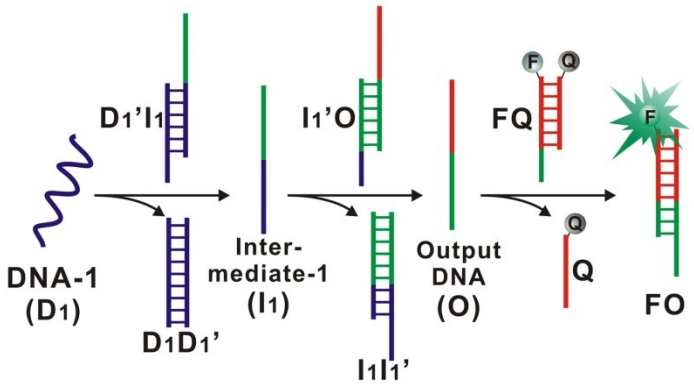

Figure 5.2 Schematic illustrating the sequential DNA strand displacement reactions and strand displacement beacon (**FQ**) to quantify DNA-1 (**D_1**) in PBS buffer.

Figure 5.3 shows the overall kinetic profile of the sequential DNA strand displacement reactions from **D_1** (target) to **FO** (signal read-out). A continuous increase in fluorescence signal (blue curve) is observed over the course of 120 min after the addition of 50 nM of DNA-1 (**D1)** to an incubation solution containing **D_1'I_1**, **I_1'O**, and **FQ**. Only background fluorescence is observed from the negative control that contains all the reagents (**D_1'I_1**, **I_1'O**, and **FQ**) but no target DNA (**D_1**) (red curve). These results suggest that our strand displacement beacon can respond quickly to the target DNA. There is no apparent increase in background fluorescence generated over 2 h after premixing all the probes and reagents.

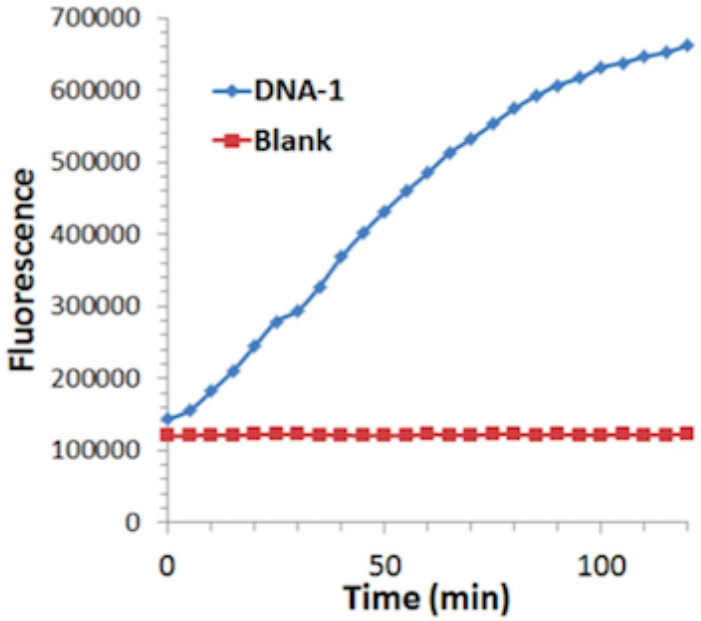

Figure 5.3 Kinetics of sequential DNA strand displacement reactions observed from monitoring the specific DNA-1 (50 nM) and reagent blank.

Calibrations between the fluorescence intensities and concentrations of $\mathbf{D_1}$ (Figure 5.4) are linear within the concentration range from 0 nM to 30 nM, at both 30 min ($R^2 = 0.9967$) and 60 min ($R^2 = 0.9966$).

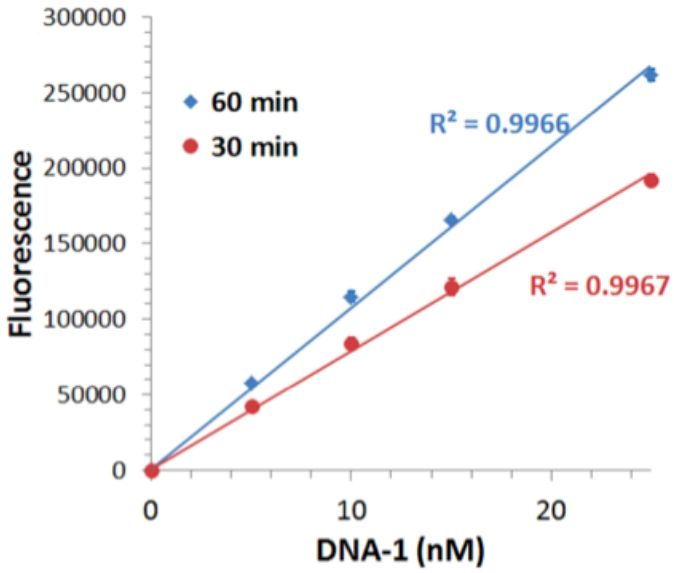

Figure 5.4 Fluorescence intensity from the displacement beacon analysis as a function of concentrations of DNA-1 (**D_1**) in solution after 30 and 60 min incubation.

To test the specificity of the approach, probes that are specifically designed for the target DNA-1 (**D_1**) were used to detect the target DNA (**D_1**) and a non-specific DNA were used. Figure 5.5 shows that the assay gives a concentration-dependent fluorescence response from the target DNA (blue circles) and that there is no fluorescence increase from the analysis of the non-specific DNA (red squares). The results suggest that the sequential strand displacement assay is able to quantify specific DNA sequences without interference from other DNA that may be present in the same sample.

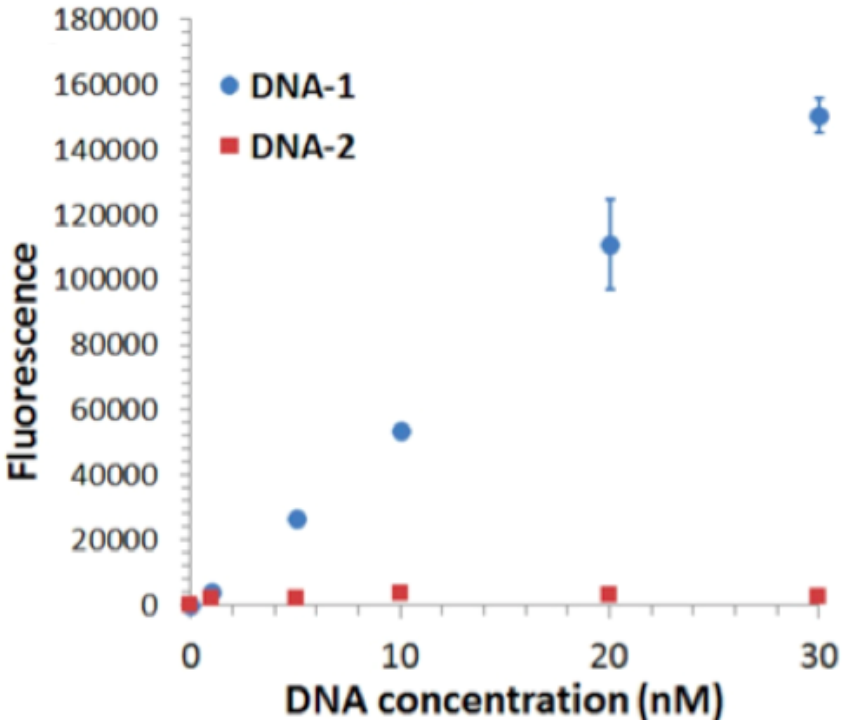

Figure 5.5 Specificity test of the sequential strand displacement assay, showing the concentration dependence for the specific DNA-1 and a negligible background from a non-specific DNA (DNA-2).

5.3.2 Quantification of DNA Conjugated to AuNPs

The surface density of a DNA sequence conjugated to AuNPs was quantified to demonstrate an application of this technique. $\mathbf{D_1}$ was conjugated to AuNPs through sulfur−gold bonds according to a previously reported method.[58] The concentration of $\mathbf{D_1}$ and AuNPs used in the reaction was in a ratio of 1000 to 1. $\mathbf{D_1}$ was released from AuNPs by adding 50 mM ME, and the DNA concentration in this solution was

determined using the sequential strand displacement assay. A mixture of beacon probes (**D_1'I_1**, **I_1'O**, and **FQ**) was added to the solution and incubated for 60 min in the dark. In parallel, unconjugated **D_1** served as an external standard for calibration (Figure 5.6). The amount of specific DNA (**D1)** released from the gold nanoparticle (**D_1**-AuNPs) was able to be quantified.

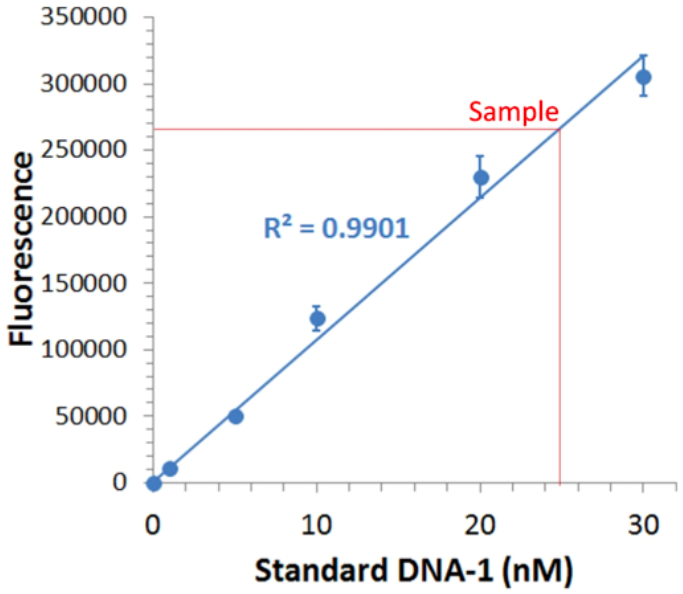

Figure 5.6 Standard curve of unconjugated D_1 to quantify DNA released from AuNP using strand displacement reaction.

Under the given conditions of DNA conjugation to the AuNPs, we measured the density of the DNA on AuNPs to be 201 ± 11 oligonucleotides per AuNP (Figure 5.6). A previously reported OliGreen assay[167] (Figure 5.7) was used to measure the density of DNA on AuNPs, and a value of 207 ± 22 oligonucleotides per AuNP was obtained. The

good agreement between the values obtained with the sequential strand displacement assay and the OliGreen assay supports the accuracy of the assay.

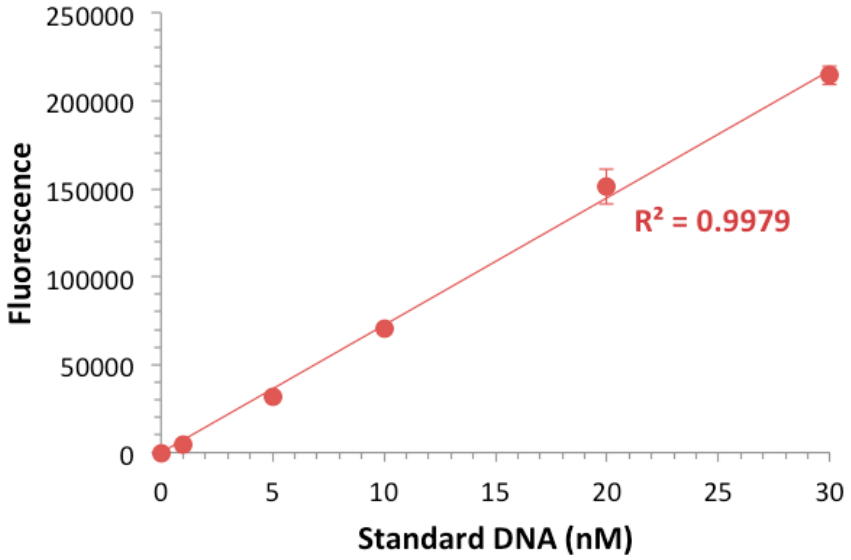

Figure 5.7 Standard curve using OliGreen assay to determine DNA released from AuNP.

The sequential strand displacement assay was applied further to the detection of different DNA densities on AuNPs. A series of DNA−AuNPs was prepared with different densities by co-conjugating DNA-1 and a short polyT DNA oligonucleotide (spacer oligo). The overall number of DNA oligonucleotides on each AuNP was kept constant. By tuning the ratio between DNA-1 and the spacer oligo (from 1000:0, 750:250, 500:500, 250:750, and 0: 1000) at the conjugation step, different densities of DNA-1 on the AuNP were achieved. As shown in Figure 5.8, the measured densities of

DNA-1 on AuNP decreased as the amount of DNA-1 was reduced at the conjugation step. The results demonstrate that the assay is able to quantify a range of DNA densities on AuNPs. The measurement background is negligible when no DNA-1 is added during the conjugation step. This is consistent with the excellent specificity of the assay.

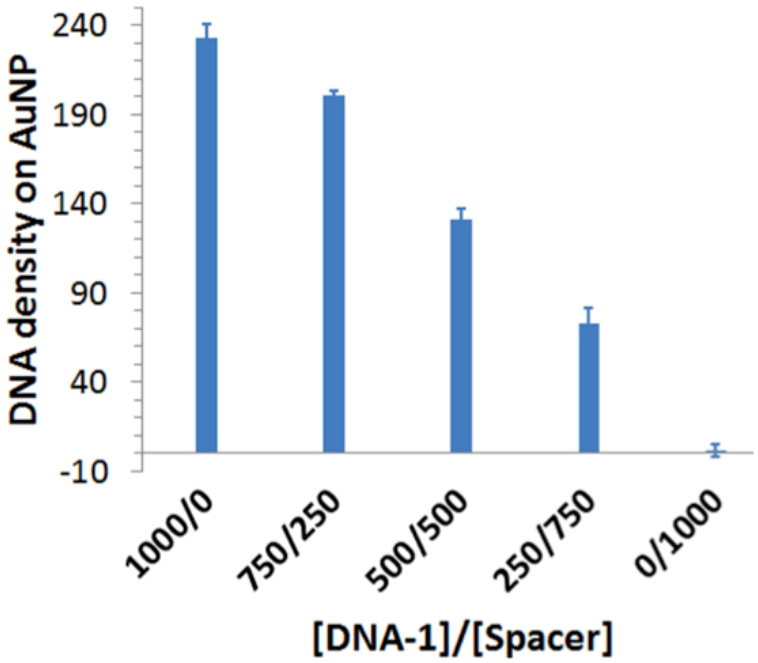

Figure 5.8 Quantifying DNA densities of control functionalized AuNPs using strand displacement reactions.

DNA used for feasibility testing was ordered from IDT as HPLC purified products. This procedure increases the cost of the DNA compared to standard desalted samples. Figure 5.9 compares DNA densities determined using the developed sequential strand displacement assay method of HPLC purified DNA and standard desalted DNA. DNA sequences with modifications (thiolated, with FAM, or with quencher) were

HPLC purified in order for the assay to have optimal results. From Figure 5.9, it is clear that the standard desalting was sufficient for the purification of unmodified sequences as the determined densities are comparable (222 ± 8 for HPLC purified and 236 ± 24 for standard desalting).

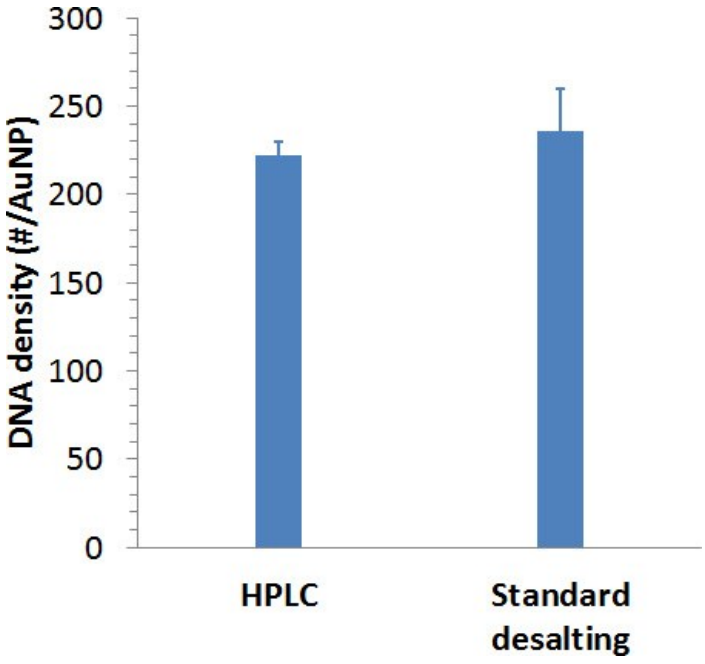

Figure 5.9 Comparison of HPLC purification and standard desalting of DNA for the determination of DNA density on AuNP using sequential strand displacement assay.

5.3.3 Quantification of DNA Density on Multifunctionalized AuNP

Unlike other existing methods that require labeling multiple DNA oligonucleotides with different fluorescent dyes, our technique has the ability to quantify multiple unlabelled DNA oligonucleotides co-conjugated on the same AuNP. As an example, the detection of two DNA sequences ($\mathbf{D_1}$ and $\mathbf{D_2}$) co-conjugated to the same AuNPs is shown (Table

5.1). The density of **D_1** and **D_2** was measured in parallel by applying specific DNA probes: **D_1'I_1** and**I_1'O** for detection of **D_1** and **D_2'I_2** and **I_2'O** for detection of **D_2**. The measured values are 93 ± 6 DNA sequence **D_1** per AuNP and 117 ± 4 DNA sequence **D_2** per AuNP (Table 5.2). **D_1** and **D_2** were conjugated separately to different AuNPs, and the densities of each sequence on AuNPs were determined. The total amount of DNA was kept constant for the different conjugation experiments. The measured DNA density values, 222 ± 8 and 233 ±12, are consistent with the sum of **D_1** and **D_2** co-conjugated on the same AuNP (210 ± 10) (Table 5.2). The results further confirm that the sequential strand displacement assay has the ability to quantify multiple DNA oligonucleotides from AuNPs.

Table 5.2 DNA densities on multi-functionalized **D_1-D_2**-AuNP and mono-functionalized **D_1**-AuNP and **D_2**-AuNP.

Density (#/AuNP)	D_1-D_2-AuNP	D_1-AuNP	D_2-AuNP
D_1 (DNA-1)	93 ± 6	222 ± 8	0
D_2 (DNA-2)	117 ± 4	0	233 ± 12
Total	210 ± 10	222 ± 8	233 ± 12

5.3.4 Comparison of Developed Method with Conventional Fluorescent Labelled Techniques

Having established the method to determine unlabelled DNA oligonucleotides on AuNPs, we assessed the ability of the fluorescent labelling used in the conventional method to observe the influence of DNA density on AuNPs. FAM and tetramethylrhodamine (TAMRA) were tested, as they are the two most widely used

fluorescence labels for measuring DNA oligonucleotides by fluorescence turn-on assays. The results are summarized in Table 5.3. The density of **D_1**-AuNP was measured by the sequential strand displacement assay and the density of FAM-**D_1**-AuNP was measured by the fluorescence turn-on assay. The density of TAMRA-**D_1**-AuNP was measured by both the fluorescence turn-on assay and the sequential strand displacement assay. When the DNA is labelled with FAM, the density measured (226 ± 10) using a fluorescence turn-on assay is comparable to the density of the unlabelled DNA (222 ± 8) measured using the sequential strand displacement assay. However, when the DNA is labelled with TAMRA the density of this DNA conjugated on AuNPs is 153 ± 5, a decrease of more than 30% from the unlabeled DNA (222 ± 8). The values obtained from the sequential strand displacement assay (147 ± 2) and from the fluorescence turn-on assay (153 ± 5) are consistent. These results confirm that the TAMRA labelling of DNA decreases the number of the DNA molecules being conjugated on the surface of AuNPs. This observation is consistent with previous reports that TAMRA has a strong interaction with the surface of AuNPs.[169] Thus, TAMRA labelling may alter the interaction between DNA and AuNPs, leading to a decrease in the surface coverage of DNA.

Table 5.3 DNA densities on various DNA-AuNP conjugates: **D_1**-AuNP, FAM-**D_1**-AuNP, and TAMRA-**D_1**-AuNP.

Density (#DNA/AuNP)	Strand displacement assay	Fluorescence turn-on assay
D_1 (DNA-1)	222 ± 8	N.A.
FAM-D_1	N.A.	226 ± 10
TAMRA-D_1	147 ± 2	153 ± 5

5.4 Conclusions

In summary, a simple, low-cost sequential strand displacement assay that is able to measure the average number of DNA molecules on each AuNP directly has been developed successfully. The sequential strand displacement assay does not require fluorescent labeling of the target DNA, thereby eliminating the effect of fluorescent dyes on the surface coverage of DNA. Particularly, multiple DNA oligonucleotides that are co-conjugated on the same AuNP can be quantified specifically through unique DNA strand displacement reactions and a universal displacement beacon. Furthermore, the developed method has a subnanomolar detection limit. This is comparable to that obtained by most fluorescence-based assays, such as the conventional fluorescence turn-on assay (OliGreen assay). Another benefit is that the strand displacement probes do not need to be purified with HPLC; a simple desalting procedure is sufficient, eliminating the HPLC purification step and reducing the reagent costs. The universal strand displacement strategy is not limited to DNA−AuNPs but can be expanded to other DNA hybrid materials, allowing for better characterizations and applications.

Chapter 6: Overall Conclusions and Future Work

I have developed assays for the specific detection of DNA, microRNA, and proteins that utilize DNA nanostructures. This work explores the use of nanomaterials as both a tool for detection and as scaffolding in the construction of DNA nanostructures. Specifically, Chapters 2 and 3 utilize QDs as a FRET donor after the formation of a 3WJ for the detection of both DNA and microRNA. Chapter 4 also uses QDs as a FRET donor, but using BINDA, for the detection of a protein target. Chapter 5 utilizes toehold−mediated strand displacement for the characterization of DNA functionalized AuNPs.

In Chapter 2, I focused on the development of a target−responsive 3WJ with FRET detection. In this Chapter, the assay was optimized with a DNA target to understand important assay parameters. I found that the assay was able to detect a target DNA sequence with high specificity and pM detection limits. This assay also was used for the detection of SNPs. By designing the probes to have common mismatches in the middle of the hybridization region, I was able to detect SNPs with very high discrimination factor (DF). The strength of this assay lies in the ability to design the 3WJ probes specifically for the desired target. This assay uses the novel approach of QDs both as a scaffold for construction of a 3WJ probe and as a FRET donor when the 3WJ is formed. Without the presence of the target, the 3WJ cannot form and FRET detection cannot occur, resulting in little background signal.

In Chapter 3, I extended the assay principle from Chapter 2 to the detection of microRNA detection. microRNA detection has unique challenges compared to DNA

detection, including weakened DNA/RNA hybridization, short microRNA length, and RNA stability due to the RNAse activity and contamination. Through re-optimization of important assay parameters, I was able to detect pM levels of a microRNA target specifically. This novel use of QD for FRET detection of microRNA with a 3WJ was rapid and sensitive to the desired target compared to a non-specific target. In comparison to other non-amplification detection methods, this 3WJ FRET strategy is comparable.[147,148]

In Chapter 4, I described the use of the same QD/Cy5 FRET detection method used in Chapters 2 and 3, but for the detection of a protein target. Using two different affinity ligands for affinity probes, a single target was able to be detected specifically with low pM limits. This developed assay utilizes the highly sensitive BINDA technique combined in a novel way with QD FRET detection. Without the binding of both affinity probes to the same target protein, FRET detection cannot occur, resulting in a minimal background signal. This developed assay can be applied to other targets with multiple affinity ligands, such as **p**latelet-**d**erived **g**rowth **f**actor (PDGF), which plays an important role in regulating cell growth and division and is commonly misregualted in various cancers.[170,171]

In Chapter 5, I developed an assay to characterize surface coverage of unlabeled DNA functionalized AuNPs through a series of toehold−mediated strand displacement reactions. This assay was able to characterize mono- and di- functionalized AuNPs but can easily be amendable to a multifunctionalized AuNP by simply changing strand displacement probes. The achieved sub nanomolar detection limits are relevant for functionalized AuNPs used in assays such as for drug delivery or biomolecule

detection.[172–175] This developed assay was able to confirm previous findings that TAMRA has a strong interaction with the surface of AuNPs, and should not be used as a labeling dye for oligonucleotides in the presence of AuNPs.[169]

Detection of biomolecules is important for many aspects of disease diagnosis and prognosis. Testing methods, notably those in resource limited settings, are aimed towards achieving **p**oint **o**f **c**are (POC) detection. POC assays have many goals, particularly diagnostic testing of non-invasive samples at the time and place of patient care. POC assays aimed to meet ASSURED criteria are:[176]

-Affordable

-Sensitive with few false negatives

-Specific with few false positives

-User-friendly with simple to perform actions

-Rapid and Robust

-Equipment free

-Deliverable to those in need

These criteria aim to provide detection of disease biomarkers but, also importantly, to reduce emergency room wait times, reduce outpatient visits, and ensure optimal use of trained professionals' time. My developed FRET assays are affordable, sensitive to low levels of target, specific for desired target, user-friendly with no separation steps required, and rapid with under 30-min detection times. To achieve ASSURED criteria,

the developed assays would require a longer shelf life, which could potentially be achieved, as DNA is very stable; however, work would need to be done to ensure that the functionalization to QDs is stable. The only equipment required for detection is a fluorescence reader, which is relatively inexpensive. The developed assay could be considered deliverable with a handheld fluorescence reader.[177,178] The robustness of the assay has yet to be tested with real−world samples.

The use of aptamers and nanotechnology as part of POC testing have established a new focus in diagnostics and biosensing.[179,180] Aptamers have incurred increasingly great interest for diagnostics and therapeutics due to their ease of functionalization with nanomaterials and fluorophores, little synthesis variation, high stability, and high specificity.[181] Combining aptamers, DNA nanostructures, and nanomaterials shows promise in improving the sensitivity of detection systems with simple readout. Specifically, the developed assays do not require amplification for sensitive detection, allowing for very little technical training and hands on work and short analysis time with homogeneous detection in a simple fluorescence plate reader. Also, by combining DNA nanostructure and nanomaterials for diagnostics and biosensing, the characterization of nanomaterials is important to obtain quantitative results.

For all experiments FRET Fold Change (Eq. 2-1) values were reported. This expression was used because the absolute measured emission from dye was very low when compared to the emission from the QD donor. Using Eq. 2-1 takes into account the signal of the dye acceptor and QD donor, as well as measurements for blank signals. This is not the traditional way to express a FRET ratio. Conventionally, the FRET Ratio is calculated by:

$$FRET\ Ratio = \frac{I_A - I_A^*}{I_D} \quad \text{(Eq. 6-1)}$$

where I_A is emission intensity of the acceptor (A) in the presence of target and donor (D), I_A^* is the intensity of the acceptor in the absence of the donor but excited at the donor excitation wavelength, and I_D is the emission intensity of the donor upon excitation.[182] This formula does not take into account any potential target non-specific interactions between donor and acceptors on the QD and Dye probes, which is determined with measurement of a blank.

Equation 6-1 can be amended to account for signal from non-specific interactions with blank measurements to the formula below:

$$S/B\ Ratio = \frac{(I_{680} - I_{680}*) \,/\, I_D}{(B_{680} - I_{680}*) \,/\, I_{DB}} \quad \text{(Eq. 6-2)}$$

where I_{680} is emission intensity of the acceptor in the presence of target and donor, I_{680}^* is the intensity of the acceptor in the absence of the donor but excited at the donor excitation wavelength, B_{680} is the emission of the acceptor in the presence of the donor but with no target, I_D is the emission intensity of the donor upon excitation in the presence of target, and I_{DB} is the emission intensity of the donor upon excitation in the absence of target. This equation takes into account signal due to FRET in the presence of a target and the FRET signal due to target non-specific interactions in a blank sample.

Below is a summary of raw values used to make Figure 2.3, reported as mean ± standard deviation (Table 6.1). These values can be used to calculate FRET Fold Change (Eq. 2-1), FRET Ratio (Eq. 6-1), and S/B Ratio (Eq. 6-3).

Table 6.1 Emission values measured for the detection of 5 nM Target DNA used to make Figure 2.3. Values are reported as mean ± standard deviation. NC (I_A^*) is the same value for all **c**/**c*** lengths.

	Sample		Blank		Control
Length of Region **c**/**c***	S_{680} (I_A)	S_{605} (I_D)	B_{680} (I_A)	B_{605} (I_{DB})	NC (I_A^*)
5 nt	7574 ± 429	440836 ± 19188	1757 ± 71	489209 ± 8194	824 ± 82
6 nt	6413 ± 285	454548 ± 17231	1751 ± 93	484351 ± 3707	
7 nt	8463 ± 74	488532 ± 9992	2929 ± 237	488940 ± 27945	

From this raw data, it is clear that the measured emission intensities of the QD donors are 2 orders of magnitude larger than emission from the dye acceptors. If these values were used in Eq. 6-1, calculated FRET Ratios would be much smaller than those calculated by Eq. 2-1 or 6-2. Equation 2-1 takes into account emission from both the dye acceptor and QD donor in both the presence and absence of a target. This equation does, however, inherently subtract 1 from overall ratios and this should be considered when interpreting results.

From the success of protein detection, the developed BINDA-FRET assay could be applied further to another protein target to show assay application, such as in serum. Using the 3WJ FRET, detection of DNA can be performed also in serum to show assay applicability, with further optimization of microRNA detection for serum or testing in cells. Alternate microRNA sequences also could be assessed to show that the developed assay can be used to detect any target. Detection of biomolecule targets in real samples

requires consideration of many factors, including matrix effects, low target concentrations, and the presence of interfering molecules for targeting and sensing. These considerations highlight the balance that needs to be achieved in a clinical setting between sensitivity and specificity to distinguish between false negatives and false positives. High sensitivity assays have the ability to confirm samples without the biomolecule, while assays with high specificity confirm the presence of the target biomolecule. With a balance between these parameters, an assay can be extended from a qualitative to quantitative result for better prognosis.

References

(1) Watson, J. D.; Crick, F. H. C. Molecular Structure of Nucleic Aids: A Structure for Deoxyribose Nucleic Acid. *Nature* **1953**, *171* (4356), 737–738.

(2) Mandelkern, M.; Elias, J. G.; Eden, D.; Crothers, D. M. The Dimensions of DNA in Solution. *J. Mol. Biol.* **1981**, *152* (1), 153–161.

(3) Clausen-Schaumann, H.; Rief, M.; Tolksdorf, C.; Gaub, H. E. Mechanical Stability of Single DNA Molecules. *Biophys. J.* **2000**, *78* (4), 1997–2007.

(4) Bockelmann, U.; Essevaz-Roulet, B.; Heslot, F. Molecular Stick-Slip Motion Revealed by Opening DNA with Piconewton Forces. *Phys. Rev. Lett.* **1997**, *79* (22), 4489–4492.

(5) Clausen-Schaumann, H.; Rief, M.; Gaub, H. E. Sequence Dependent Mechanics of Single DNA Molecules. *Biophys. J.* **1999**, *76* (1), A151–A151.

(6) Chalikian, T. V.; Volker, J.; Plum, G. E.; Breslauer, K. J. A More Unified Picture for the Thermodynamics of Nucleic Acid Duplex Melting: A Characterization by Calorimetric and Volumetric Techniques. *Proc. Natl. Acad. Sci. U. S. A.* **1999**, *96* (14), 7853–7858.

(7) Rich, A.; Davies, D. R. A New Two Stranded Helical Structure: Polyadenylic Acid and Polyuridylic Acid. *J. Am. Chem. Soc.* **1956**, *78* (14), 3548–3549.

(8) Rich, A. A Hybrid Helix Containing Both Deoxyribose and Ribose

Polynucleotides and Its Relation to the Transfer of Information between the Nucleic Acids. *Proc. Natl. Acad. Sci. U. S. A.* **1960**, *46* (8), 1044–1053.

(9) Holley, R.; Apgar, J.; Everett, G.; Madison, J.; Marquisse, M.; Merrill, S.; Penswick, J.; Zamir, A. Structure of a Ribonucleic Acid. *Science* **1965**, *147* (3664), 1462–1465.

(10) Britten, R. J.; Davidson, E. H. Gene Regulation for Higher Cells : A Theory. *Science* **1969**, *165* (3891), 349–357.

(11) Bartel, D. P. MicroRNAs: Genomics, Biogenesis, Mechanism, and Function. *Cell* **2004**, *116* (2), 281–297.

(12) Ambros, V. The Functions of Animal microRNAs. *Nature* **2004**, *431* (7006), 350–355.

(13) Olsen, P. H.; Ambros, V. The Lin-4 Regulatory RNA Controls Developmental Timing in Caenorhabditis Elegans by Blocking LIN-14 Protein Synthesis after the Initiation of Translation. *Dev. Biol.* **1999**, *216* (2), 671–680.

(14) Seggerson, K.; Tang, L.; Moss, E. G. Two Genetic Circuits Repress the Caenorhabditis Elegans Heterochronic Gene Lin-28 after Translation Initiation. *Dev. Biol.* **2002**, *243* (2), 215–225.

(15) Bartel, D. P. MicroRNA Target Recognition and Regulatory Functions. *Cell* **2009**, *136* (2), 215–233.

(16) Fabian, M. R.; Sonenberg, N.; Filipowicz, W. Regulation of mRNA Translation and Stability by microRNAs. *Annu. Rev. Biochem.* **2010**, *79* (1), 351–379.

(17) Grimson, A.; Farh, K. K. H.; Johnston, W. K.; Garrett-Engele, P.; Lim, L. P.; Bartel, D. P. MicroRNA Targeting Specificity in Mammals: Determinants beyond Seed Pairing. *Mol. Cell* **2007**, *27* (1), 91–105.

(18) Doench, J. G.; Sharp, P. A. Specificity of microRNA Target Selection in Translational Repression. *Genes (Basel).* **2004**, *504* (5), 504–511.

(19) Jiang, Q.; Wang, Y.; Hao, Y.; Juan, Y.; Teng, M.; Zhang, X.; Li, M.; Wang, G.; Liu, Y. miR2Disease: A Manually Curated Database for microRNA Deregulation in Human Disease. *Nucleic Acids Res* **2009**, *37*, D98-104.

(20) Lee, R. C.; Feinbaum, R. L.; Ambros, V. The C. Elegans\rheterochronic Gene Lin-4 Encodes Small RNAs with Antisense\rcomplementarity to Lin-14. *Cell* **1993**, *75: 843–85*, 843–854.

(21) Carthew, R. W.; Sontheimer, E. J. Origins and Mechanisms of miRNAs and siRNAs. *Cell* **2009**, *136* (4), 642–655.

(22) Verma, P.; Pandey, R. K.; Prajapati, P.; Prajapati, V. K. Circulating microRNAs: Potential and Emerging Biomarkers for Diagnosis of Human Infectious Diseases. *Front. Microbiol.* **2016**, *7* (AUG), 1–7.

(23) Chen, X.; Ba, Y.; Ma, L.; Cai, X.; Yin, Y.; Wang, K.; Guo, J.; Zhang, Y.; Chen, J.; Guo, X.; et al. Characterization of microRNAs in Serum: A Novel Class of Biomarkers for Diagnosis of Cancer and Other Diseases. *Cell Res.* **2008**, *18* (10), 997–1006.

(24) Bruinsma, I. B.; van Dijk, M.; Bridel, C.; van de Lisdonk, T.; Haverkort, S. Q.;

Runia, T. F.; Steinman, L.; Hintzen, R. Q.; Killestein, J.; Verbeek, M. M.; et al. Regulator of Oligodendrocyte Maturation, miR-219, a Potential Biomarker for MS. *J. Neuroinflammation* **2017**, *14* (1), 1–7.

(25) Chen, C.; Lu, C.; Qian, Y.; Li, H.; Tan, Y.; Cai, L.; Weng, H. Urinary miR-21 as a Potential Biomarker of Hypertensive Kidney Injury and Fibrosis. *Sci. Rep.* **2017**, *7* (1), 1–9.

(26) Bode, A. M.; Dong, Z. Post-Translational Modification of p53 in Tumorigenesis. *Nat. Rev. Cancer* **2004**, *4* (10), 793–805.

(27) Isogai, S.; Shirakawa, M. Protein Modification by SUMO. *Seikagaku* **2007**, *79* (12), 1120–1130.

(28) Cress, W.; Seto, E. Histone Deacetlyases, Transcriptional Control, and Cancer. *J. Cell. Physiol.* **2000**, *184* (1), 1–16.

(29) Zhang, H.; Li, F.; Dever, B.; Li, X.-F.; Le, X. C. DNA-Mediated Homogeneous Binding Assays for Nucleic Acids and Proteins. *Chem. Rev.* **2013**, *113* (4), 2812–2841.

(30) Zhang, H.; Li, F.; Dever, B.; Wang, C.; Li, X.-F.; Le, X. C. Assembling DNA through Affinity Binding to Achieve Ultrasensitive Protein Detection. *Angew. Chem. Int. Ed. Engl.* **2013**, *52* (41), 10698–10705.

(31) Marras, S. A. E.; Tyagi, S.; Kramer, F. R. Real-Time Assays with Molecular Beacons and Other Fluorescent Nucleic Acid Hybridization Probes. *Clin. Chim. Acta* **2006**, *363* (1–2), 48–60.

(32) Engvall, E.; Perlmann, P. Enzyme-Linked Immunosorbent Assay (ELISA) Quantitative Assay of Immunoglobulin G. *Immunochemistry* **1971**, *8* (9), 871–874.

(33) Voller, A.; Bartlett, A.; Bidwell, D. E. Enzyme Immunoassays with Special Reference to ELISA Techniques. *J. Clin. Pathol.* **1978**, *31*, 507–520.

(34) Engvall, E.; Perlmann, P. Enzyme-Linked Immunosorbent Assay, ELISA III. Quantitation of Specific Antibodies by Enzyme-Labelled Anti-Immunoglobulin in Antigen-Coated-Tubes. *J. Immunol* **1972**, *109*, 129–135.

(35) Belanger, L.; Sylvestre, C.; Dufour, D. Enzyme-Linked Immunoassay for Alpha-Fetoprotein by Competitive and Sandwich Procedures. *Clin. Chim. Acta* **1973**, *48* (1), 15–18.

(36) Domon, B.; Aebersold, R. Mass Spectrometry and Protein Analysis. *Science* **2006**, *312* (5771), 212–217.

(37) Cooks, R. G.; Ouyang, Z.; Takats, Z.; Wiseman, J. M. Detection Technologies. Ambient Mass Spectrometry. *Science (80-.).* **2006**, *311* (5767), 1566–1570.

(38) Tyagi, S.; Kramer, F. R. Molecular Beacons: Probes That Fluoresce upon Hybridization. *Nat. Biotechnol.* **1996**, *14*, 303.

(39) Wang, K.; Tang, Z.; Yang, C. J.; Kim, Y.; Fang, X.; Li, W.; Wu, Y.; Medley, C. D.; Cao, Z.; Li, J.; et al. Molecular Engineering of DNA: Molecular Beacons. *Angew. Chemie - Int. Ed.* **2009**, *48* (5), 856–870.

(40) Tan, W.; Wang, K.; Drake, T. J. Molecular Beacons. *Curr. Opin. Chem. Biol.*

2004, *8* (5), 547–553.

(41) Sassolas, A.; Blum, L. J.; Leca-Bouvier, B. D. Homogeneous Assays Using Aptamers. *Analyst* **2011**, *136* (2), 257–274.

(42) Jhaveri, S.; Rajendran, M.; Ellington, A. D. In Vitro Selection of Signaling Aptamers. *Nat. Biotechnol.* **2000**, *18* (12), 1293–1297.

(43) Vallée-Bélisle, A.; Plaxco, K. W. Structure-Switching Biosensors: Inspired by Nature. *Curr. Opin. Struct. Biol.* **2010**, *20* (4), 518–526.

(44) Tang, Z.; Mallikaratchy, P.; Yang, R.; Kim, Y.; Zhu, Z.; Wang, H.; Tan, W. Aptamer Switch Probe Based on Intramolecular Displacement. *J. Am. Chem. Soc.* **2008**, *130* (34), 11268–11269.

(45) Yamamoto, R.; Kumar, P. K. R. Molecular Beacon Aptamer Fluoresces in the Presence of Tat Protein of HIV-1. *Genes to Cells* **2000**, *5* (5), 389–396.

(46) Hamaguchi, N.; Ellington, A.; Stanton, M. Aptamer Beacons for the Direct Detection of Proteins. *Anal. Biochem.* **2001**, *294* (2), 126–131.

(47) Tok, J.; Lai, J.; Leung, T.; Li, S. F. Y. Molecular Aptamer Beacon for Myotonic Dystrophy Kinase-Related Cdc42-Binding Kinase α. *Talanta* **2010**, *81* (1–2), 732–736.

(48) Li, J. J.; Fang, X.; Tan, W. Molecular Aptamer Beacons for Real-Time Protein Recognition. *Biochem. Biophys. Res. Commun.* **2002**, *292* (1), 31–40.

(49) Mullis, K. B.; Faloon, F. A. Specific Synthesis of DNA in Vitro via a

Polymerase-Catalyzed Chain Reaction. In *Recombinant DNA Methodology*; Elsevier, 1989; pp 189–204.

(50) Lizardi, P. M.; Huang, X.; Zhu, Z.; Bray-Ward, P.; Thomas, D. C.; Ward, D. C. Mutation Detection and Single-Molecule Counting Using Isothermal Rolling-Circle-Amplification. *Nat. Genet.* **1998**, *19* (3), 225–232.

(51) Nilsson, M.; Gullberg, M.; Dahl, F.; Szuhai, K.; Raap, A. K. Real-Time Monitoring of Rolling-Circle Ampli ® Cation Using a Modi ® Ed Molecular Beacon Design. *Nucleic Acids Res.* **2002**, *30* (14), 1–7.

(52) Pickering, J.; Bamford, A.; Godbole, V.; Briggs, J.; Scozzafava, G.; Roe, P.; Wheeler, C.; Ghouze, F.; Cuss, S. Integration of DNA Ligation and Rolling Circle Amplification for the Homogeneous, End-Point Detection of Single Nucleotide Polymorphisms. *Nucleic Acids Res.* **2002**, *30* (12), e60.

(53) Cheng, Y.; Li, Z.; Zhang, X.; Du, B.; Fan, Y. Homogeneous and Label-Free Fluorescence Detection of Single-Nucleotide Polymorphism Using Target-Primed Branched Rolling Circle Amplification. *Anal. Biochem.* **2008**, *378* (2), 123–126.

(54) Dirks, R. M.; Pierce, N. A. From The Cover: Triggered Amplification by Hybridization Chain Reaction. *Proc. Natl. Acad. Sci. U. S. A.* **2004**, *101* (43), 15275–15278.

(55) Söderberg, O.; Gullberg, M.; Jarvius, M.; Ridderstråle, K.; Leuchowius, K. J.; Jarvius, J.; Wester, K.; Hydbring, P.; Bahram, F.; Larsson, L. G.; et al. Direct Observation of Individual Endogenous Protein Complexes in Situ by Proximity

Ligation. *Nat. Methods* **2006**, *3* (12), 995–1000.

(56) Fredriksson, S.; Gullberg, M.; Jarvius, J.; Olsson, C.; Pietras, K.; Gústafsdóttir, S. M.; Östman, A.; Landegren, U. Protein Detection Using Proximity-Dependent DNA Ligation Assays. *Nat. Biotechnol.* **2002**, *20* (5), 473–477.

(57) Zhang, H.; Li, X.-F.; Le, X. C. Binding-Induced DNA Assembly and Its Application to Yoctomole Detection of Proteins. *Anal. Chem.* **2012**, *84* (2), 877–884.

(58) Li, F.; Zhang, H.; Lai, C.; Li, X.-F.; Le, X. C. A Molecular Translator That Acts by Binding-Induced DNA Strand Displacement for a Homogeneous Protein Assay. *Angew. Chem. Int. Ed. Engl.* **2012**, *51* (37), 9317–9320.

(59) Zhang, H.; Li, F.; Li, X.-F.; Le, X. C. Yoctomole Detection of Proteins Using Solid Phase Binding-Induced DNA Assembly. *Methods* **2013**, *64* (3), 322–330.

(60) Li, F.; Zhang, H.; Wang, Z.; Li, X.; Li, X.-F.; Le, X. C. Dynamic DNA Assemblies Mediated by Binding-Induced DNA Strand Displacement. *J. Am. Chem. Soc.* **2013**, *135* (7), 2443–2446.

(61) Heid, C.; Livak, K.; Stevens, J.; Williams, P. Real Time Quantitative PCR. *Genome Res.* **1996**, *6*, 986–994.

(62) Mocellin, S.; Rossi, C. R.; Pilati, P.; Nitti, D.; Marincola, F. M. Quantitative Real-Time PCR: A Powerful Ally in Cancer Research. *Trends Mol. Med.* **2003**, *9* (5), 189–195.

(63) Wilhelm, J.; Pingoud, A. Real-Time Polymerase Chain Reaction. *ChemBioChem*

2003, *4* (11), 1120–1128.

(64) Klein, D. Quantification Using Real-Time PCR Technology: Applications and Limitations. *Trends Mol. Med.* **2002**, *8* (6), 257–260.

(65) Zipper, H.; Brunner, H.; Bernhagen, J.; Vitzthum, F. Investigations on DNA Intercalation and Surface Binding by SYBR Green I, Its Structure Determination and Methodological Implications. *Nucleic Acids Res.* **2004**, *32* (12).

(66) Ellington, A. D.; Szotsak, J. W. In Vitro Selection of RNA Molecules That Bind Specific Ligands. *Nature* **1990**, *346* (6287), 818–822.

(67) Ellington, A.; Szostak, J. Selection in Vitro of Single-Stranded DNA Molecules That Fold into Specific Ligand-Binding Structures. *Nature* **1992**, *355*, 850–852.

(68) Bock, L. C.; Griffin, L. C.; Latham, J. A.; Vermaas, E. H.; Toole, J. J. Selection of Single-Stranded DNA Molecules That Bind and Inhibit Human Thrombin. *Nature* **1992**, *355* (6360), 564–566.

(69) Charlton, J.; Sennello, J.; Smith, D. In Viva Imaging of Inflammation Human Neutrophil Elastase. *Chem. Biol.*

(70) Sun, H.; Zhu, X.; Lu, P. Y.; Rosato, R. R.; Tan, W.; Zu, Y. Oligonucleotide Aptamers: New Tools for Targeted Cancer Therapy. *Mol. Ther. - Nucleic Acids* **2014**, *3* (May), e182.

(71) Nimjee, S. M.; Rusconi, C. P.; Sullenger, B. A. Aptamers: An Emerging Class of Therapeutics. *Annu. Rev. Med.* **2005**, *56* (1), 555–583.

(72) Tuerk, C.; Gold, L. Systematic Evolution of Ligands by Exponential Enrichment: RNA Ligands to Bacteriophage T4 DNA Polymerase. *Science* **1990**, *249* (4968), 505–510.

(73) Jayasena, S. D. Aptamers: An Emerging Class of Molecules That Rival Antibodies in Diagnostics. *Clin. Chem.* **1999**, *45* (9), 1628–1650.

(74) Forster, T. Energiewanderung Und Fluoreszenz. *Naturwissenschaften* **1946**, *33* (6), 166–175.

(75) Lakowicz, J. R. *Principles of Fluorescence Spectroscopy Principles of Fluorescence Spectroscopy*; 2006.

(76) Jablonski, A. Über Den Mechanismus Der Photolumineszenz von Farbstoffphosphoren. *Z Phys* **1935**, *94* (1–2), 38–46.

(77) Algar, W. R.; Krull, U. J. Quantum Dots as Donors in Fluorescence Resonance Energy Transfer for the Bioanalysis of Nucleic Acids, Proteins, and Other Biological Molecules. *Anal. Bioanal. Chem.* **2008**, *391* (5), 1609–1618.

(78) Algar, W. R.; Tavares, A. J.; Krull, U. J. Beyond Labels: A Review of the Application of Quantum Dots as Integrated Components of Assays, Bioprobes, and Biosensors Utilizing Optical Transduction. *Anal. Chim. Acta* **2010**, *673* (1), 1–25.

(79) Zhang, C.-Y.; Yeh, H.-C.; Kuroki, M. T.; Wang, T.-H. Single-Quantum-Dot-Based DNA Nanosensor. *Nat. Mater.* **2005**, *4* (11), 826–831.

(80) Borm, P. J. A.; Robbins, D.; Haubold, S.; Kuhlbusch, T.; Fissan, H.; Donaldson,

K.; Schins, R.; Stone, V.; Kreyling, W.; Lademann, J.; et al. *The Potential Risks of Nanomaterials: A Review Carried out for ECETOC*; 2006; Vol. 3.

(81) Buzea, C.; Pacheco, I. I.; Robbie, K. Nanomaterials and Nanoparticles: Sources and Toxicity. *Biointerphases* **2007**, *2* (4), MR17-MR71.

(82) Roduner, E. Size Matters: Why Nanomaterials Are Different. *Chem. Soc. Rev.* **2006**, *35* (7), 583.

(83) Biju, V. Chemical Modifications and Bioconjugate Reactions of Nanomaterials for Sensing, Imaging, Drug Delivery and Therapy. *Chem. Soc. Rev.* **2014**, *43* (3), 744–764.

(84) Larson, D.; Zipfel, W.; Williams, R.; Clark, S.; Bruchez, M.; Wise, F.; Webb, W. Water-Soluble Quantum Dots for Multiphoton Fluorescence Imaging in Vivo. **2003**, *300* (5624), 1434–1436.

(85) Alivisatos, A. Semiconductor Clusters, Nanocrystals, and Quantum Dots. *Science (80-.).* **1996**, *271* (5251), 933–937.

(86) Michalet, X.; Pinaud, F.; Bentolila, L.; Tsay, J.; Doose, S.; Li, J.; Sundaresan, G.; Wu, A.; Gambhir, S.; Weiss, S. Quantum Dots for Live Cells, in Vivo Imaging, and Diagnostics. *Science* **2005**, *307* (5709), 538–545.

(87) Giersig, M.; Mulvaney, P.; Solomentsev, Y.; Èhmer, M.; Anderson, J. L. Shape Control of CdSe Nanocrystals. *Nat. Langmuir Langmuir J. Appl. Phys* **1993**, *404* (35), 3408–3413.

(88) Medintz, I. L.; Uyeda, H. T.; Goldman, E. R.; Mattoussi, H. Quantum Dot

Bioconjugates for Imaging, Labelling and Sensing. *Nat. Mater.* **2005**, *4* (6), 435–446.

(89) Murray, C. B.; Norris, D. J.; Bawendi, M. G. Synthesis and Characterization of Nearly Monodisperse CdE (E = S, Se, Te) Semiconductor Nanocrystallites. *J. Am. Chem. Soc.* **1993**, *115* (19), 8706–8715.

(90) Mirkin, C. A.; Letsinger, R. L.; Mucic, R. C.; Storhoff, J. J. A DNA-Based Method for Rationally Assembling Nanoparticles into Macroscopic Materials. *Nature*. 1996, pp 607–609.

(91) Daniel, M.-C.; Astruc, D. Gold Nanoparticles: Assembly, Supramolecular Chemistry, Quantum-Size-Related Properties, and Applications toward Biology, Catalysis, and Nanotechnology. *Chem. Rev.* **2004**, *104* (1), 293–346.

(92) Kelly, K. L.; Coronado, E.; Zhao, L. L.; Schatz, G. C. The Optical Properties of Metal Nanoparticles: The Influence of Size, Shape, and Dielectric Environment. *J. Phys. Chem. B* **2003**, *107* (3), 668–677.

(93) Underwood, S.; Mulvaney, P. Effect of the Solution Refractive Index on the Color of Gold Colloids. *Langmuir* **1994**, *10* (10), 3427–3430.

(94) Mulvaney, P. Surface Plasmon Spectroscopy of Nanosized Metal Particles. *Langmuir* **1996**, *12* (3), 788–800.

(95) Zhao, W.; Brook, M. A.; Li, Y. Design of Gold Nanoparticle-Based Colorimetric Biosensing Assays. *ChemBioChem* **2008**, *9* (15), 2363–2371.

(96) Hutter, E.; Fendler, J. H. Exploitation of Localized Surface Plasmon Resonance.

Adv. Mater. **2004**, *16* (19), 1685–1706.

(97) Song, T.; Liang, H. Synchronized Assembly of Gold Nanoparticles Driven by a Dynamic DNA-Fueled Molecular Machine. *J. Am. Chem. Soc.* **2012**, *134* (26), 10803–10806.

(98) Zhang, L.; Gu, F.; Wang, A.; Langer, R.; Farokhzad, O. Nanoparticles In Medicine: Therapeutic Applications and Developments. *Clin. Pharmacol. Ther.* **2008**, *83* (5), 761–769.

(99) Liong, M.; Lu, J.; Kovochich, M.; Xia, T.; Ruehm, S. G.; Nel, A. E.; Tamanoi, F.; Zink, J. I. Multifunctional Inorganic Nanoparticles for Imaging, Targeting, and Drug Delivery. TL - 2. *ACS Nano* **2008**, *2* (5), 889–896.

(100) Huang, Y.; Zhao, S.; Liang, H.; Chen, Z. F.; Liu, Y. M. Multiplex Detection of Endonucleases by Using a Multicolor Gold Nanobeacon. *Chem. - A Eur. J.* **2011**, *17* (26), 7313–7319.

(101) Song, S.; Liang, Z.; Zhang, J.; Wang, L.; Li, G.; Fan, C. Gold-Nanoparticle-Based Multicolor Nanobeacons for Sequence-Specific DNA Analysis. *Angew. Chemie - Int. Ed.* **2009**, *48* (46), 8670–8674.

(102) Hazarika, P.; Ceyhan, B.; Niemeyer, C. M. Sensitive Detection of Proteins Using Difunctional DMA-Gold Nanoparticles. *Small* **2005**, *1* (8–9), 844–848.

(103) Liu, J.; Lu, Y. Smart Nanomaterials Responsive to Multiple Chemical Stimuli with Controllable Cooperativity. *Adv. Mater.* **2006**, *18* (13), 1667–1671.

(104) Prigodich, A. E.; Randeria, P. S.; Briley, W. E.; Kim, N. J.; Daniel, W. L.;

Giljohann, D. A.; Mirkin, C. A. Multiplexed Nanoflares: MRNA Detection in Live Cells. *Anal. Chem.* **2012**, *84* (4), 2062–2066.

(105) Díaz, J. A.; Grewer, D. M.; Gibbs-Davis, J. M. Tuning Ratios, Densities, and Supramolecular Spacing in Bifunctional DNA-Modified Gold Nanoparticles. *Small* **2012**, *8* (6), 873–883.

(106) Li, X.; Guo, J.; Asong, J.; Wolfert, M. A.; Boons, G. J. Multifunctional Surface Modification of Gold-Stabilized Nanoparticles by Bioorthogonal Reactions. *J. Am. Chem. Soc.* **2011**, *133* (29), 11147–11153.

(107) Seeman, N. C. Nanomaterials Based on DNA. *Annu. Rev. Biochem.* **2010**, *79* (1), 65–87.

(108) LePecq, J. B.; Paoletti, C. A Fluorescent Complex between Ethidium Bromide and Nucleic Acids. Physical-Chemical Characterization. *J. Mol. Biol.* **1967**, *27* (1), 87–106.

(109) Duckett, D. R.; Lilley, D. M. The Three-Way DNA Junction Is a Y-Shaped Molecule in Which There Is No Helix-Helix Stacking. *EMBO J.* **1990**, *9* (5), 1659–1664.

(110) Li, F.; Lin, Y.; Le, X. C. Binding-Induced Formation of DNA Three-Way Junctions and Its Application to Protein Detection and DNA Strand Displacement. *Anal. Chem.* **2013**, *85* (22), 10835–10841.

(111) Zhang, D. Y.; Seelig, G. Dynamic DNA Nanotechnology Using Strand-Displacement Reactions. *Nat. Chem.* **2011**, *3* (2), 103–113.

(112) Zhang, D. Y.; Winfree, E. Control of DNA Strand Displacement Kinetics Using Toehold Exchange. *J. Am. Chem. Soc.* **2009**, *131* (47), 17303–17314.

(113) Lander, E. S. Initial Sequencing and Analysis of the Human Genome. *Nature* **2001**, *409* (6822), 860–921.

(114) Venter, J. C.; Adams, M. D.; Myers, E. W.; Li, P. W.; Mural, R. J.; Sutton, G. G.; Smith, H. O.; Yandell, M.; Evans, C. A.; Holt, R. A.; et al. The Sequence of the Human Genome. *Science* **2001**, *291* (5507), 1304–1351.

(115) Rosi, N. L.; Mirkin, C. A. Nanostructures in Biodiagnostics. *Chem. Rev.* **2005**, *105* (4), 1547–1562.

(116) Burton, P. R.; Clayton, D. G.; Cardon, L. R.; Craddock, N.; Deloukas, P.; Duncanson, A.; Kwiatkowski, D. P.; McCarthy, M. I.; Ouwehand, W. H.; Samani, N. J.; et al. Genome-Wide Association Study of 14,000 Cases of Seven Common Diseases and 3,000 Shared Controls. *Nature* **2007**, *447* (7145), 661–678.

(117) Seeman, N. C. Nucleic Acid Junctions and Lattices. *J. Theor. Biol.* **1982**, *99* (2), 237–247.

(118) Seeman, N. C.; Kallenbach, N. R. DNA Branched Junctions. *Annu. Rev. Biophys. Biomol. Struct.* **1994**, *23*, 53–86.

(119) Goodman, R.; Schaap, I.; Tardin, C.; Erben, C.; Berry, R.; Schmidt, C.; Turberfield, A. Rapid Chiral Assembly of Rigid DNA Building Blocks for Molecular Nanofabrication. *Science* **2005**, *310*, 1661–1665.

(120) Boer, D. R.; Kerckhoffs, J. M. C. A.; Parajo, Y.; Pascu, M.; Usón, I.; Lincoln, P.; Hannon, M. J.; Coll, M. Self-Assembly of Functionalizable Two-Component 3D DNA Arrays through the Induced Formation of DNA Three-Way-Junction Branch Points by Supramolecular Cylinders. *Angew. Chemie* **2010**, *122* (13), 2386–2389.

(121) Shu, D.; Shu, Y.; Haque, F.; Abdelmawla, S.; Guo, P. Thermodynamically Stable RNA Three-Way Junction for Constructing Multifunctional Nanoparticles for Delivery of Therapeutics. *Nat. Nanotechnol.* **2011**, *6* (10), 658–667.

(122) Müller, J.; Lippert, B. Imposing a Three-Way Junction on DNA or Recognizing One: A Metal Triple Helicate Meets Double Helix. *Angew. Chemie - Int. Ed.* **2006**, *45* (16), 2503–2505.

(123) Hamada, S.; Murata, S. Substrate-Assisted Assembly of Interconnected Single-Duplex DNA Nanostructures. *Angew. Chemie - Int. Ed.* **2009**, *48* (37), 6820–6823.

(124) Thomas, J. M.; Yu, H. Z.; Sen, D. A Mechano-Electronic DNA Switch. *J. Am. Chem. Soc.* **2012**, *134* (33), 13738–13748.

(125) Seemann, I. T.; Singh, V.; Azarkh, M.; Drescher, M.; Hartig, J. S. Small-Molecule-Triggered Manipulation of DNA Three-Way Junctions. *J. Am. Chem. Soc.* **2011**, *133* (13), 4706–4709.

(126) Thomas, J. M.; Chakraborty, B.; Sen, D.; Yu, H. Z. Analyte-Driven Switching of DNA Charge Transport: De Novo Creation of Electronic Sensors for an Early

Lung Cancer Biomarker. *J. Am. Chem. Soc.* **2012**, *134* (33), 13823–13833.

(127) Ge, B.; Huang, Y. C.; Sen, D.; Yu, H. Z. A Robust Electronic Switch Made of Immobilized Duplex/quadruplex DNA. *Angew. Chemie - Int. Ed.* **2010**, *49* (51), 9965–9967.

(128) Nutiu, R.; Li, Y. In Vitro Selection of Structure-Switching Signaling Aptamers. *Angew. Chemie - Int. Ed.* **2003**, *125*, 4771–4778.

(129) Wu, T.; Xiao, X.; Zhang, Z.; Zhao, M. Enzyme-Mediated Single-Nucleotide Variation Detection at Room Temperature with High Discrimination Factor. *Chem. Sci.* **2015**, *6* (2), 1206–1211.

(130) Brunk, C. F.; Jones, K. C.; James, T. W. Assay for Nanogram Quantities in C : Ellular Homogenates of DNA. *Anal. Biochem.* **1979**, *92*, 497–500.

(131) Georgiou, C. D.; Papapostolou, I. Assay for the Quantification of Intact/fragmented Genomic DNA. *Anal. Biochem.* **2006**, *358* (2), 247–256.

(132) Lapitan Jr., L. D. S.; Guo, Y.; Zhou, D. Nano-Enabled Bioanalytical Approaches to Ultrasensitive Detection of Low Abundance Single Nucleotide Polymorphisms. *Analyst* **2015**, *140* (12), 3872–3887.

(133) Ngo, H. T.; Gandra, N.; Fales, A. M.; Taylor, S. M.; Vo-Dinh, T. Sensitive DNA Detection and SNP Discrimination Using Ultrabright SERS Nanorattles and Magnetic Beads for Malaria Diagnostics. *Biosens. Bioelectron.* **2016**, *81*, 8–14.

(134) Hwang, M. T.; Landon, P. B.; Lee, J.; Choi, D.; Mo, A. H.; Glinsky, G.; Lal, R. Highly Specific SNP Detection Using 2D Graphene Electronics and DNA Strand

Displacement. *Proc. Natl. Acad. Sci.* **2016**, *113* (26), 7088–7093.

(135) Cai, B.; Wang, S.; Huang, L.; Ning, Y.; Zhang, Z.; Zhang, G. J. Ultrasensitive Label-Free Detection of PNA-DNA Hybridization by Reduced Graphene Oxide Field-Effect Transistor Biosensor. *ACS Nano* **2014**, *8* (3), 2632–2638.

(136) Krichevsky, A. M.; Gabriely, G. miR-21: A Small Multi-Faceted RNA. *J. Cell. Mol. Med.* **2009**, *13* (1), 39–53.

(137) Volinia, S.; Calin, G. A.; Liu, C.-G.; Ambs, S.; Cimmino, A.; Petrocca, F.; Visone, R.; Iorio, M.; Roldo, C.; Ferracin, M.; et al. A microRNA Expression Signature of Human Solid Tumors Defines Cancer Gene Targets. *Proc. Natl. Acad. Sci. U. S. A.* **2006**, *103* (7), 2257–2261.

(138) Zhang, Z.; Li, Z.; Gao, C.; Chen, P.; Chen, J.; Liu, W.; Xiao, S.; Lu, H. miR-21 Plays a Pivotal Role in Gastric Cancer Pathogenesis and Progression. *Lab. Investig.* **2008**, *88* (12), 1358–1366.

(139) Iorio, M. V.; Visone, R.; Di Leva, G.; Donati, V.; Petrocca, F.; Casalini, P.; Taccioli, C.; Volinia, S.; Liu, C. G.; Alder, H.; et al. MicroRNA Signatures in Human Ovarian Cancer. *Cancer Res.* **2007**, *67* (18), 8699–8707.

(140) Nam, E. J.; Yoon, H.; Kim, S. W.; Kim, H.; Kim, Y. T.; Kim, J. H.; Kim, J. W.; Kim, S. MicroRNA Expression Profiles in Serous Ovarian Carcinoma. *Clin. Cancer Res.* **2008**, *14* (9), 2690–2695.

(141) Lui, W.-O.; Pourmand, N.; Patterson, B. K.; Fire, A. Patterns of Known and Novel Small RNAs in Human Cervical Cancer. *Cancer Res.* **2007**, *67* (13), 6031–

6043.

(142) Fulci, V.; Chiaretti, S.; Goldoni, M.; Azzalin, G.; Carucci, N.; Tavolaro, S.; Castellano, L.; Magrelli, A.; Citarella, F.; Messina, M.; et al. Quantitative Technologies Establish a Novel microRNA Profile of Chronic Lymphocytic Leukemia. *Blood* **2007**, *109* (11), 4944–4951.

(143) Tran, N.; McLean, T.; Zhang, X.; Zhao, C. J.; Thomson, J. M.; O'Brien, C.; Rose, B. MicroRNA Expression Profiles in Head and Neck Cancer Cell Lines. *Biochem. Biophys. Res. Commun.* **2007**, *358* (1), 12–17.

(144) Tetzlaff, M. T.; Liu, A.; Xu, X.; Master, S. R.; Baldwin, D. A.; Tobias, J. W.; Livolsi, V. A.; Baloch, Z. W. Differential Expression of miRNAs in Papillary Thyroid Carcinoma Compared to Multinodular Goiter Using Formalin Fixed Paraffin Embedded Tissues. *Endocr. Pathol.* **2007**, *18* (3), 163–173.

(145) Kutay, H.; Bai, S.; Datta, J.; Motiwala, T.; Pogribny, I.; Frankel, W.; Jacob, S. T.; Ghoshal, K. Downregulation of miR-122 in the Rodent and Human Hepatocellular Carcinomas. *J. Cell. Biochem.* **2006**, *99*, 671–678.

(146) Lesnik, E. A.; Freier, S. M. Relative Thermodynamic Stability of DNA, RNA, and DNA:RNA Hybrid Duplexes: Relationship with Base Composition and Structure. *Biochemistry* **1995**, *34* (34), 10807–10815.

(147) Yang, L.; Liu, B.; Wang, M.; Li, J.; Pan, W.; Gao, X.; Li, N.; Tang, B. A Highly Sensitive Strategy for Fluorescence Imaging of MicroRNA in Living Cells and in Vivo Based on Graphene Oxide Enhanced Signal Molecules Quenching of

Molecular Beacon. *ACS Appl. Mater. Interfaces* **2018**, acsami.7b19284.

(148) Jin, Z.; Geibler, D.; Qiu, X.; Wegner, K. D.; Hildebrandt, N. A Rapid, Amplification-Free, and Sensitive Diagnostic Assay for Single-Step Multiplexed Fluorescence Detection of MicroRNA. *Angew. Chemie - Int. Ed.* **2015**, *54* (34), 10024–10029.

(149) de Planell-Saguer, M.; Rodicio, M. C. Analytical Aspects of microRNA in Diagnostics: A Review. *Anal. Chim. Acta* **2011**, *699* (2), 134–152.

(150) de Planell-Saguer, M.; Rodicio, M. C. Detection Methods for microRNAs in Clinic Practice. *Clin. Biochem.* **2013**, *46* (10–11), 869–878.

(151) Stahlhut, C.; Slack, F. J. MicroRNAs and the Cancer Phenotype: Profiling, Signatures and Clinical Implications. *Genome Med.* **2013**, *5* (12), 111.

(152) Huntington, J. A. Molecular Recognition Mechanisms of Thrombin. *J. Thromb. Haemost.* **2005**, *3* (8), 1861–1872.

(153) Davie, E. W.; Kulman, J. D. An Overview of the Structure and Function of Thrombin. *Semin. Thromb. Hemost.* **2006**, *32* (Suppl 1), 3–15.

(154) Crawley, J. T. B.; Zanardelli, S.; Chion, C. K. N. K.; Lane, D. A. The Central Role of Thrombin in Hemostasis. *J. Thromb. Haemost.* **2007**, *5* (Suppl 1), 95–101.

(155) Di Cera, E. Thrombin. *Mol. Aspects Med.* **2008**, *29* (4), 203–254.

(156) Sokolova, E.; Resier, G. Prothrombin/thrombin and the Thrombin Receptors

PAR-1 and PAR-4 in the Brain: Localization, Expression and Participation in Neurodegenerative Diseases. *Thromb. Haemost.* **2008**, *100* (4), 576–581.

(157) Franchini, M.; Mannucci, P. M. Thrombin and Cancer: From Molecular Basis to Therapeutic Implications. *Semin. Thromb. Hemost.* **2012**, *38* (1), 95–101.

(158) Shuman, M. A.; Majerus, P. W. The Measurement of Thrombin in Clotting Blood by Radioimmunoassay. *J. Clin. Invest.* **1976**, *58* (5), 1249–1258.

(159) Brummel-Ziedins, K. E.; Vossen, C. Y.; Butenas, S.; Mann, K. G.; Rosendaal, F. R. Thrombin Generation Profiles in Deep Venous Thrombosis. *J. Thromb. Haemost.* **2005**, *3* (11), 2497–2505.

(160) Deng, B.; Lin, Y.; Wang, C.; Li, F.; Wang, Z.; Zhang, H.; Li, X.; Le, X. C. Aptamer Binding Assays for Proteins : The Thrombin Example — A Review. *Anal. Chim. Acta* **2014**, *837*, 1–15.

(161) Tasset, D. M.; Kubik, M. F.; Steiner, W. Oligonucleotide Inhibitors of Human Thrombin That Bind Distinct Epitopes. *J. Mol. Biol.* **1997**, *272* (5), 688–698.

(162) Kong, D.; Xu, J.; Shen, H. Positive Effects of ATP on G-Quadruplex-Hemin DNAzyme-Mediated Reactions. *Anal. Chem.* **2010**, *82* (14), 6148–6153.

(163) Yang, L.; Ellington, A. D. Real-Time PCR Detection of Protein Analytes with Conformation-Switching Aptamers. *Anal. Biochem.* **2008**, *380* (2), 164–173.

(164) Heyduk, E.; Heyduk, T. Nucleic Acid-Based Fluorescence Sensors for Detecting Proteins. *Anal. Chem.* **2005**, *77* (4), 1147–1156.

(165) Demers, L. M.; Mirkin, C. a.; Mucic, R. C.; Reynolds, R. a.; Letsinger, R. L.; Elghanian, R.; Viswanadham, G. A Fluorescence-Based Method for Determining the Surface Coverage and Hybridization Efficiency of Thiol-Capped Oligonucleotides Bound to Gold Thin Films and Nanoparticles. *Anal. Chem.* **2000**, *72* (22), 5535–5541.

(166) Hurst, S. J.; Lytton-Jean, A. K. R.; Mirkin, C. A. Maximizing DNA Loading on a Range of Gold Nanoparticle Sizes. *Anal. Chem.* **2006**, *78* (24), 8313–8318.

(167) Liu, C. W.; Huang, C. C.; Chang, H. T. Control over Surface DNA Density on Gold Nanoparticles Allows Selective and Sensitive Detection of mercury(II). *Langmuir* **2008**, *24* (15), 8346–8350.

(168) Kim, E. Y.; Stanton, J.; Vega, R. A.; Kunstman, K. J.; Mirkin, C. A.; Wolinsky, S. M. A Real-Time PCR-Based Method for Determining the Surface Coverage of Thiol-Capped Oligonucleotides Bound onto Gold Nanoparticles. *Nucleic Acids Res.* **2006**, *34* (7).

(169) Maxwell, D. J.; Taylor, J. R.; Nie, S. Self-Assembled Nanoparticle Probes for Recognition and Detection of Biomolecules. *J. Am. Chem. Soc.* **2002**, *124* (32), 9606–9612.

(170) Yancopoulos, G. D. Vascular-Specific Growth Factors and Blood Vessel Formation. *Nature* **2000**, *407* (September), 242–248.

(171) Hellström, M.; Kalén, M.; Lindahl, P.; Abramsson, A.; Betsholtz, C. Role of PDGF-B and PDGFR-Beta in Recruitment of Vascular Smooth Muscle Cells and

Pericytes during Embryonic Blood Vessel Formation in the Mouse. *Development* **1999**, *126* (14), 3047–3055.

(172) Giljohann, D. A.; Seferos, D. S.; Daniel, W. L.; Massich, M. D.; Patel, P. C.; Mirkin, C. A. Gold Nanoparticles for Biology and Medicine. *Angew. Chemie - Int. Ed.* **2010**, *49* (19), 3280–3294.

(173) Kyriazi, M.-E.; Giust, D.; El-Sagheer, A. H.; Lackie, P. M.; Muskens, O. L.; Brown, T.; Kanaras, A. G. Multiplexed mRNA Sensing and Combinatorial-Targeted Drug Delivery Using DNA-Gold Nanoparticle Dimers. *ACS Nano* **2018**, acsnano.7b08620.

(174) Zheng, J.; Li, N.; Li, C.; Wang, X.; Liu, Y.; Mao, G.; Ji, X.; He, Z. A Nonenzymatic DNA Nanomachine for Biomolecular Detection by Target Recycling of Hairpin DNA Cascade Amplification. *Biosens. Bioelectron.* **2018**, *107* (January), 40–46.

(175) Peng, H.; Li, X.-F.; Zhang, H.; Le, X. C. A microRNA-Initiated DNAzyme Motor Operating in Living Cells. *Nat. Commun.* **2017**, *8* (May 2016), 14378.

(176) Wu, G.; Zaman, M. H. Low-Cost Tools for Diagnosing and Monitoring HIV Infection in Low-Resource Settings. *Bull. World Health Organ.* **2012**, *90* (12), 914–920.

(177) Kozma, P.; Lehmann, A.; Wunderlich, K.; Michel, D.; Schumacher, S.; Ehrentreich-Förster, E.; Bier, F. F. A Novel Handheld Fluorescent Microarray Reader for Point-of-Care Diagnostic. *Biosens. Bioelectron.* **2013**, *47*, 415–420.

(178) Fang, X. X.; Li, H. Y.; Fang, P.; Pan, J. Z.; Fang, Q. A Handheld Laser-Induced Fluorescence Detector for Multiple Applications. *Talanta* **2016**, *150*, 135–141.

(179) Dhiman, A.; Kalra, P.; Bansal, V.; Bruno, J. G.; Sharma, T. K. Aptamer-Based Point-of-Care Diagnostic Platforms. *Sensors Actuators, B Chem.* **2017**, *246*, 535–553.

(180) Syedmoradi, L.; Daneshpour, M.; Alvandipour, M.; Gomez, F. A.; Hajghassem, H.; Omidfar, K. Point of Care Testing: The Impact of Nanotechnology. *Biosens. Bioelectron.* **2017**, *87*, 373–387.

(181) Ozer, A.; Pagano, J. M.; Lis, J. T. New Technologies Provide Quantum Changes in the Scale, Speed, and Success of SELEX Methods and Aptamer Characterization. *Mol. Ther. - Nucleic Acids* **2014**, *3* (June), e183.

(182) Hildebrandt, N.; Spillmann, C. M.; Algar, W. R.; Pons, T.; Stewart, M. H.; Oh, E.; Susumu, K.; Díaz, S. A.; Delehanty, J. B.; Medintz, I. L. Energy Transfer with Semiconductor Quantum Dot Bioconjugates: A Versatile Platform for Biosensing, Energy Harvesting, and Other Developing Applications. *Chem. Rev.* **2016**, acs.chemrev.6b00030.

(183) Paliwoda, R. E.; Li, F.; Reid, M. S.; Lin, Y.; Le, X. C. Sequential Strand Displacement Beacon for Detection of DNA Coverage on Functionalized Gold Nanoparticles. *Anal. Chem.* **2014**, *86* (12), 6138–6143.

Appendix A: List of Publications

1) Reid, M.S.; **Paliwoda, R.E.**; Zhang, H.; Le, X.C. Reduction of background generated from template-template hybridizations in the Exponential Amplification Reaction. Submitted to *Analytical Chemistry*, June 2018 (manuscript number: ac-2018-02788w).

2) **Paliwoda, R.E.**; Newbigging, A.N.; Wang, Z.; Le, X.C. Benefits and risks associated with consumption of Great Lakes fish containing omega-3 fatty acids and polychlorinated biphenyls (PCBs). *Journal of Environmental Science*, 2016, *41*, 1-5.

3) Newbigging, A.N.*; **Paliwoda, R.E.***; Le, X.C. Rice: Reducing arsenic content by controlling water irrigation. *Journal of Environmental Science*. 2015, *30*, 129-131. (*These authors contributed equally to the publication)

4) **Paliwoda, R.E.**; Li, F.; Reid, M.S.; Lin, Y.; Le, X.C. Sequential Strand Displacement Beacon for Detection of DNA Coverage on Functionalized Gold Nanoparticles. *Analytical Chemistry*. 2014, *86*, 6138-6143. (**Chapter 5**)